# SCALABLE TOPOGRAPHY-INDUCED CELL ALIGNMENT FOR

# TISSUE ENGINERING APPLICATIONS



## ANENE-NZELU CHUKWUEMEKA ONYEKA GEORGE

*(M.D) Cuba*

## A THESIS SUBMITTED

## FOR THE DEGREE

## DOCTOR OF PHILOSOPHY (PH.D)

## DEPARTMENT OF BIOMEDICAL ENGINEERING

## NATIONAL UNIVERSITY OF SINGAPORE

## 2014

# DECLARATION

**I hereby declare that this thesis is my original work and has been written by me in entirety. I have duly acknowledged all sources of information which have been used in the thesis**

**This thesis has not been submitted for any degree in any university previously**

**Anene-Nzelu Chukwuemeka George Onyeka**
**4th August 2014**

# ACKNOWLEDGEMENTS

Willyams, Milvia, Miguelito, Amos, Jimada, Okechukwu, Pastor Mayito and family. I do hope to meet you guys some day in the future

Finally I want to thank my awesome family for the great support. Words can't describe how much I love you all, I'm sure the best years of our lives are yet to come. Thanks to Dad, Mum, Amara, Ken, Uche, Onyi, Chinua, Ebuka. I love you all immensely. Above all, all glory to Jesus for your great love which is better than life. I am reminded that "though the mountains are shaken and the hills are removed, your unfailing love for me would not be shaken".

**TABLE OF CONTENTS**

# LIST OF PUBLICATIONS AND CONFERENCE PROCEEDINGS

1. **Anene-Nzelu C.G et al** (2013) Scalable alignment of three-dimensional cellular constructs in a microfluidic chip, Oral Presentation, International Conference on biomedical engineering (ICBME), Dec 4-7, Singapore

2. **Anene-Nzelu C.G et al** (2013) Scalable alignment of three-dimensional cellular constructs in a microfluidic chip, *Lab on a Chip* 13 (20): 4124-4133

3. **Anene-Nzelu C.G et al** (2013) Gratings on a dish. A scalable cell alignment substrate on optical media. Oral Presentation, *ASME Summer bioengineering conference*, June 26-29 Oregon USA

4. **Anene-Nzelu C.G et al** (2013) Scalable Cell alignment on optical media substrates, *Biomaterials* 34(21): 5078-87

5. **Anene-Nzelu C.G et al** (2012) *In vitro* platform for the study of drug induced cardiotoxicity. Poster Presentation, *3<sup>rd</sup> World congress, Tissue engineering and regenerative medicine TERMIS*, September 5-8 Vienna Austria

6. Nugraha B, **Anene-Nzelu C.G**, Toh Y.C et al (2012) *In vitro* toxicology models based on tissue engineered constructs. Poster Presentation. A*STAR scientific conference, October 18-19 Singapore

7. **Anene-Nzelu C.G et al** (2011) Liver tissue model for drug toxicity screening, *Journal of mechanics in medicine and biology* 11(02): 369-390

8. Wang Y, Sunsanado T, Lei X, **Anene-Nzelu C.G et al** (2010) Current development of bioreactors for extracorporeal bioartificial liver, *Biointerphases* 5(3) 116-130

9. **Anene-Nzelu C.G et al** (2014) High throughput aligned *in vitro* platform for physiological and pharmacological studies of the heart (in preparation)

# LIST OF PATENTS

1) IBN-303 "Gratings-on-a-Dish- Processing of Large-Area, Low-Cost Diffraction Gratings (Holographic Gratings and Optical Discs CD/DVD) for Cell Culture/Cell Alignment".

# SUMMARY

*In vitro* cell alignment has been shown over the years to be important for dictating cellular response such as cell morphology, differentiation, maturation and proliferation. Recreating cell alignment *in vitro* is hence very important for cell biologist, biomedical engineers, stem cell scientists and any researcher interested in harnessing all the benefits of *in vitro* platforms.

Current technologies used to fabricate micro/nanogrooves *in vitro* are photolithography, ultraviolet-laser irradiation, UV embossing, nanoimprint lithography and electron-beam lithography. Though these methods can been used to achieve nanoscale resolution, they involve costly clean-room equipments, lengthy procedures and highly skilled labor and protocols. In addition, the high cost of acquiring these machines makes it difficult for labs to explore the various applications of alignment *in vitro*

In order to make cell alignment a routine feature of cell culture, commercially available optical media are explored as cost effective, scalable platforms with micro/nano grooves for cell culture. These commercially available optical media are optical devices with periodic structure, which is able to split and diffract light into several beams travelling in various directions. Here, we demonstrate that the optical media can directly support cell attachment, growth, alignment and differentiation. We also show its use as molds for patterning PDMS used for both 2D and 3D microfluidic cell culture. Finally we show that these commercially available optical media can serve as platforms for cardiotoxicity drug screening, as they are not only scalable for large scale and high throughput studies, but also amenable to the various tests

required in drug screening. Commercially available optical media can therefore be exploited as a scalable and cost-effective source of micro-grooved cell culture substrates. This will allow researchers to incorporate cell alignment for routine culture of cardiac, skeletal or neuronal cells to support cell and tissue research and drug testing applications

# LIST OF FIGURES

# LIST OF TABLES

## LIST OF SYMBOLS AND ABBREVIATIONS

| | |
|---|---|
| 2D | Two Dimensional |
| 3D | Three Dimensional |
| AFM | Atomic Force Microscope |
| ANP | A type Natriuretic peptide |
| ATP | Adenosine Tri Phosphate |
| BNP | B type Natriuretic peptide |
| CD | Compact Disc |
| CHO | Chinese Hamster Ovary |
| CICR | Calcium Induced Calcium Release |
| CX-43 | Connexin 43 |
| DNA | Deoxyribonucleic Acid |
| DVD | Digital Versatile Disc |
| EC | Endothelial Cells |
| ECM | Extra Cellular Matrix |
| EF | Electrical Field |
| ER | Endoplasmic Reticulum |
| FBS | Fetal Bovine Serum |
| FFT | Forward Fourier Transform |
| GJ | Gap Junction |
| HBSS | Hanks Balanced Salt Solution |
| HERG | Human Ether-a-go-go-Related Gene |
| HESC | Human Embryonic Stem Cells |
| HMSC | Human Mesenchymal Stem Cells |
| IPSC | Induced Pluripotent Stem Cells |
| MEA | Multi Electrode Array |

| | |
|---|---|
| MHC | Myosin Heavy Chain |
| MLC | Myosin Light Chain |
| NIL | Nano Imprint Lithography |
| NRVM | Neonatal Rat Ventricular Myocytes |
| PC | Polycarbonate |
| PCL | Polycaprolactone |
| PDMS | Poly Di-Methyl Siloxane |
| PEG | Polyethylene Glycol |
| PET | Polyethylene Terephthalate |
| PMMA | Polymethyl Methacrylate |
| PS | Polystyrene |
| RGD | Arg-Gly-Asp |
| RNA | Riboxy Nucleic Acid |
| RT | Reverse Transcriptase |
| SC | Schwann Cells |
| SMC | Smooth Muscle Cells |
| TCP | Tissue Culture Plastic |
| TDP | Torsades de Pointes |
| UV | Ultra Violet |
| VCM | Ventricular Cardiomyocytes |
| WCA | Water Contact Angle |

# CHAPTER 1: INTRODUCTION

## 1.1 Cell alignment *in vitro* and *in vivo*

Cell alignment refers to the spatial and oriented organization of cells [1]. This plays an important role in various cell behaviors including cytoskeleton reorganization, membrane protein relocation, cell-adhesion complexes spatial disposition, gene expression, and ECM remodeling [1]. Cell alignment has also been shown over the years to be important for dictating cellular response such as cell morphology, differentiation, maturation and proliferation [2]. They also serve as platforms for studying effect of mechanical cues on cells [3, 4], and recent evidence suggests cell alignment affects the epigenetic state of the cells [5]. Alignment *in vivo* can be observed at various organizational levels in different tissues and organs. They can be seen at the extracellular matrices (ECMs) level such as the collagen fiber bundles in ligaments [6], in the blood-vessel epithelium which is made up of cells aligned along the direction of the flow [7], in striated muscle cells [8], neuron cells [9], and cardiomyocytes [10]. Cell alignment ensures pattern formation during embryogenesis [11], aids tissue maturation [12] and regeneration [13] and is important hierarchical organization of cells and tissues [1, 14]. Aligned organization of cells also results in secretion and deposition of a highly anisotropic ECM, which is specific to tissue type and critical in determining tissue function [1, 15]. Recreating cell alignment *in vitro* is hence very important for cell biologist, biomedical engineers, stem cell scientists and any researcher interested in regeneration of structured and functional tissue equivalents [1].

1

## 1.2 Cell alignment for differentiation and maturation

Cell differentiation and maturation *in vitro* is important for studies related to developmental biology, disease modeling, regenerative medicine and drug development [16]. Differentiating cells into a target organ using for example, patient-derived iPSCs as an autologous source of cells potentially circumvents the need for immunosuppressant therapy after transplantation. This therapeutic potential of stem cell-based regenerative medicine has been demonstrated in animal models with good results [16]. Apart from its potential in regenerative medicine, stem cells can be used to elucidate disease mechanisms *in vitro*. Equipped with the knowledge gleaned from the said disease mechanism elucidation, scientists can look for how to prevent or cure the disease [16]. In addition, to the therapeutic potentials, stem cells when differentiated to a target organ can serve as cell source for drug development [16]. To reap the benefits of stem cells *in vitro*, cells must be cultured under the right set of conditions for successful differentiation into the desired lineage [4]. While some researchers direct their effort towards finding the right molecules or transcription factors needed for differentiation, it is becoming apparent that physical (micro environmental) factors are also important for induction into the right lineage [2]. One of such physical cues required for cell differentiation is alignment of cells by underlying topography [2]. Alignment has been shown to be beneficial for differentiation and maturation of cells into the skeletal, cardiac and neuronal lineage.

*1.2.1. Cell alignment for skeletal muscle differentiation and maturation*

Skeletal muscle is composed of highly aligned bundles of parallel multinucleated myotubes, formed by fusion of differentiated mononuclear myoblast [17]. This parallel arrangement of myofibers in skeletal muscles is necessary for developing high contractile forces. Skeletal muscle is needed for movement, breathing and carrying out daily physical activities. Hence, any damage to the muscle would greatly impair a patient's day-to-day activities. To treat such patients, differentiation and tissue engineering of skeletal muscle is a potential alternative. Not only would it serve as therapy, skeletal muscle tissue engineering can also serve as a platform for drug development and to study insulin metabolism. Unfortunately, myoblasts cannot differentiate into organized arrays of myotubes autonomously when cultured in typical cell culture flask [17]. They form disordered and branched myotubes and this may lead to failure in clinical applications. To solve this problem, many research efforts have been focused on techniques promoting alignment of skeletal myotubes.

Myoblast alignment is suggested as a critical step before fusion during myotube formation. During musculoskeletal myogenesis, tracks (depth of 1–4.5μm and width of 2–3μm) formed by primary and secondary mature muscle fibers bring myoblasts into conformable alignment with the mature fibers before fusion [17]. Myoblasts lie and grow in the grooves between the adjacent fibers and differentiate into a fused and aligned muscle tissue [17]. Due to this aligned process during tissue development *in vivo*, physical

topography (grooves and ridges) may act as biomimetic platforms for myoblast differentiation and spatial organization.

Many *in vitro* studies indicate that anisotropic topography is an effective parameter for alignment of skeletal myoblasts and myotubes. Dang *et al* showed an induction into the myogenic lineage by aligning human mesenchymal stem cells (hMSC) *in vitro* [18]. Culturing hMSC on nanofibers induced a cytoskeletal and nuclear alignment and elongation. These morphological changes led to an upregulation of genes indicative of myogenic lineage even while the cells were cultured in proliferative, non-differentiating medium [18]. In another experiment, Wang *et al* showed enhanced alignment, fusion and maturation of myoblast when C2C12 cells were cultured on grooved substrates as compared to the cells cultured on flat substrates [17]. Ricotti *et al* showed that culturing C2C12 cells on electrospun nanofibers reduced their proliferative capacity and enhanced their maturation [19]. Many other experiments have shown the importance of alignment for skeletal muscle tissue engineering. The alignment can be achieved through various means such as: micropatterning [20, 21], mechanical stretch [22], electrical stimulation [23], abrasive-ground patterned surfaces [24], microchip with linearly aligned microgrooves [25], and bio-printing technology [26]. In all these experiments, it was shown that differentiation of skeletal myocytes on aligned platforms yielded more matured and electrically coupled myotubes than cells cultured on flat surfaces [20-24]. More recently scientists have been able to generate skeletal muscle grafts of aligned tissue for regenerative medicine [27]. The graft was used to treat mice models of Duchenne Muscular

Dystrophy (DMD), and the transplant led to the formation of a significantly greater number of dystrophin-positive muscle fibers [27]. This result indicates that dystrophin replacement and myogenesis is achievable *in vivo* with this approach [27]. Due to the fact that skeletal muscle is a highly organized tissue in which the ECM is composed of highly-aligned cables of collagen with nanoscale features, transplanting of aligned skeletal muscle graft is a more biomimetic approach as it leads to better integration and electrical coupling [27]. The grafting of unaligned tissues or the direct injection of cells into muscles for regenerative therapy often results in suboptimal functional improvement due to a failure to integrate with native tissue properly [27]. Cell alignment hence offers benefits not only for enhanced differentiation and maturation but also for a better integration of tissue grafts into host tissue [27].

*1.2.2 Cell alignment for neuronal differentiation*

Cell alignment is important in nerve tissue for differentiation, polarity selection and axonal regeneration. With respect to differentiation, Yim et al showed that by culturing hMSC on nanogratings of 350nm width, there was an upregulation of neuronal markers [4] (Fig 1). They argued that cytoskeleton rearrangement and nuclei elongation of the hMSC played an important role in creating the signal transduction for the transdifferentiation [4]. The cytoskeletal and nuclear elongation have been correlated with changes in gene expression profile and cell differentiation in other studies [4]. They further showed that the combination of topographical and chemical cues enhanced the differentiation of the hMSC into neuronal lineage [4]. In another study, they showed that by culturing human embryonic stem cells hESC on topographies

of different dimensions, they could direct the differentiation of these cells into

either the neuronal lineage or the glial lineage [28].
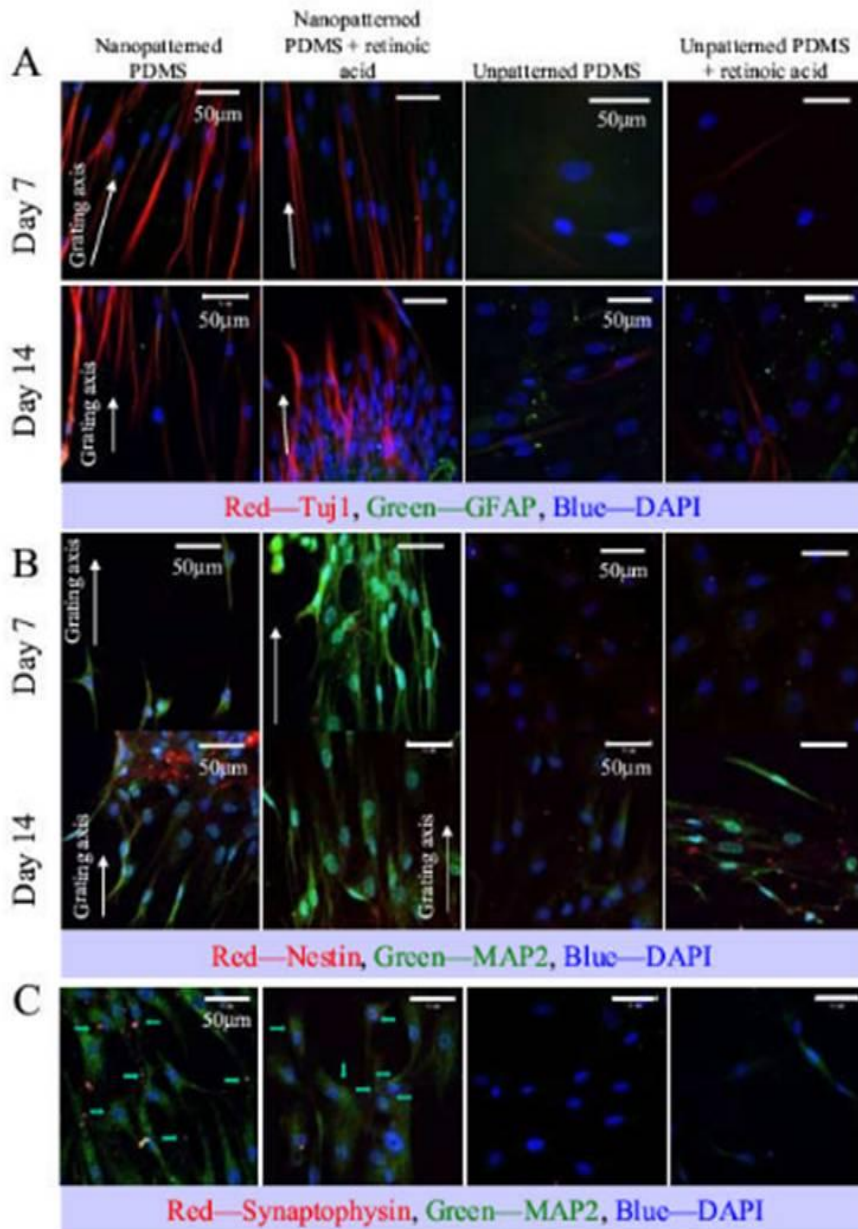


**Figure 1: Enhanced differentiation of human mesenchymal stem cells into neuronal lineage**. Immunofluorescent staining of (A) Tuj1 and GFAP, (B) MAP2 and nestin and (C) synaptophysin and MAP2 of hMSCs cultured on nano-patterned PDMS, nano-patterned PDMS in the presence of retinoic acid (RA), unpatterned PDMS and unpatterned PDMS in the presence of RA. (A) Tuj1 is in red, GFAP in green; (B) nestin is in red, MAP2 in green and (C) synaptophysin is in red and marked by arrows, while MAP2 is shown in green. In all panels the DAPI nuclei counter-stain is shown in blue. The direction of the gratings is indicated with a white arrow. Images were taken at representative areas of the samples. Scale bar 50μm [4]

In axonal regeneration, neural cells orient parallel to aligned Schwann cells (SCs) in both peripheral and central nerve injuries *in vivo* [1, 29, 30]. After a nerve lesion, SCs start to proliferate and generate longitudinal cell strands called bands of Büngner [31]. This causes the nerve lumen to become restructured by hundreds of microchannels along the major axis of the nerve [1]. Aligned SCs and their ECM hence act as a guide for axonal regrowth [1]. A number of studies have demonstrated that SC alignment via longitudinally orientated microgrooves imitate the formation of bands of Büngner, suggesting that topography cues of the nerve *in vivo* may induce SC alignment [32, 33]. A recent study showed that culturing dorsal root ganglion cells on PDMS with micro and nano-scale topography of SCs enhanced neurite alignment and neuronal adhesion (Fig 2) [12]. Besides just providing a physical topography, the aligned SCs also secret ECM molecules, cell adhesion molecules and neurotrophic factors which are necessary for nerve regeneration. It is possible that the alignment is partially responsible for triggering the secretion of those molecules considering the fact that human SCs oriented to aligned electrospun poly(e-caprolactone) fibers had an enhanced mature state which is pro-myelinating state [34]. Transplantation of nerve conduits seeded with aligned SCs has also been used to promote nerve regeneration [1, 35, 36], This is due to the improved rate and extent of neurite elongation cultured on aligned SCs. Due to all the promising *in vitro* results, many researchers are developing biomaterials which induce SC alignment for artificial nerve grafts [1, 37, 38].
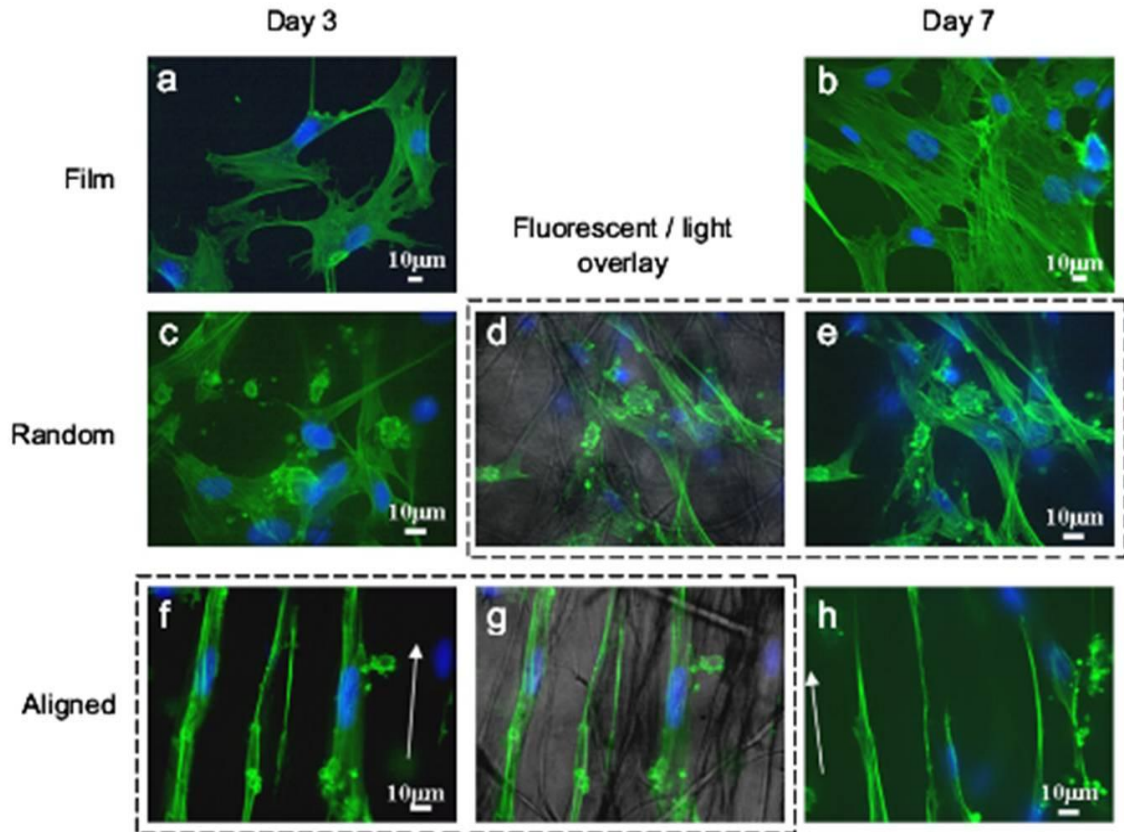
**Figure 2: Confocal images of human Schwann cells cultured on PCL scaffolds for 3 days (a, c and f) and 7 days (b, e and h).** A) And B) PCL film; C-E) randomly oriented PCL fibers; and F-H) aligned PCL electrospun fibers, arrows depict directions of fiber alignment. D) And G) Fluorescent-light images overlay. Green: actin cytoskeleton, blue: DAPI [12]

Alignment *in vitro* has also been shown to direct the differentiation of PC12 cell lines into bipolar morphology as compared to the multipolar morphology obtained when cultured on flat surfaces [39]. Neuronal polarity *in vivo* is determined by a series of events preceded by cytoskeletal rearrangement that leads to activation of signaling pathways, selective protein and organelle trafficking and focal adhesion distribution [39-42]. Polarity selection is important in neural differentiation as different cells have different functions [39-42]. Manipulating neuronal polarity in vitro hence can serve as a tool to study neural development [39-42]. These and many more studies

8

highlight the importance of cell alignment for differentiation and maturation of

cells [43, 44]. Table 1 shows the various applications of cell alignment *in vitro*

**Table 1: Effects of cell alignment using micro/nanogrooves *in vitro*** [45]

| Cell Type | Dimension | Materials | Results |
|---|---|---|---|
| Cardiomyocytes | -Depth of 2-5μm and widths of 5-10μm<br><br>-Depth of 100 and 350nm and width of 450nm<br><br>-Wrinkle widths of 20nm -10 μm<br><br>-Depths of 200-500nm and widths from 50-800nm<br><br>-Electrospun fiber widths of 3μm | PDMS<br><br>-Polystyrene<br><br>-Polyurethane<br><br>-PDMS<br><br>-PEG<br><br>-Polyurethane | -Cell alignment, and a more physiological localization of N-cadherin and Connexin 43. More synchronous activity<br><br>-Cell alignment regardless of material. Beating rates dependent on topography and stiffness<br><br>-Better sarcomeric organization and localization of connexin 43 and N-cadherin<br><br>-Better sarcomeric organization, faster action potential conduction<br><br>-Alignment and enhanced differentiation of mESC |

| | | | |
|---|---|---|---|
| Skeletal Myoblasts/C2C12 | -Fibers of diameter ranging from 400nm to 1.5μm<br><br>-Groove width of 450 and 900nm and depth of 100 and 350nm<br><br>-Average fiber diameter 200-400nm | -Nylon<br><br>-Polystyrene<br><br>-Polyhydroxybutyrate | -Cell alignment with enhanced differentiation and maturation<br><br>-Cell alignment, formation of longer myotubes<br><br>-Cell alignment, formation of longer myotubes |
| Neuronal cells/PC12 | Depth of 250nm and Width of 500nm<br><br>Depth of 200nm and width ranging from 500nm - 5μm<br><br>Depth of 80nm -2μm and groove/ridge width of 250nm – 2μm | -PMMA<br><br>-Polystyrene<br><br>-PDMS | -Neuronal polarity selection<br><br>-Neuronal polarity selection.<br><br>-Submicron topography more effective<br><br>-Enhance neural differentiation |

**1.3 Cell alignment incorporated into *in vitro* platforms for drug screening**

*1.3.1 In vitro drug testing*

Over the past decade, drug safety issues caused about 30-40% of drug attrition at all phases of development, including drug discovery, preclinical evaluation, clinical evaluation, and post market surveillance both in the US and worldwide [46]. This is a huge burden for the pharmaceutical companies considering the cost of developing a new drug which could range from 500 million to 2,000 million dollars depending on the therapy or the developing firm [47]. Figure 3 shows the rapid increase in cost of developing a drug over the years both in the preclinical and the clinical phase. The pharmaceutical industry has recognized the urgent need to decide in the early preclinical development stage when a drug candidate is sufficiently characterized and capable to be selected for human testing. This way, greater value can be generated while minimizing escalating development costs, this is because failure to detect drug toxicities during preclinical testing contributes to drug candidate failure during clinical testing. To achieve this goal, proper *in vitro* testing models and assays have to be used at a very early stage to streamline hit-to-lead generation and to identify the most promising lead.
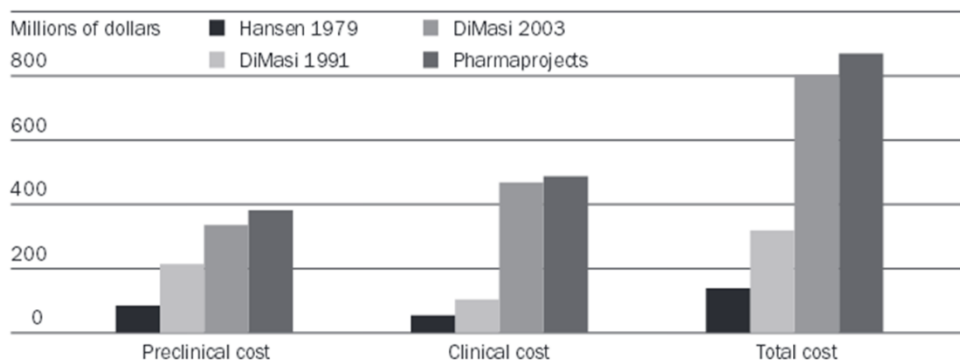
**Figure 3: The cost of developing a new drug**. The estimated cost of drug development has been consistently increasing over the years, both in the preclinical and the clinical phases [47]

*In vitro* studies can be designed to identify a lead candidate from several hits and develop the best procedure for new drug scale-up. They also help for detailed study of the drugs absorption, distribution, metabolism, excretion and toxicity (ADMET) which are of fundamental importance for the success of the drug [48]. In addition, due to high cost, unavailability and ethical concerns of using animal and human models, *in vitro* platforms are a formidable alternative for research in drug development. Compared to animal models and cadaveric tissues, the *in vitro* models are amenable to systematic, repetitive, controlled and quantitative investigation of cell or tissue physiology in drug discovery and development [49]. *In vitro* models can be used to assess a large number of different combinations of experimental parameters [50]. Effective *in vitro* models can therefore help predict *in vivo* situations and also help elucidate the mechanism of action of those drugs. Figure 4 shows a schematic of drug discovery process and the place of preclinical studies.

12
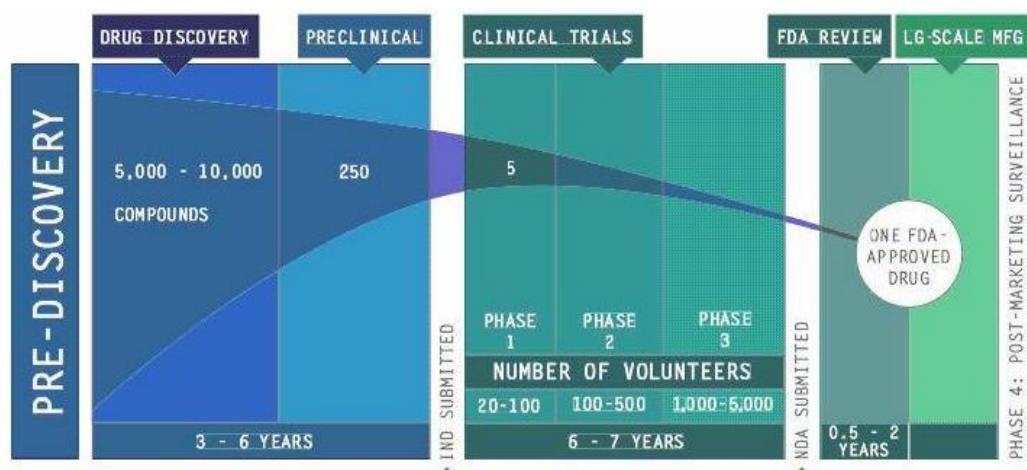
**Figure 4: Drug discovery process** (Adapted from http://www.gsdpharmaconsulting.com)

*1.3.2 Importance of drug induced cardiotoxicity and clinical manifestations*

Of all the drugs that have been withdrawn from the market, cardiovascular related toxicities remain a leading cause, ranking second after hepatotoxicity [51]. In other studies, cardiovascular toxicities ranked as high as hepatotoxicity or even higher (Figure 5), this underscores the importance of screening drugs for cardiotoxicity during development [46, 52, 53]. Many drugs, both cardiac and non cardiac pharmaceuticals can have deleterious effect on the heart and patients can present with different symptoms such as arrythmias, contractility toxicity, ischaemic toxicity, secondary cardiotoxicity (eg induced hypertension) and valve toxicity [54]. Drug induced arrhythmias accounts for approximately half of the cardiotoxicities, with torsades de pointes (TdP), a potentially life-threatening polymorphic ventricular tachycardia as a common manifestation [54, 55].

13

| Worldwide withdrawal (121 compounds) | | US Withdrawal (95 compounds) | |
| --- | --- | --- | --- |
| Reason | Percent | Reason | Percent |
| Hepatotoxicity | 26 | Cardiovascular safety (proarrhythmia) | 19 (12) |
| Hematologic toxicity | 10 | Neuropsychiatric effects | 12 |
| Cardiovascular safety | 9 | Hepatotoxicity | 9 |
| Dermatologic effects | 6 | Bone marrow toxicity | 7 |
| Carcinogenicity | 6 | Allergic reactions | 6 |

**Figure 5: Leading reasons for drug withdrawal from the market** [46]

*1.3.3. Mechanistic understanding of drug induced cardiotoxicity*

The drug induced alterations are manifest at molecular level, electrophysiology and macro-mechanical function of the heart. Majority of these alterations are caused by interactions of these drugs with the various ion channels and adrenergic receptors found on the cell membrane [55-57]. The most commonly affected channel is the 'rapid' delayed rectifier current ($I_{Kr}$) also known as human-ether-a-go (hERG) channel. This channel conducts potassium ($K^+$) ions out of the muscle cells of the heart, and this current is critical in correctly timing the return to the resting state of the cell membrane during the cardiac action potential [58]. The drugs generally bind to these channels and block the passage of potassium ions through them. Certain drugs also inhibit the trafficking of these channels to the cell membrane [59]. Although the hERG is a major target, other drugs cause cardiotoxicity by affecting other ion channels in the heart, especially those channels involved in

the action potential generation of the heart [56]. Another major molecular player involved in drug induced cardiotoxicity is calcium. Recent evidence seems to suggest that calcium homeostasis is a unifying pathway for clinical manifestation of most drug induced cardiotoxicity as it is responsible for the excitation-contraction coupling of the heart, hence, attention should be paid to calcium transients, calcium ion channels, calcium receptors and calcium trafficking proteins [60]. The most common manifestation of these alterations *in vitro* are prolonged or reduced action potential duration, reduced calcium transients, downregulation or upregulation of receptors and ion channels and reduced trafficking of channels to the membrane. Other mechanisms include: ATP depletion, disruption of ER integrity, drug-induced apoptosis, oxidative stress, mitochondrial toxicity and more recently through alteration of cardiac cytochrome P450 (CYP) metabolism [61-63]. These alterations (Fig 6) ultimately lead to arrhythmias, cell death and various cardiomyopathies [64] and hence, to avoid these, *in vitro* platforms for study of cardiac physiology and pharmacology must be amenable to evaluating these parameters. In addition a good *in vitro* platform must have a network of functionally coupled cells while replicating tissue microenvironments with *in vivo* phenotype of the cells and can be scaled up for high throughput [64-66].
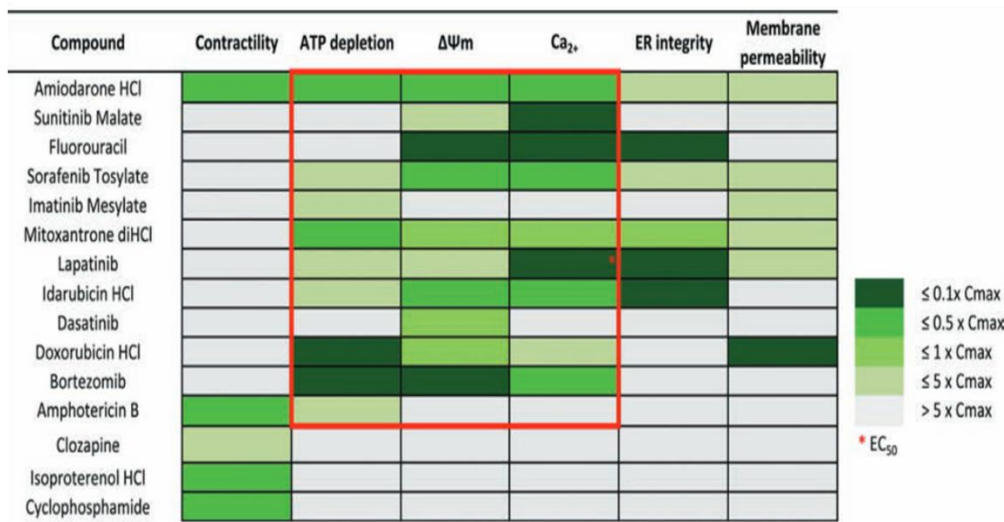
**Figure 6: Mechanisms that lead to the development of drug induced cardiotoxicity** [67].

*1.3.4. Importance of replication of tissue microenvironment in vitro*

The heart is a highly anisotropic organ which means that its properties are dependent on the direction. In the heart, the muscle fibers are arranged longitudinally and connect end to end via intercalated disks. They polarize their intracellular contractile apparatus and align with neighboring cells to facilitate the rapid spread of electrical activation and to increase the force of contraction [65]. The proper arrangement of all these structures guarantees proper functioning of the heart. Both the electrical sequence of depolarization and repolarization, and the mechanical sequence of contraction and relaxation depend on the architecture of the heart to be carried out without anomalies [68]. Alteration of cardiomyocyte shape, mass or interconnectivity has been shown to be related to a number of pathologies [69]. As can be seen in Fig 7, extensive deposition of extra cellular matrix (ECM) which leads to fibrosis and alteration in cardiomyocyte width and length are characteristic of cardiac dysfunction.
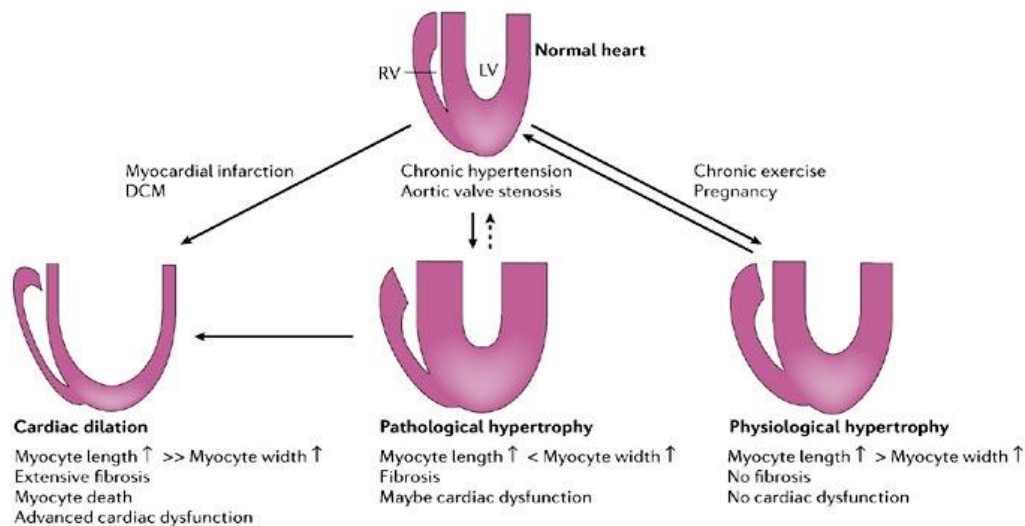
16

**Figure 7: Structure-Function relationship in the heart** [69]

The shape and alignment of the cardiomyocytes *in vivo* is a result of the ECM fiber arrangement in the heart. These collagen fibers with submicron dimensions are arranged to form a network of grooves and ridges and thus direct the morphology of cardiomyocytes [10]. In tissue engineering, directing the cells into the right phenotype and function also requires the microenvironment providing the same factors that govern cellular processes *in vivo* [70]. Replicating this microenvironment *in vitro* not only allows the study of individual cells and tissue constructs in a more accurate anatomical state, but also provides important cues for inducing proper phenotypic and physiologic responses [71]. *In vitro* experiments have shown that culturing cells on grooved substrates restores the cardiomyocyte morphology and alignment. This restoration in turn has been shown to increase force of contraction, speed of anisotropic action potential propagation, enhanced calcium homeostasis, electrical stability and more physiological response to

pro-arrhythmic drugs [10, 65, 71-73]. Recapitulating this native milieu is therefore necessary for a good *in vitro* platform for physiological and pharmacological study of the cardiomyocytes

## 1.4. Cell alignment in microfluidic chips as *in vitro* tools for biological applications

Microfluidic platforms hold great promise for the creation of advanced cell culture models as they enable us to control the local microenvironment [74-76]. Microfluidic systems enable temporal and spatial control of molecules and cells in the micrometer scale and thus can be used for various biological applications such as tissue engineering, drug discovery and bioassays [74-76]. The micro-scale of the cell culture means that fewer cells and reagents are used, thus reducing cost, and enabling high throughput applications. Most microfluidic chips are made from PDMS due to its numerous advantages over silicon and glass.

Poly dimethyl siloxane (PDMS) has been widely used in cell biology for microfluidic chips, microfabrication and for studying the effect of stiffness on cells [76-78]. PDMS is elastically deformable, non toxic, cheap and exhibits excellent optical properties. With respect to microfabrication and microfluidic chips, PDMS is the material of choice due to its deformability, permeability and ability to be molded to a resolution in nanometer scale [76, 77]. It can also be covalently bonded to glass by plasma treatment to form a sealed microfluidic device. In addition, by varying the ratio of the elastomer base and cross linker, PDMS with different elastic modulus can be obtained

18

and used to study the effect of stiffness on cells [76-78]. One major drawback of PDMS is that it can absorb small hydrophobic molecules like drugs and thus is not ideal for studying drug dose response [77]. Regardless of these limitations, PDMS is still widely used in cell biology especially in mechanobiology where the effects of the mechanical environment; such as topography and stiffness, on cells are studied [76, 77]. Depending on the application, the PDMS' physical and biochemical environment can be optimized to meet the need [76, 77]. One of such important features is cell alignment. Being able to incorporate grooved PDMS in microfluidic chips would be beneficial for cell types like skeletal and cardiac muscle, that way the various benefits of microfluidic technology can be harnessed for cell culture of the above mentioned cells [79].

### 1.4.1 Embedding micro and nanoscale cues in microfluidic chips

Despite the numerous benefits of cell alignment *in vitro*, there have been relatively few attempts to incorporate engineered features for aligning cells in microfluidic systems [79]. ECM patterning on glass substrates in microfluidic devices have been explored in the past [65, 80]. In this case, the alignment was produced by geometrically constraining cell attachment and spreading to only the desired area. While this technique has proved efficient in both static monolayer culture and microfluidic devices, they are limited to aligning a monolayer of cells but not 3D constructs [81]. In addition it is more challenging in microfluidic chips to ensure proper attachment and confinement of cells to the desired regions [79, 81]. Other methods such as electrical stimulation have been explored for aligning cells in chips. In one of such

studies, the researchers cultured rabbit ventricular cardiomyocytes in a microfluidic chip exposed to electrical stimulation to study the contraction of cardiomyocytes under stimulation [82]. In another study the researchers set out to engineer cardiac tissue-like structure via a combination of dielectrophoresis and electro-orientation inside a microfluidic chip (Fig 8) [83]. Their results showed that the cardiac cells aligned in the microfluidic chip due to the electrical field [83].
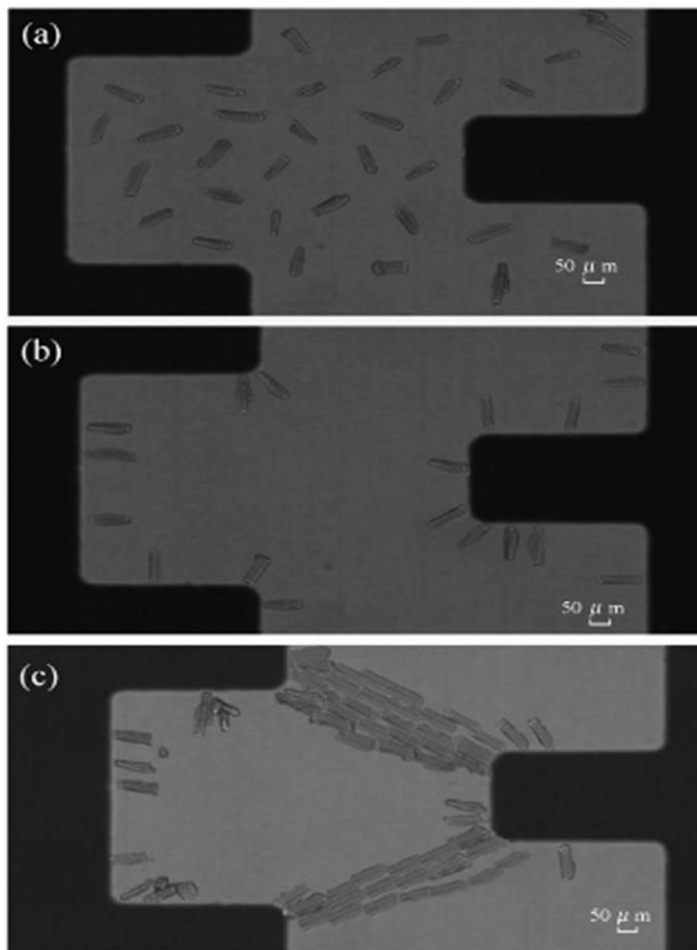


**Figure 8: Optical micrographs of cell orientation in the microfluidic device**. A) Cell randomly distributed when no voltage was applied; B) cells only accumulate to the edge for relatively low concentration ($2.1 \times 10^3$ cells/ml) and low amplitude of applied ac electric field (2 Vp-p); C) a tissue-like monolayer was formed between the interdigitated-castellated electrodes for $5.4 \times 10^4$ cells/ml of concentration and 4 Vp-p of applied electric field [83].

A number of other cell types such as neuronal cells have also been used to study the effect of electrical stimulation in microfluidic chips. Though this method is valid, it also requires specialized set-up and skill [84].

Microfluidic platforms embedded with microgrooves have also been used for cell alignment; however a major challenge of making topographical cues, such as micro-grooves, a routine feature of microfluidic platforms is the high cost of fabrication. Yang *et al.* proposed a stitching method to generate large surface areas of micro-grooved substrate (Fig 9). This consists of pre-fabricating micro-grooved substrates using photolithography or electron beam lithography and then stitching them together [79].
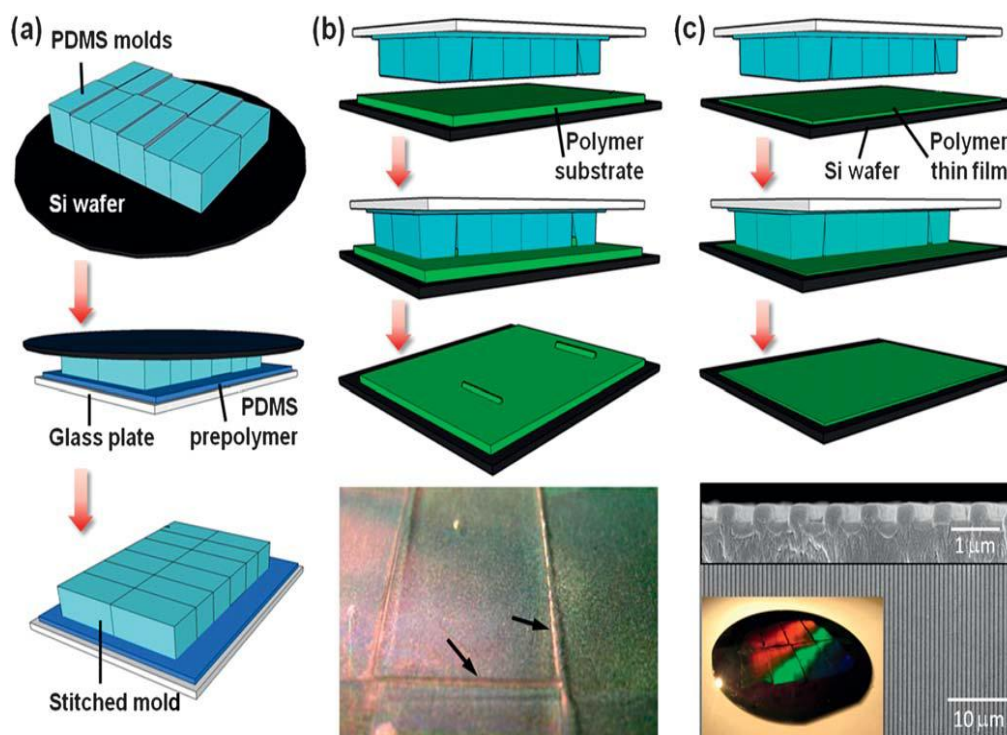


**Figure 9: Stitching technique**. A) Schematic illustration of stitching technique. B) When the stitched mold was embossed into a thick polymer substrate, the polymer was squeezed into interstices as indicated by the arrows

in the optical image. C) A large area of nanopattern on PS thin film spin-coated on a 75 mm wafer (the inset optical image). SEM images show both the top and cross-sectional views of final transferred PS nanogratings [79].

Other researchers created aligned and random patterns using [85] in polydimethysiloxane (PDMS) microfluidic chips. However, both methods require costly or specialized photolithography or electrospinning equipment.

Methods for creating aligned 3D constructs in microfluidic systems have not been demonstrated so far. Most of the cell alignment experiments in microfluidic chips have been done in 2D monolayer and hence protocols compatible with the implementation of microfluidic 3D cell culture should be explored [79, 80]. So far, generation of aligned 3D cellular constructs has been developed in static cultures using cell sheet, scaffolds or hydrogels [86-88]. Hence, the ability to create aligned 3D culture of cells from anisotropic tissues, which require polarity or alignment for proper functioning, will enable one to customize microfluidic cell models of these specific tissues and fully realize their potential in desired applications, such as drug screening.

## 1.5. Current methods used for creating cell alignment *in vitro* and the drawbacks

To engineer this cell alignment *in vitro*, (both for microfluidic chips and direct cell culture) the most commonly used techniques include: Mechanical stimulation (stretch or fluid shear stress), Electrical stimulation, Surface chemistry and micro/nanogrooved substrates [89] or patterning of ECM molecules with the desired shape on the substrate [90].

*1.5.1 Mechanical stimulation*

      *In vivo*, cells experience various mechanical cues which are important for the structures, compositions, and functions of living tissues [91]. The mechanical stimulations can induce physiological or pathological alterations in ECM, leading to an adaptive tissue organization. In vitro, the types of mechanical stimulations used include stretch, Flow shear stress.

1.5.1.1 Stretch

      Applying cyclic mechanical stretch to substrates or scaffolds seeded with cells is routinely used to align cells [92]. This method has been applied to a number of cells such as Mesenchymal stem cells (MSC), Cardiomyocytes, Fibroblasts, Smooth muscle cells (SMC) and Endothelial cells (EC). Cyclic mechanical stretch applied *in vitro* (typically, 0.5–2 Hz, 2–20% strain) is similar to the periodic mechanical loading seen in skeletal muscle, veins, arteries and tendons *in vivo*. Cells cultured on a 2D substrate that is subjected to uniaxial cyclic stretch tend to align perpendicular to the direction of principal cyclic strain (i.e., the direction of minimal substrate deformation) [1, 93-95]. For the cells in 3D scaffolds and hydrogels, stretch-induced cell orientation is more complex. For instance, uniaxial cyclic stretch can induce alignment at the gel surface but not within the gel [96, 97]. Yet in another study, more than 90% of SMCs seeded in fibronectin coated scaffolds made of poly(glycolide) and collagen (type I) were aligned after exposure to cyclic stretching (7% strain, 1 Hz) for 10 weeks [98]. The reason for this complexity could be that other factors such as the contact guidance of the ECM fibers in the scaffolds may also affect stretch-induced alignment.

Cyclic stretch is dependent on duration, magnitude and frequency. With respect to duration, cellular stress fibers have been observed to initiate alignment as early as 5 min after mechanical stretch [99]. In another experiment with SMC's, Crouchley et al showed that, SMCs generated stable cell alignment within 24 h when subjected to 10–24% strain [100], and this alignment of vascular SMCs can be maintained for up to 48 h after removing the stretch. Stretch magnitude also affects cell alignment. Cells have been shown to align more rapidly under higher stretch amplitudes [101]. However, the minimum strain necessary for inducing cell alignment varies from case to case. Given that the orientation tendency is to align in the direction of minimal substrate deformation, the alignment-force field of cyclic stretch is dependent on the mechanical properties of substrates (engineering cell alignment). Another factor that determines the efficiency of mechanical stretch is the stretch frequency. Higher frequencies (1-2Hz) tend to align cells in shorter time (<12 hrs) whereas lower frequencies (0.5 Hz) achieve the same with longer duration (>24 hrs) [102].

Although it is known that cell alignment generally begins with a process of cytoskeleton reorganization, the underlying mechanism for stretch-induced cell alignment remains elusive (engineering cell alignment). Stress fiber alignment is one of the earliest events in cell alignment often responding in as little as 5 mins with a resultant polymerization along the direction of the minimal substrate deformation. This rapid alignment response of stress fibers complete much faster than cell reorientation (more than 3 h) and focal adhesions changes. A number of cytoskeletal modifications have been observed during SMC reorientation in response to cyclic stretch. These

changes include attenuation of stress induced cell alignment with cytochalasin D, the formation of cellular pseudopods in the same direction as SMCs realignment, and a similar change tendency of F-actin/G-actin ratio [1]. All these cytoskeletal reorganization suggest a key role of mechanotransduction, which might initiate the down-stream effects of stretch-induced cell alignment and greatly determine further stable patterns in the long run. Some molecules such as integrin-ß1, p38mitogen-activated protein kinase (MAPK), nitric oxide etc. play important modulating role in stretch-induced SMC alignment [1]. In addition, cyclic stretch can lead to the secretion of autocrine and paracrine growth factors in vascular SMCs, including transforming growth factor-beta, vascular endothelial growth factor, platelet-derived growth factor, and fibroblast growth factor [1]. However, the relationship between these factors and the rapid cell alignment response is still not clear [1].

While mechanical stretch can lead to cell alignment, one of the major drawbacks of such method is that it can lead to pathological hypertrophy of the cells with an induction of the fetal gene program in cardiac cells. It also leads to cell apoptosis and arrhythmogenesis. Thus stretch-induced alignment may be more suitable for disease modeling [103].

1.5.1.2 Fluid shear stress

Physiological and pathological growth and remodeling of some tissues like the cardiovascular tissue are affected by mechanical stimuli, such as strain and fluid shear stress [104]. Vascular smooth muscle cells (SMCs), for example are contractile cells that participate in the regulation of wall tensile stress are arranged in various patterns. A straight blood vessel mainly contains circumferentially aligned SMCs, whereas a curved blood vessel, such as the

aortic arch, is composed of axially aligned SMCs in regions of convex curvature [105]. The vascular endothelium is another example. These cells play an important role by sensing the alterations in biological, chemical and physical properties of blood flow to maintain homoeostasis [103]. One of the physical properties of the blood flow is the laminar shear stress which exerts both cellular and molecular effects on endothelial structure and functions [103]. This shear stress-induced alignment is also present *in vitro*. A number of scientists have studied the effect of shear stress on the alignment of endothelial cells, cardiac cells and smooth muscle cells. One of the earliest experiments to report the effect of shear stress on alignment was done with SMC's. In their experiments, Ann Lee *et al* exposed SMC's to shear stresses ranging from 0 to 20 dynes/cm$^2$ and their results revealed that SMC's alignment is dependent on the magnitude of and exposure time to applied fluid shear stress [104]. Endothelial cells have also been shown to elongate and align with shear stress [103]. Shear stress induces reorientation of the microtubule-organizing centre to the leading edge of migrating cells and this leads to cytoskeletal alignment [103]. Other molecules such as integrins and c-Jun N terminal Kinases (JNK) have been implicated in cytoskeletal re-arrangement produced under shear stress in endothelial cells [106, 107]. Just like the mechanical stretch, this method may lead to upregulation of proteins which may not necessarily be useful for different cell types. These proteins include transcriptional regulators, enzymes, GPCRs (G-protein-coupled receptors), cytokines, cytoskeletal and matrix proteins etc. Shear stress therefore has profound effects on the molecular response and physiological function of the vascular endothelium [103].

## 1.5.2 ECM Patterning

ECM patterning is one of the most common ways to control cell morphology *in vitro*. The basic strategy to achieve cell patterning is to fabricate cytophilic and cytophobic patterns at the microscale [108]. Cells attach to the cytophilic regions and take the shape of the preadsorbed ECM proteins [109]. The microcontact printing can either be "positive patterning", where ECM molecules are stamped on hydrophobic surfaces or "negative patterning" which involves stamping of cell repellent molecules on cytophilic surfaces [108].
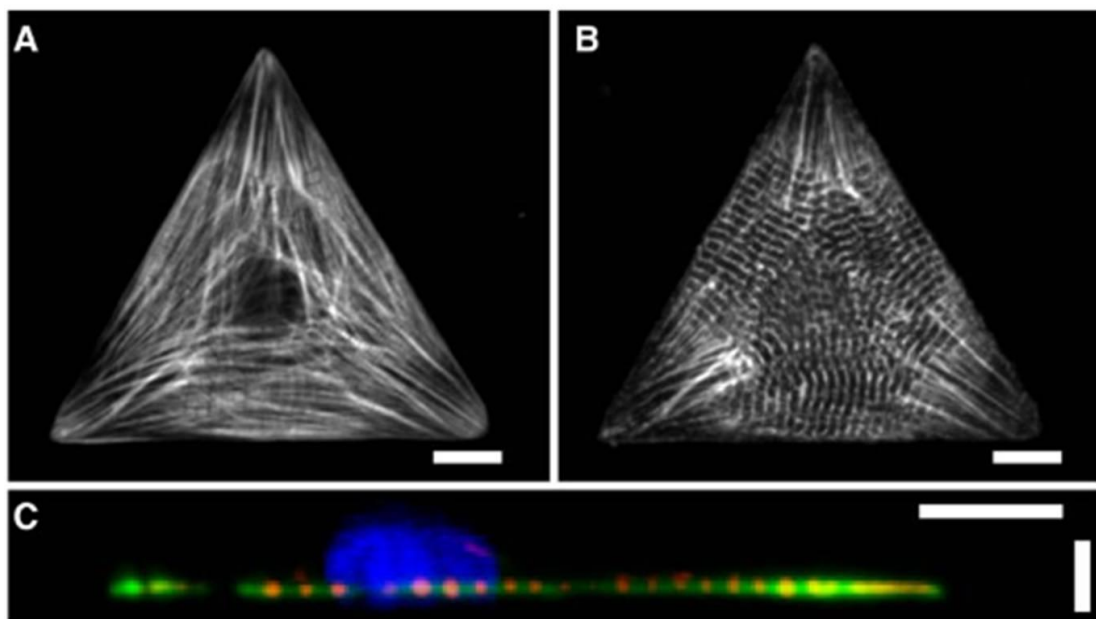


**Figure 10: Micropatterned myocytes on triangular ECM islands.** The image shows a triaxial alignment of myofibrils as revealed by fluorescence microscopy of actin (A) and sarcomeric α-actinin stains (B). XZ projections of the confocal stack show that these myocytes adopt a similar, pseudo 2D arrangement of the nucleus and myofibrils (C) [110].

This method has been used for many cells including cardiomyocytes, endothelial cells, stem cells etc and the cells can be made to take any desired shape (Fig 10) [110]. Although this can be used for cell alignment, this method faces a number of challenges. The chemical modification of the surface can be cumbersome [81], lack of homogeneity in the thickness of deposited ECM layer would affect the mechanical and chemical properties of the material [111] and it is difficult to precisely control cell-adhesive ligand density. This last problem is mainly due to the poor transfer efficiency and the deterioration of adsorbed protein over time [108]. Furthermore, it is challenging to achieve single-cell positioning on each pattern without cells adhering to the background. A lot of research lately has been directed towards enhancing attachment of cells to the pattern [108]. Despite the benefits of controlling cell shape through patterning, the effect of patterning over a long period of time is still not fully elucidated. Some studies have shown an increase in apoptosis [112]. In other studies the cells spread and extended beyond the boundaries of the patterned areas over time. In addition, only few studies have assessed gene expression and differentiation of cells on patterned substrates [108].

*1.5.3 Electrical Stimulation*

Cells within an electrical field change their morphology and in turn align perpendicular to the applied direct current [113, 114]. This method has been used in vitro for cell alignment with a variety of cell types such as fibroblasts, neuronal cells and cardiac cells. The cytoskeletal re-arrangement of cells in response to electrical stimulation is both dependent on electric field

28

and cell type. Just like stretch induced cell alignment, the electric field strength affects the speed and efficiency of cell alignment. In an experiment that compared the rate of alignment with field strength, the researchers found that with a field of 0.4V/mm, human skin fibroblasts aligned within 3 hours, in contrast, the cells aligned in about 24 hours with a field strength of 0.1 V/mm [115]  Different cell types also respond differently to electric stimulation. Cardiac and neuronal cells seem to respond easier and faster to electrical stimulation than other cell types. In an experiment, rat neural cells (PC-12) aligned and elongated perpendicular to a 7 V/cm field for 1 h, whereas MSCs did not show alignment when placed within the same field for the same time duration [116, 117]. Electrical stimulation changes the voltage gradients that neurons maintain across their membranes and this triggers neuronal responses such as migration and alignment [118]. For cardiac cells, electrical stimulation has been shown to lead to a synchronized contraction of cardiac muscle cells [119]. In addition, electrical stimulation leads to alignment, reduced excitation threshold, increased maximum capture rate, increased amplitude of contraction and a more mature phenotype in general [120]. Though an increasing number of studies have focused on inducing cell alignment with electrical field, the mechanism by which EF induces alignment remains unclear. In addition, electrical stimulation requires specialized equipment, making it difficult for routine use. Figure 11 shows an example of alignment with electrical stimulation and nanogrooves.

29
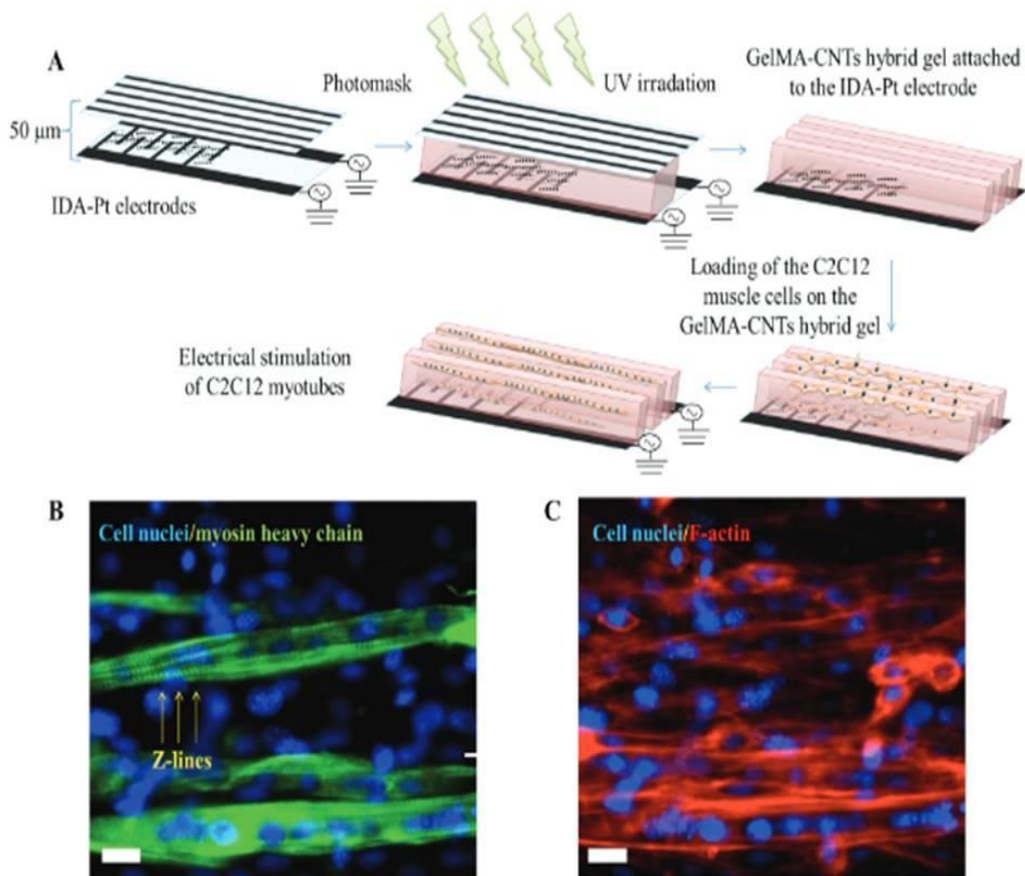
**Figure 11: C2C12 alignment within GelMA hydrogel with topography and electrical stimulation**. A) Schematic representation of the procedure to fabricate a grooved topography within the GelMA-CNT hybrid gel (0.3 mg/ml CNTs). B) Immunostaining of cell nuclei/myosin heavy chain. C) Cell nuclei/F-actin [121].

*1.5.4 Micro/Nanogrooves*

Micro/nanogrooved substrates constitute physical methods of regulating cell function without involving biomolecules [108]. Substrate topography provides a biomimetic cell-stimulating cue, because cells *in vivo* contact textured not smooth interfaces [108]. Basement membranes of various tissues are composed of complex mixtures of nanoscale (5–200 nm) pits, pores, protrusions, striations, particulates, and fibers [3], hence fabricating grooved substrates is a desired feature of cell culture [10]. With respect to the

30

use of micro/nano grooves, these substrates have been explored over the years for orienting/aligning cells in a particular direction for tissue engineering [89]. Cells align along the grooves by "contact guidance" which occurs when a cell assumes a corresponding orientation and moves along the line [122, 123]. It has also been shown that the focal adhesion complexes are formed within the grooves [124]. Many methods have been used to generate grooves (Fig 12); one of the earliest methods for making grooves for cell culture was done by D.M. Brunette [122].
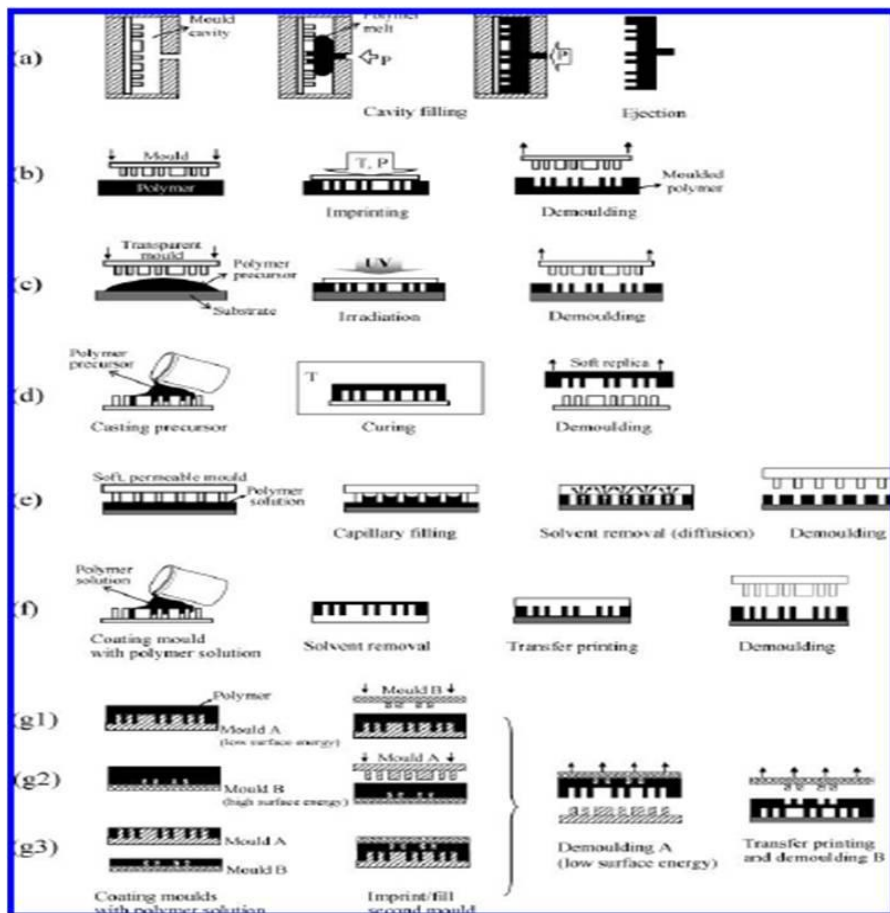


**Figure 12: Comparison of different molding processes.** A) Injection molding (NIL). B) Hot embossing or nanoimprint lithography. C) UV NIL. D) Soft lithography. E) Solvent-assisted molding. F) Reversal imprinting or transfer molding. G) Multilayer printing: "duo-mould" approach. The schematic g1, g2, and g3 represent three variants of this process [125]

In his experiments, the grooves were produced in silicon wafers by micromachining, a process which is based on the methods used to fabricate microelectronic components, and the grooved surfaces were then replicated in epon [122]. Another method used for creating grooves is by laser-irradiation. Studies have shown that grooves can be generated on different surfaces such as Polystyrene (PS) and PDMS using laser irradiation. When cells are cultured on these surfaces, they align along the direction of the grooves [126, 127]. Another method-UV embossing is a technique which offers many advantages such as rapid processing, low cost and good dimensional replication. It involves using polymers films coated with an UV-curable polyester resin, then imprinted with an embossing material containing the micro/nanopattern and subsequently photo polymerized [128, 129]. Nanoimprint lithography is a more recent development, it uses compression molding to create a thickness contrast pattern in a thin resist film coated on a substrate [43, 44, 130]. This is followed by anisotropic etching to transfer the pattern through the entire thickness of the resist. Electron-beam lithography another relatively new technology involves fabrication of grooves on electron beam mask plates which are further cut with a diamond saw [43, 44, 131].Though these methods can been used to achieve nanoscale resolution, they involve costly clean-room equipments, lengthy procedures and highly skilled labor and protocols. Table 2 shows the cost of equipment needed for photolithography.

**Table 2: Cost of ownership of photolithographic equipment [132]**

| Technology | Tool Cost | Fixed/Recurring cost | Throughput |
|---|---|---|---|
|  | $M | $/Hr | W/Hr |
| 193 Optical binary mask | 9.5 | 1432 | 35.8 |
| 157 Optical binary mask | 11 | 1597 | 36.3 |
| Extreme Ultraviolet Lithography (EUVL)- SEMATECH | 17.5 | 2006 | 34 |
| Electron-beam Projection Lithography (EPL)- SCALPEL | 8.9 | 1035 | 23 |
| Multi-Column and Multi-Beam electron beam lithography (MXM) Single module | 12 | 1333 | 30 |

The high cost of acquiring these machines makes it difficult for labs to explore the various applications of alignment *in vitro*. Cheaper alternative methods of producing micro-grooved substrates have been developed, such as micropatterned surfaces ground with abrasives [24] or using metal wrinkles [71]. The metallic wrinkle (Fig 13) is a tunable, rapid, robust, and inexpensive non photolithographic fabrication method to create cell culture substrates with

controllable nano- and microscale cues [71]. The grooves were created by leveraging the mismatch in stiffness between a prestressed polymer sheet and an overlying thin metal film [71]. When the plastic sheet retracts upon heating, the stiffer metal film buckles in a controllable manner causing wrinkles. The authors were able to achieve controllable heterogeneous wrinkle length-scales based on varying thickness of metal coating on prestressed polystyrene (PS) sheets [71]. Coating thicknesses ranged from 15 to 90 nm, with all thicknesses generating wrinkles ranging from 20 nm to 10μm and average wrinkles thicknesses ranging from 800 nm to 1μm and increasing proportionally with coating thickness [71]. The abrasives grinding also presents an easy, simple, and low-cost method for aligning cells, utilizing surfaces with micro-scale features fabricated by grinding with abrasives [24]. Rectangular iron blocks of which the surface had been finished with a surface grinder were ground with abrasives at a pressure of approximately 0.4 kg/cm$^2$ along a straight rail to fabricate linear patterns [24]. Different kinds of abrasives such as sand papers were used to control the sizes of the microscale features. The iron blocks were then used as molds for PDMS [24].
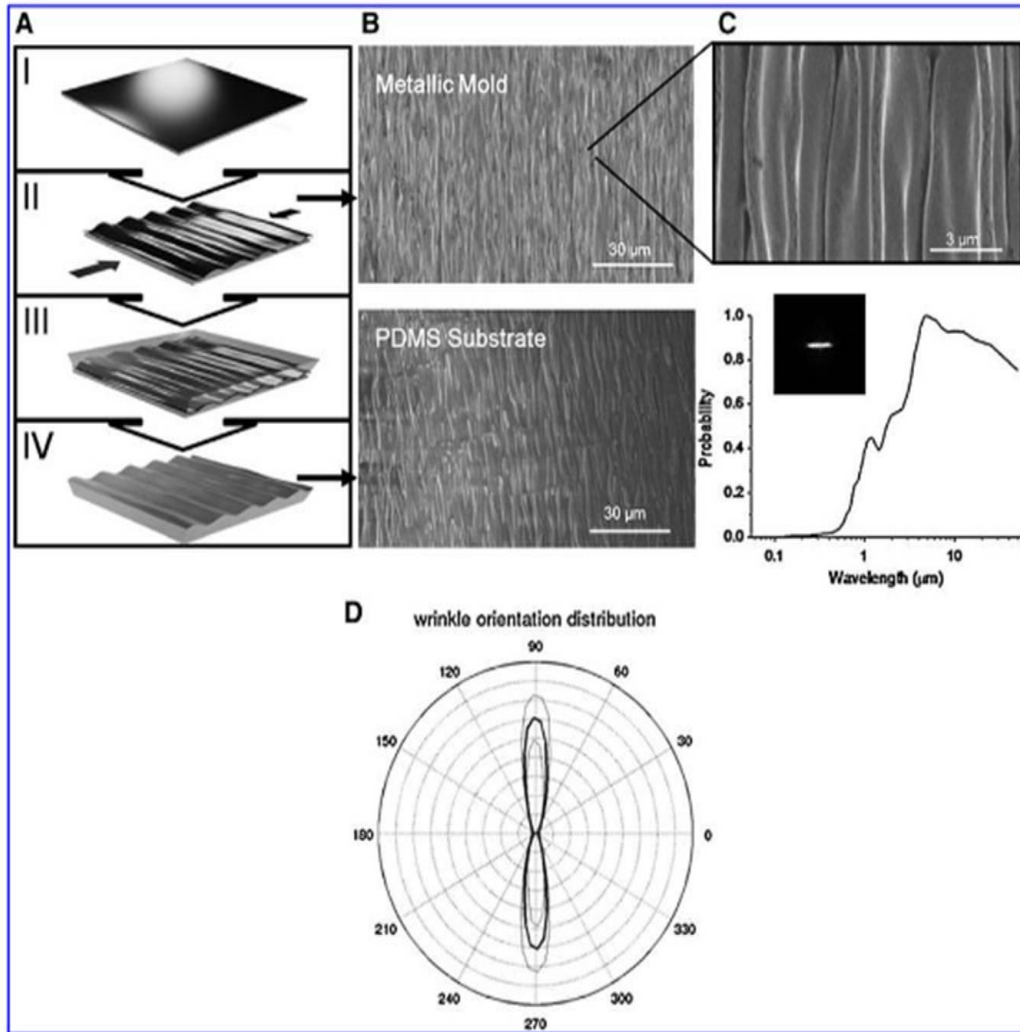
**Figure 13: Fabrication and characterization of multiscale wrinkle substrate.** A) (I) Metallic layer is deposited on PS prestressed sheet. (II) PS is induced to thermally shrink while constrained from opposite sides to generate aligned anisotropic wrinkles. (III) The metal wrinkles are used as a soft lithography mold to generate a PDMS substrate (IV), which is used to culture CMs. B) Scanning electron micrographs (SEMs) of metal wrinkles (with high-resolution inset) and PDMS substrate. C) The length scale distribution from Fast Fourier transform of SEM images. Inset shows high degree of anisotropy, as quantified by D) computing a histogram of gradient orientations (thick lines) and standard deviation (thin lines) [71].

Although these techniques are inexpensive, they still require some level of skill, and are not scalable for high throughput or large scale culture. In addition, the dimensions on the grooves are usually not uniform [81]. In order

to make cell alignment a routine feature of cell culture, commercially available optical media are explored as cost effective, scalable platforms with micro/nano grooves for cell culture.

## 1.6 Commercially available optical media

Commercially available optical media are optical devices with periodic structure, which is able to split and diffract light into several beams travelling in various directions (Fig 14). The directions of those beams will depend on the spacing of the grating and the wavelength of the light so that the grating acts as a dispersive element. Diffraction is observed when the phase of a wave front of light is changed by a partial obstruction such as a slit; this changes the direction of the light. Those gratings are usually employed in spectrometers, holograms, optical storage mediums and monochromators. Diffraction gratings can be generated mechanically or holographically [133].

### 1.6.1 Mechanically Ruled Gratings

The first method and the preferred method for producing diffraction gratings was to use a diamond cutting tool to make grooves up to 30,000/inch (12,000/cm) [133]. To obtain a master grating using this method, the metal-coated grating blank is mounted on a carriage and a diamond cutting tool is mounted above the carriage. The cutter repeatedly moves across the blank cutting grooves. The master grating produced by this method is not commonly used in spectroscopy; instead it is kept as a mold and used to make replicas [133].

*1.6.2 Holographically Ruled Gratings*

This is a newer method for producing gratings; the major difference is that the blank is coated with a photoresist instead of a metal [133]. A laser beam generates an interference pattern which consists of alternate lines of light and dark, and the coated blank is exposed to it. This ensures that the photoresist is exposed to different intensities of light at different points on its surface. After developing, the photoresist is washed away in proportion to the extent of this exposure, forming grooves. The grooves formed by this method usually have a sinusoidal shape in cross-section [133].

*1.6.3 Replication of the gratings*

To make this process cost effective, both holographically and mechanically ruled gratings can be replicated. This process involves covering the ruled surface by a thin film of epoxy [133]. Another blank is fitted on top of the epoxy layer and allowed to cure. After curing, the two blanks are pulled off. Both mechanically ruled and holographically ruled gratings can be replicated using this method [133].

The most common examples of these optical media are CD and DVD. Both are made from polycarbonate and the patterns are drilled in the form of a single spiral track [134]. The DVD has two joined layers of polycarbonate surface which could be dislodged by applying force between them. The periodicity of the CD is about 1500 nm while the DVD-R is 800 nm [134]. Diffraction gratings can also be purchased from optic companies. They consist of large numbers of equally spaced parallel slits ranging from a few hundreds to thousands per centimeter. They can be made from different materials such

as polyethylene terephthalate or glass [135]. A number of studies have explored using these optical media to generate submicron-scale color patterns, print ECM tracks or imprint other polymers such as PDMS, collagen membranes and silk films [134-137].
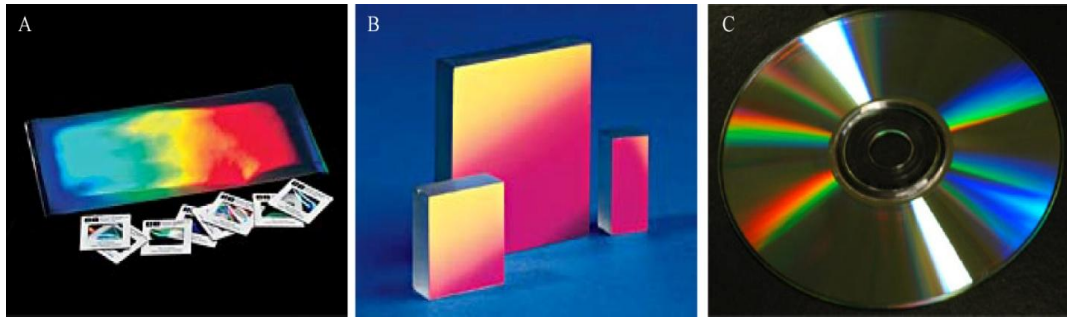


**Figure 14: Examples of Optical media**. A) Holographic diffraction grating film. B) Reflective ruled diffraction grating. C) Optical storage medium. Adapted from www.edmundoptics.com

## 1.7 Use of optical media in biological research

A few studies have explored the use of commercially available optical media as templates for forming microgrooves on different materials such as collagen membranes, Silk films and PDMS [135, 137]. In one of these experiments, micro-grooved collagen membranes fabricated using optical gratings were used to culture human dermal fibroblasts (HDFs) and human umbilical artery smooth muscle cells (HUASMCs) [135]. Collagen hydrogels were air-dried onto microgrooved templates and removed after they had formed films/membranes [135]. The templates were made from commercially available grooved materials—vinyl phonograph records (PRs), plane-ruled diffraction gratings (PRDGs) (Fig 15). The grooved CMs were highly effective at inducing HDFs and HUASMCs to elongate and align [135].
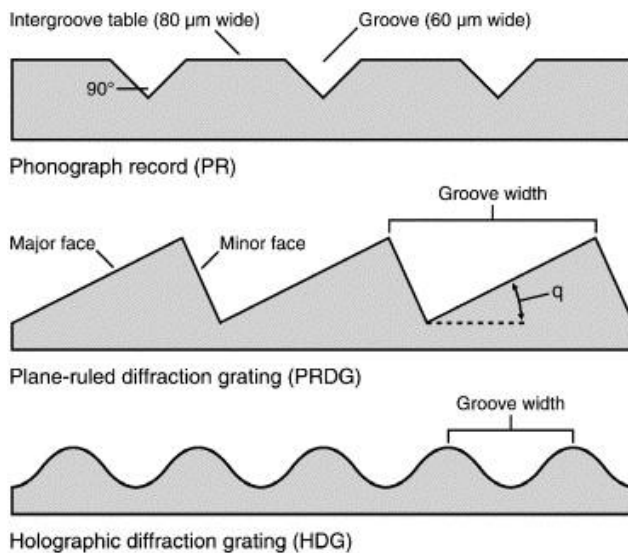
**Figure 15: Illustration of profiles of grooved templates viewed at right angles to the long axes of the grooves**. Dimensions of the profiles are not in scale [135].

In a similar study, reflective diffraction gratings were used to form grooves in PDMS and this in turn was used as a mold for obtaining micro-grooved silk films [137]. Human corneal fibroblasts cultured on the silk films responded by aligning along the direction of the grooves [137]. Though these commercially available optical media have been used for patterning other polymers, to the best of our knowledge, there has been no report of direct cell culture on these optical media. In addition, their use has not been explored for microfluidic or other high throughput applications. In this study we exploit the various advantages of commercially optical media for biological applications. Some of the benefits are highlighted below:

- A standard size CD-R or optical grating costing between 1-5 USD can produce enough micro-grooved cell culture inserts for seven 24-well plates.

39

- The materials of the optical media, polycarbonate (CD-Rs and DVD-Rs) and polyester (optical gratings), have been shown to support cell culture [138, 139].

- The dimensions fall within the published range for producing cell alignment *in vitro* [43].

- They do not require costly clean room equipments or lengthy protocols.

- They are transparent making biological imaging feasible on the substrates.

- There has been no report on direct culturing and alignment of cells on these optical media or its use for large surface area PDMS for microfluidic chips.

In this study, we demonstrate that the optical media can directly support cell attachment, growth, alignment and differentiation. We also show its use as molds for patterning PDMS used for both 2D and 3D microfluidic cell culture. Finally we show that these commercially available optical media can serve as platforms for cardiotoxicity drug screening, as they are not only scalable for large scale and high throughput studies, but also amenable to the various tests required in drug screening. Commercially available optical media can therefore be exploited as a scalable and cost-effective source of micro-grooved cell culture substrates. This will allow researchers to incorporate cell alignment for routine culture of cardiac, skeletal or neuronal cells to support cell and tissue research and drug testing applications.

## CHAPTER 2: OBJECTIVE AND SPECIFIC AIMS

The thesis aims to propose a cost effective and scalable platform for the various applications requiring cell alignment *in vitro*. As highlighted previously, cells respond to their physical environment and by engineering a more physiological microenvironment, differentiation and maturation of certain cell types can be enhanced *in vitro*. An important feature which has been shown to be beneficial for a number of cell types is grooves in the underlying substrate, though this has been proven important for many cell types, making it a routine feature for cell culture has not yet been achieved. This is mainly due to the cost of fabrication and the specialized equipment and skill needed. To address this problem, we show that commercially available optical media can serve as platforms for direct culture of cells. We show that it can be customized to be used for differentiation, maturation, mechanobiology studies and as a platform for drug screening. In addition, we explore its use as a mold for patterning large surface area of PDMS which can be incorporates into microfludic chips.

## MAIN HYPOTHESIS

Nano/Microgrooved substrates from commercially available optical media serve as molds for large scale patterning of PDMS used in microfluidic chip and also provide a biomimetic *in vitro* platform for differentiation, maturation and pharmacological studies involving skeletal, cardiac and neuronal cells

## 2.1 Specific Aim 1: Harnessing nanogrooved commercially available optical media as platforms for aligning cardiac, skeletal and neuronal cells in culture

### 2.1.1 Objective:

This section investigates the feasibility of using nanogrooved commercially available optical media as substrates to act as topographical cues for aligning cells in culture. It also investigates effects of alignment on proliferation and maturation of various cells. This would provide a cost effective and readily available substrate for tissue engineering application

### 2.1.2 Experimental design

1) Optimize preparation of commercially available optical media as substrates for cell culture

2) Characterize optical media's surface using AFM, SEM

3) Make surface amenable for cell culture by various treatment methods: Plasma treatment, ECM coating, chemical conjugation of ligand

4) Cell culture of H9C2, PC12, C2C12 and Primary rat hepatocytes

5) Analysis of proliferation, alignment, immunostaining and gene expression of cultured cells

## 2.2 Specific Aim 2: Engineering scalable 2D and 3D cellular constructs of aligned skeletal myoblasts in PDMS microfluidic chips embedded with nanogrooves

*2.2.1 Objective:*

Extending from specific aim 1, this section explores the usefulness of the commercially available gratings as molds for replica molding of large surface areas of PDMS. The nanogrooved PDMS are subsequently used in microfluidic chips to generate 2D and 3D cellular constructs of aligned skeletal myoblasts. This provides a scalable method for engineering microfluidic chips with embedded nano/microscale cues

*2.2.2 Experimental design*

1) Generation of large surface area of micro-grooved PDMS using optical media as mold

2) Physical characterization of PDMS using SEM and AFM

3) 2Dand 3D microfluidic chip setup

4) Cell culture using C2C12 myoblasts for both 2D and 3D

5) Analysis of myoblast and myotubes alignment in microfluidic chip

## 2.3 Specific Aim 3: Developing a high throughput *in vitro* platform for physiological and pharmacological study of neonatal rat cardiomyocytes

*2.3.1 Objective:*

This section explores the utility of the biomimetic platform to restore cardiomyocyte morphology, enhance their function and increase their potential for drug screening applications

*2.3.2 Experimental design:*

1) Isolation and culture of neonatal rat cardiomyocytes

2) Morphological and molecular characterization of rat cardiomyocytes

3) Electrophysiological characterization of rat cardiomyocytes

4) Drug testing using paradigm drugs

# CHAPTER 3: HARNESSING NANOGROOVED COMMERCIALLY AVAILABLE OPTICAL MEDIA AS PLATFORMS FOR ALIGNING CARDIAC, SKELETAL AND NEURONAL CELLS IN CULTURE

This chapter discusses the feasibility of using nanogrooved commercially available optical media as substrates to act as topographical cues for aligning cells in culture. It explains the steps taken to make the commercially optical media amenable for cell culture, and the various surface modification techniques for different cell types. It also investigates effects of alignment on proliferation, differentiation and maturation of various cells.

## 3.1. Introduction

Cells in many organs are presented with different topographical features by the respective extracellular matrix (ECM) in their basement membrane [140]. The basement membrane consists of ECM components such as glycosaminoglycans, fibrous proteins like fibronectin and collagen, growth factors and cytokines anchored on ECM fibers, hyaluronic acid, laminin etc. displaying unique features of pores, fibers and ridges in the scale of nanometers [113]. The arrangement of these ECM molecules presents morphological and differentiation cues to the cells lying on them. A good example is the heart *in vivo* which is a highly anisotropic organ, and the cardiomyocytes in the heart are aligned because of the parallel arrangement of the collagen fibers [10].

Just as these topographical cues regulate biological processes *in vivo*, presenting cells with topographical features *in vitro* can also affect cellular

morphology and differentiation capabilities [110]. Cell alignment *in vitro* can be achieved either through micropatterning ECM molecules into line geometries [110] or by creating grooves and ridges on the substrates [10]. Published reports have shown that grooves and ridges with dimensions ranging from 35 nm to 25 µm in width and 14 nm to 5 µm in depth can induce cell alignment [43, 131]. This cell alignment has been used for various applications such as engineering muscle tissues [89], stem cell differentiation [2], mechanobiology studies [124], cell proliferation [3, 44], and ECM production [141]. In an interesting study, researchers have shown that topographical cues from micro-grooved substrates alone were sufficient to direct the switch of stem cells towards a particular cell fate such as neuronal or myogenic pathways without the aid of specific induction growth factors [4, 18]. Other cell types such as cardiomyocytes and skeletal myocytes exhibit a more mature functional phenotype when they are aligned in culture [19, 120, 142]. Replicating this aligned cellular structure *in vitro* can therefore be used for applications such as models to study differentiation, for functional electrophysiological studies of the cardiac muscle [143], and as *in vitro* ensembles for pharmacological studies and drug screening platforms [65].

Current technologies used to fabricate micro/nanogrooved substrates for cell culture include: photolithography, electron beam lithography, nanoimprint lithography, electrospinning and UV embossing [43, 132]. Besides the high cost of fabrication, these techniques involve lengthy procedures, specialized clean room facilities, highly skilled labor and are technically challenging to scale up to large surface areas [79]. Hence, despite

the various advantages of aligning cells in culture, the challenges greatly limit the translation of interesting findings relating cell alignment to cell function into practical and routine cell culture applications.

Here, we propose that commercially available optical media such as CD-R, DVD-R, and optical gratings, present a readily available source of nano/micro-grooved substrates that fulfills the needs of aligning cells in a cost-effective manner. A standard size CD-R or optical grating costing between 1-5 USD can produce enough micro-grooved cell culture inserts for seven 24-well plates. The materials of the optical media, polycarbonate (CD-Rs and DVD-Rs) and polyester (optical gratings), have been shown to support cell culture [138, 139], and the dimensions fall within the published range for producing cell alignment *in vitro* [43]. Although some forms of the optical media have previously been used to pattern other polymers for cell culture [135, 137], there has been no report on direct culturing and alignment of cells on these optical media. Therefore we demonstrate here that the optical media can directly support cell attachment, growth, alignment and differentiation. Commercially available optical media can therefore be exploited as a scalable and cost-effective source of micro-grooved cell culture substrates. This will allow researchers to incorporate cell alignment for routine culture of cardiac, skeletal or neuronal cells to support cell and tissue research and drug testing applications.

## 3.2. Materials and methods

### 3.2.1. Cell lines

All the cell lines used were below passage 20. They include H9C2, C2C12 and PC12 cells from ATCC.

### 3.2.2. Processing of CD-R/DVD-R/ and optical gratings for cell culture

Three examples of commercially available optical media include CD-R (Imation, Singapore), DVD-R (Verbatim, Singapore) and optical grating (Edmund optics, Singapore). For the CD-Rs, the label, acrylic and the aluminum layers on top were peeled off with an adhesive tape to expose the polycarbonate layer. For the DVD-R, we peel off the top cover layer to expose the grooved polycarbonate layer in the middle for further processing and cell culture. The exposed polycarbonate surfaces of CD-Rs/DVD-Rs were cut into pieces (1 cm X 1 cm), so that they can fit in 24-well plates. For the optical gratings, 13mm diameter pieces were punched out using a metal punch (Helmold, Ilinois USA). CD-R/DVD-R and optical grating pieces were then treated with absolute methanol for 1 hour, sonicated for 30 min and then rinsed with DI water to remove any dust particles and chemicals, especially the organic dyes in case of optical discs. The optical media pieces were sterilized by treating with 70% ethanol for 1 hour, and rinsed with sterile DI water or autoclaved at 105 ºC for 21 mins. The optical media pieces were then placed in a well plate to complete "Gratings in a dish" device. The substrates will be made available through Bio-Byblos (Taiwan, ROC) as Vivoalign™.

### 3.2.3. Surface characterization by Atomic Force Microscopy (AFM) and Scanning Electron Microscopy (SEM)

SEM/AFM samples were prepared by cutting appropriate sizes of the optical media. For SEM, the samples were viewed with a JSM 5600 scanning electron microscope (Jeol, Japan) at 5 kV. Prior to imaging, the gratings were sputter-coated with platinum for 60s. For CD-R samples with 0.1% gelatin, the protein was fixed by glutaraldehyde and serially dehydrated with ethanol before SEM was done. Atomic force microscope, DI Nanoscope Dimension 3100 (Digital Instruments, USA) was used in tapping mode to identify the groove features on the optical media.

### 3.2.4. Nano indentation to determine Young's modulus

The mechanical test for the gratings was performed with a nano-indentation system [45] at ambient temperature. Superglue was used to attach specimen to the stage. A Berkovich diamond indenter with depth-control method was used during the nano-indentation test. The maximum depth was fixed at 1 μm for indentation tests across all the samples. Both loading and unloading rate were 0.1 mN/sec and the dwelling time at the maximum load was 60 seconds. Each indent was of size 100 μm.

### 3.2.5. Plasma treatment to render the surface hydrophilic

The CD-R/DVD-R and optical grating cell culture inserts were plasma treated for 3 minutes using the plasma machine (FEMTO, CUTE-B, South Korea) and then soaked in ethanol for 30 min. After the ethanol treatment, they were rinsed three times with PBS before coating with ECM for experiments with PC12 cell lines.

### 3.2.6. Water contact angle measurement of the surface

Five microliter of DI water was pipetted on the gratings surface in a random orientation. Water contact angles were measured with a goniometer (Contact Angle System OCA 30, Data Physics Instruments GmbH, Germany) using the SCA20 software.

### 3.2.7. ECM coating of CD-R/DVD-R and optical gratings

After plasma treatment, 10 µg/ml of laminin (354232, BD biosciences, Singapore) was used to coat the gratings for 1 hour in the case of PC12 cells. A solution of Fibronectin (F1141, Sigma-Aldrich, Singapore) and Gelatin (G1890, Sigma, Singapore) was used for HL-1 cells while the other cell types (H9C2, 3T3 and C2C12) did not need ECM coating.

### 3.2.8. Conjugation of RGD on PET film

The conjugation of RGD on PET film was undertaken as previously reported [144]. Briefly, after argon plasma treatment and UV induced deposition of poly-acrylic acid, PET film (12 mm in diameter) was placed into a 24-well plate for conjugation of RGD using 1-ethyl-3-(3-dimethylaminopropyl) carbodiimide (EDC) and N-Hydroxysuccinimide (NHS) cross linking. 0.2 mg RGD in 100 ml phosphate buffer (0.1 м, pH 7.4) was added into each well, respectively. The conjugated film was sterilized by soaking in 70% ethanol for 3 h and then rinsed 3 times with phosphate buffered saline (PBS, pH 7.4).

### 3.2.9 Rat hepatocyte isolation and culture

Primary hepatocytes were harvested from male Wistar rats weighing 250–300 g by a two-step *in situ* collagenase perfusion method [144]. 200–300

million cells were isolated from each rat with viability >90% as determined by the Trypan Blue exclusion assay. Freshly isolated rat hepatocytes (0.18 million cells per well) in 500 μl William's E culture media were seeded on the PET films conjugated with RGD in 24-well plates. Hepatocytes were cultured in William's E media, supplemented with 1 mg/ml bovine serum albumin (BSA), 10 ng/ml of epidermal growth factor (EGF), 0.5 mg/ml of insulin, 5 nM of dexamethasone, 50 ng/ml of linoleic acid, 100 U/ml of penicillin and 100 μg/ml of streptomycin. Culture medium was changed daily.

### 3.2.10. Picogreen assay

H9C2 cells were seeded at a density of 13,000 cells/cm$^2$ and allowed to attach for 1 hour on the tissue culture plastic (TCP) and both the grooved and flat surfaces of the optical media used. After 1 hour, unattached cells were washed off with PBS; the optical media pieces were taken to new wells and cells were lysed with 0.1% SDS, 500 microliters per well. The assay was performed with the Quanti-iT™ PicoGreen® dsDNA kit (P11495, Invitrogen, USA). A standard curve was established with known cell number of H9C2 cells.

### 3.2.11. Alamar Blue assay

H9C2 cell growth over 5 days was monitored using the alamarBlue® Cell Viability Assay Protocol (DAL1100, Invitrogen, Singapore). Cells were incubated with 10% alamarBlue® in culture media (vol/vol) for 2 hours on days 1, 3 and 5 and the fluorescence was measured with the Infinite M1000 plate reader (Tecan, Switzerland) with absorption wavelength at 560 nm and emission wavelength at 590 nm. Fluorescence intensity values for days 3 and

5 were normalized to the fluorescence intensity for day 1 as an indication of the relative cell number compared to the number of attached cell on day 1.

### 3.2.12. RNA isolation, cDNA synthesis and qPCR analysis

Cells were lysed using RLT buffer from Qiagen. Cell lysate was collected and RNA isolation was done and total RNA was reverse transcribed to cDNA according to manufacturer's protocol. Custom designed primers for cardiomyocytes (Supplementary table 1) and already published primers for C2C12 cells [19] were used for the quantitative PCR and the reactions were performed using both Roche lightcycler and Bio-Rad real time system. Analysis of each gene was performed using the relatively quantitative $\Delta\Delta CT$ method. Transcript levels were first normalized to the housekeeping gene GAPDH and expressed as relative level to that on the flat surface.

### 3.2.13. Differentiation of H9C2 cells

The H9C2 is a cell line derived from embryonic rat heart tissue and is widely used to study the rat physiology and cardiotoxicity. The cell line can differentiate into both skeletal and cardiac muscle. Upon addition of all-trans retinoic acid and reduction of serum content, the H9C2 cell differentiates into cardiac lineage [145]. The H9C2 cells were seeded at a density of 13,000 cells per $cm^2$ containing 1 cm x 1 cm square pieces of CD-R and DVD-R. After the cells attained confluence about 2 days after seeding, the cells were treated with 1 μM of all-trans retinoic acid (R2625, Sigma Singapore) daily for 5 days. At the end of the 5 days, the RNA isolation and gene expression was carried out and cells fixed for immunostaining.

### 3.2.14. Differentiation of C2C12 cells

The skeletal myoblast cell line C2C12 cells were seeded at a density of 25,000 cells per $cm^2$, in the 24-well plates containing 1 cm x 1 cm square pieces of CD and DVD, and grown in the proliferation medium that consists of DMEM (Gibco®, 31600, Invitrogen, Singapore) low glucose with 10% fetal bovine serum (FBS) (Gibco® 16000, Invitrogen, Singapore). After 2 days, (90-100% confluence) the medium was switched to differentiation medium which contains 1% FBS and 1% insulin-transferrin-sodium selenite (Gibco®, 41400, Invitrogen, Singapore) [19], and was changed daily for another 3 consecutive days. At the end of the 3 days, the cells were fixed for myosin heavy chain (MHC) and F-actin. In addition to immunostaining, RT-PCR of skeletal muscle specific genes was carried out. Fusion index was calculated as the fraction of total nuclei present inside myotubes (nuclei ≥ 2).

### 3.2.15. Differentiation of PC12 cells

The PC12 cell line is derived from a pheochromocytoma of a rat adrenal medulla. Upon addition of nerve growth factor, they differentiate into neuronal like cells. The PC 12 cells were seeded at a density of 7,500 cells per $cm^2$ in 24-well plates containing 1 cm x 1 cm square pieces of CD and DVD and cultured in DMEM high glucose with 10% Horse serum (HS) and 5% FBS. After 24 hours, the medium was switched to DMEM high glucose with 1% HS and 0.5% FBS with 50 ng/ml of Nerve growth factor (NGF) (480352, Calbiochem®, Merck Millipore, Singapore). The cells were fixed for immunostaining after 48 hours of culture.

### 3.2.16. Immunofluorescent assessment of differentiation markers and F-Actin

Cells were fixed with 3.7% PFA for 10 minutes at 37ºC, permeabilized with 0.1% Triton-X 100/PBS for 30 minutes at room temperature and blocked with 2% bovine serum albumin for 2 hours at room temperature. Washing after each step was performed with 0.1% Triton-X 100/PBS three times at 10 minutes each.

All incubations with primary antibodies were performed overnight at 4ºC. Working primary antibody concentrations were as follows: 1:200 for mouse anti alpha sarcomeric actinin (A7811, Sigma, Singapore), 1:200 for mouse anti myosin heavy chain (clone MY32, M4276, Sigma, Singapore). After primary incubation, samples were washed three times as explained above and incubated with secondary antibodies for 1 hour at room temperature. The dilution used for secondary antibody was 1:250 Alexa Fluor® 546 Donkey anti mouse IgG (H+L) (A100436, Invitrogen, Singapore). Alexa fluor phalloidin 488 (A12379, Invitrogen, Singapore) was added during the secondary antibody incubation for F-actin visualization. The samples were washed three times and counter stained with DAPI (D9542, Sigma, Singapore) at 1 µg/ml for 10 minutes at room temp. After washing, the samples were mounted (DAKO fluorescence mounting medium, Agilent technologies, Singapore) and imaged with a confocal microscope (Olympus FV1000).

### 3.2.17. Quantification of nucleus and cell orientation

Two-dimensional Fast Fourier Transform (2D FFT) turns spatial information of images into frequency domain and is used to analyze anisotropy in cells, ECM fibers, tissues and biomaterials [146, 147]. To

analyze the anisotropy, the long to short axis of the ellipse generated by the 2D FFT was used as an index [148]. In addition, the nuclei alignment angle which is the orientation of the major elliptic axis of the nucleus with respect to the horizontal axis was measured using ImageJ software and used to evaluate overall cell alignment [86]. For this analysis, the nuclei alignment angles were normalized to the mean nuclei angle for each sample and the percentage of nuclei within 20º of the mean was calculated [86].

### 3.2.18. Quantification of cell area

An ImageJ plug-in was used to analyze projected cell dimensions. For this analysis, H9C2 cells were sparsely seeded at very low density 3-5,000 cells per $cm^2$ and cultured for 2 days. Afterwards, cells were fixed and stained for nucleus (DAPI) and F-actin (Phalloidin) as described above. These images were obtained using a confocal microscope and analyzed using ImageJ software. Plug-ins to analyze cell area, long axis and short axis were used to obtain data from four different sets.

### 3.2.19. Statistical analysis

Statistical differences were performed using GraphPad prism 5 (GraphPad Software Inc. California, USA). For cell attachment and cell growth studies, analysis was performed using one way analysis of variance followed by bonferroni's multiple comparison tests. For the long to short axis index, a column statistics was performed, comparing the values to a hypothetical value of 1. For the gene expression studies, paired t-test studies were performed comparing flat and grooved for each gene. $p < 0.05$ was considered significant.

## 3.3. Results and discussion

### 3.3.1. Preparation and characterization of the optical media

Since the intended applications of commercially available optical media are for data storage and spectroscopy, it is important to process them to be cell culture compatible. Briefly, the optical media need to be stripped of any metal coatings and organic dyes to expose the micro-groove polymeric substrate (Fig 16). It is important to note that the CD-R and DVD-R used in this study are different from the conventional CDs (compact discs) or DVDs (digital versatile discs) that come with stored data, where the surface topography is completely different from the CD-Rs/DVD-Rs. The CDs/DVDs are molded from a master, which transfers the digital data in the form of pits and lands on the polycarbonate surface. While in case of CD-Rs/DVD-Rs, the spiral pre-groove (named so because it's molded before any data are written on the disc) is molded from a metal stamper. The pre-groove helps to guide the laser beam while writing and reading data. We have exploited this pre-groove for cell culture and alignment.
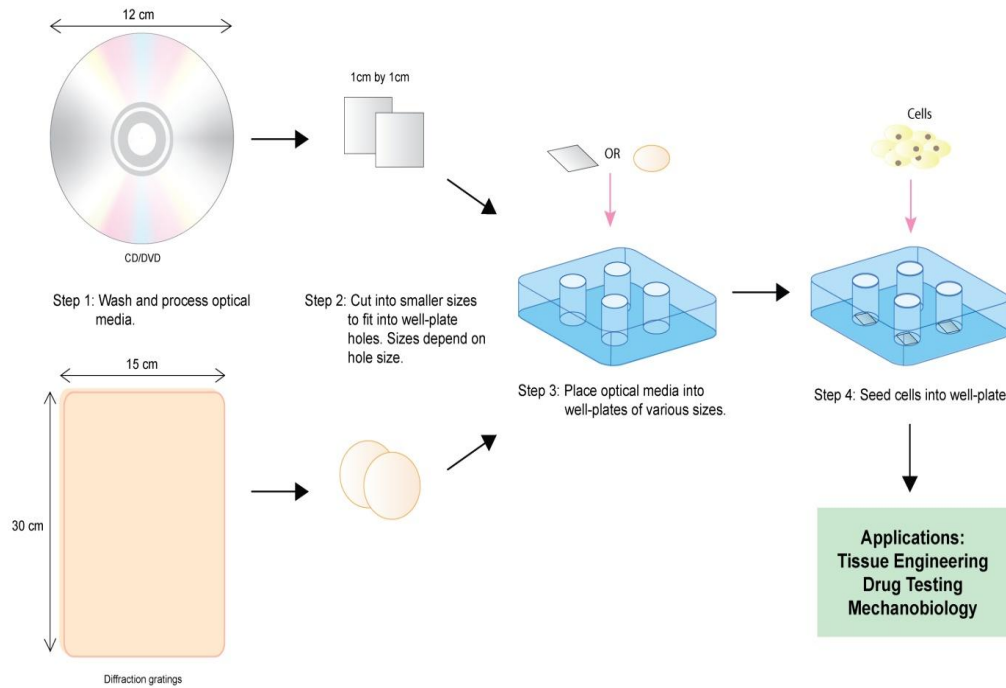
**Figure 16: Preparation of the optical media**. A standard sized CD-R or optical grating can produce enough nano/microgrooved cell culture insert for up to seven 24 well plates.

To characterize the optical media, we first performed an SEM and AFM to analyze the topography of the surface. The top view SEM of both the gratings and optical disc revealed a regular grooved pattern (Fig 17 A-C). This grooved pattern ran along the short axis of the rectangular optical grating and ran in concentric circles (pre-grooves) on the CD-Rs and DVD-Rs. In addition, SEM image of fibronectin/gelatin coated CD-Rs was taken to assess if the grooves were preserved even after the coating (Supplementary Figure 1A). The results revealed that the coating was thin enough to preserve the pattern of the grooves. The AFM image showed the profile and dimension of the optical media (Fig 17 D-F). The DVD-R exhibited a repeating trapezoid profile with a pitch of 800 nm and depth of 200 nm. The CD-R has a sine

57

wave form, with a pitch of 1.6 μm and a depth of 100 nm; the optical grating

also exhibited a sine wave form with a sharper apex than the CD-R. The pitch

of the optical grating was 1 μm and the depth was 200 nm. Although a major

limitation of the optical media is its pre-defined dimension, the dimension falls

within the range previously reported to align various cell types [43, 44].



CD-R                              DVD-R                              Optical grating
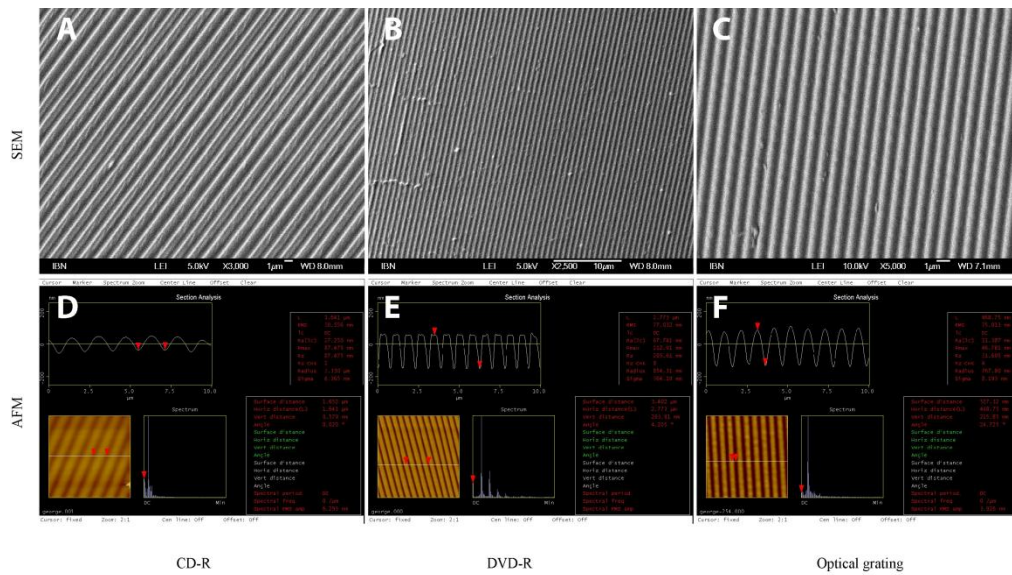


G    **Surface wettability**
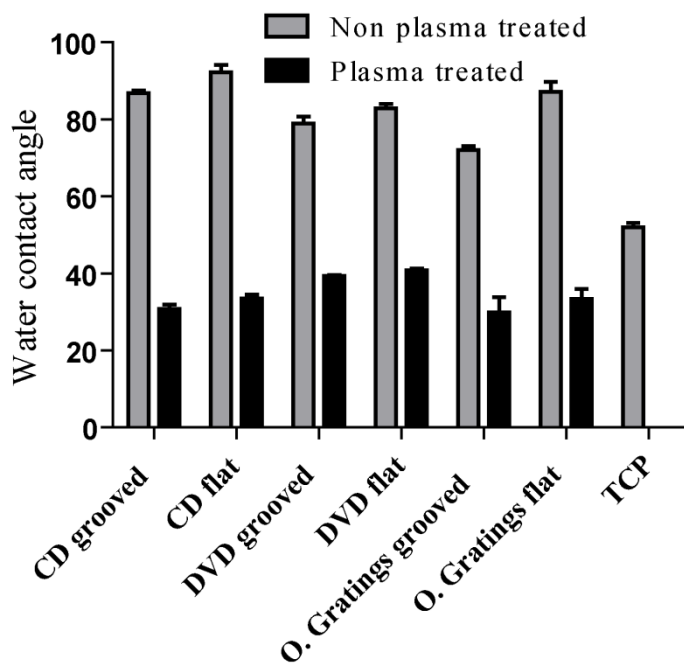
**Figure 17: Surface characterization of the optical media.** (A-C) shows the top view SEM images of the optical media used CD-R, DVD-R and optical grating respectively. The groove pattern is regular and runs in concentric circle for the CD-R/DVD-R and along the short axis for the optical grating. (D-F) shows the profile of the optical media by AFM images. The DVD-R has a trapezoid shape while CD-R and Optical gratings have a sine wave form. The dimensions are: CD-R has a pitch of 1.6 µm and depth of 100 nm. DVD-R has a pitch of 800 nm and depth of 200 nm. The optical grating has a pitch of 1µm and depth of 200 nm. (E) The water contact angles for all the optical media used shows that they are weakly hydrophilic with angles of about 70-90º much higher than the WCA for TCP which is about 50º. After plasma treatment the WCA was significantly reduced to about 30-40º

Surface properties such as wettability, measured by surface water contact angle (WCA), can affect protein adsorption, cell attachment and cell growth on a surface [149, 150]. We measured the WCA of the optical media as weakly hydrophilic with WCA of 70-90º. These values were much higher than the WCA of TCP which was ~50º (Fig 2G). To make the surface more hydrophilic and enhance cell attachment, we plasma-treated the optical media and this significantly reduced the WCA of the optical media to 30-40º. We have also measured the Young's modulus of the optical media and TCP by nano-indentation (Table 3) and the values were in the gigapascal (GPa) range, with the TCP being the stiffest material. A material's mechanical stiffness can affect cellular behavior such as growth and differentiation [151].

**Table 3: Young's modulus of optical media and TCP**

| Optical media | Young's modulus (GPa) |
|---|---|
| CD-R/DVD-R Polycarbonate | $3.1 \pm 0.04$ |
| Optical grating PET | $3.4 \pm 0.03$ |

| Tissue culture plastic Polystyrene | $4.4 \pm 0.07$ |
|---|---|

## 3.3.2. Cell attachment and growth

H9C2 cells were seeded at a density of 13,000 cells per cm$^2$ in 24-well plates containing both sides of the optical media (grooved and flat side) or control TCP. After 1 hour, the number of attached cells was quantified. To analyze the importance of wettability for cell attachment, the assay was performed both with plasma-treated and non plasma-treated optical media. We observed a 70-100% cell attachment on the plasma-treated surfaces (with WCA of 30-40º); significantly higher than the cell attachment of 40-50% on non-plasma treated surfaces (with WCA of 70-90º; Fig 18 A). The relationship between surface wettability and cell attachment has been studied extensively. Though some have reported that cells prefer hydrophilic materials, others have shown that certain cells favor hydrophobic materials [149, 150]. H9C2 cells (Fig 18A) favored hydrophilic surfaces; however, the bare surface may also be used for cells that adhere better on hydrophobic surfaces.
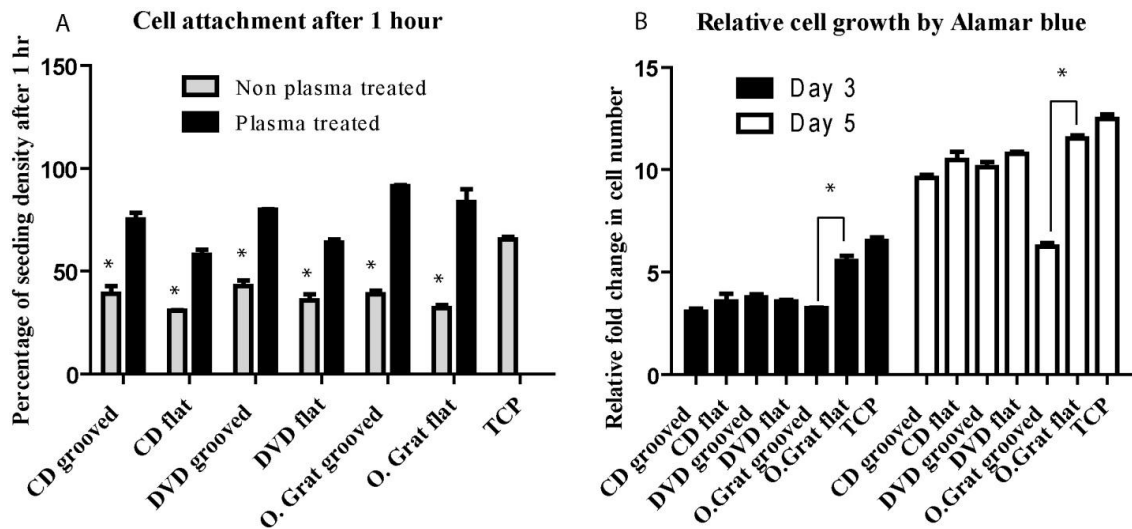
**Figure 18: Cell attachment and growth on the optical media**. (A) Cell attachment of H9C2 cells on the optical media after 1 hr. Before plasma treatment only about 40% of the initial seeding density had attached across all platforms. However, with the increase in hydrophilicity after plasma treatment, the attachment significantly increased to between 60-90%. *=$p$<0.05 comparing non plasma treated to plasma treated for each substrate. Data are average of 3 independent experiments. (B) With the alamarBlue assay, there was a significant decrease in proliferation with cells cultured on the grooved holographic gratings when compared to cells cultured on flat holographic gratings (PET) $p$<0.05. This difference, however, was not evident in the cells cultured on the CD/DVD (Polycarbonate). The TCP had a higher proliferation rate most likely due to higher young's modulus of the polystyrene.

We assessed cell growth on the optical media substrates over 5 days by alamarBlue® (Resazurin). Resazurin is a redox dye commonly used as an indicator of chemical cytotoxicity in cultured cells. The assay is based on the ability of viable, metabolically active cells to reduce resazurin to resorufin and dihydroresorufin [152]. Resazurin is non-toxic to cells, and can be used to assess cell number, and metabolic competence of cells *in vitro* [153]. For CD-R and DVD-R, there was no significant difference in growth between the grooved and flat surface; however, for the optical grating, cell growth was

significantly reduced in the grooved surface (Fig 18B). Previous studies have reported contradictory effects of cell alignment on cell growth. In some studies [141], researchers reported no significant difference in growth of fibroblasts between aligned and unaligned cells on electrospun polymeric fibers. On the other hand, others have found a significant reduction in proliferation of cells cultured on micro-grooved surfaces and on aligned electrospun polymers purportedly due to a restriction of cell spreading during cell alignment [154, 155]. In CD and DVD, the apex is broad while the optical gratings have narrow and pointed apex (Fig 17 D-F) restricting the area of cell spreading, and reducing cell growth. We also noted a correlative relationship between the materials' Young's modulus and cell growth. By comparing cell growth on only flat surfaces, we observed that H9C2 cells proliferated fastest on TCP with a young's modulus of 4.4 GPa (doubling time of 14.5 hours, Fig 18B), followed by optical gratings (PET) with a young's modulus of 3.4 Gpa (doubling time of 17.5 hours, Fig 18B). Cell growth on the CD/R and DVD/R (PC) with a young's modulus of 3.1 GPa was the slowest (doubling time of 21 hours). These observations are consistent with the positive regulation of cell growth by substrate rigidity [156, 157].

*3.3.3. Morphology and morphometric analysis*

Cells cultured on the flat control substrate had no specific orientation; however, cells cultured on the grooved surfaces displayed a predominantly spindle shaped morphology and were oriented along the direction of the grooves (Fig 19 A-F) and Video 1. This cell orientation produced on all the grooved surfaces regardless of the material (PC, PET), shows that the

topography is the key determinant of alignment [142]. Average cell area was quantified by image analysis and the results showed that the cells cultured on the grooved surfaces had significantly smaller area than the cells on flat surfaces (Fig 19 G).
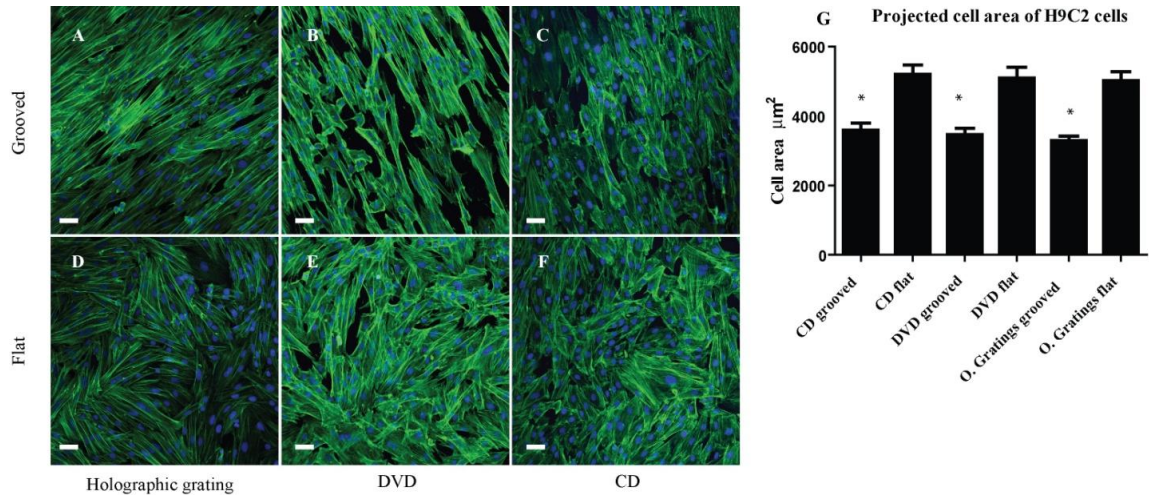


**Figure 19: Morphology and morphometric analysis of H9C2 cells on the optical media**. (A-F) shows the F-actin and DAPI staining of H9C2 cells on the optical media after 5 days. (A-C) corresponds to the grooved surfaces and (D-F) corresponds to the flat surfaces. These images show that topography is the key determinant of cell alignment regardless of material properties. Scale bar 50 μm. (G) shows the average cell area of H9C2 cells on the optical media. The average cell area is significantly reduced when cells are cultured on grooved surfaces. * indicates $p<0.05$ when comparing grooved and flat surface for each substrate.

To quantify the degree of alignment achieved across all platforms, a 2D fast Fourier transformation (FFT) was performed (Fig 20). The FFT for aligned cells exhibited a more elongated elliptical spectrum which indicated a preferred direction of alignment (Fig 20A) whereas the FFT for the unaligned cells exhibited a circular spectrum (Fig 20B) which indicated no directionality [147]. This result was consistent for the cells cultured on CD, DVD and PET gratings, supporting that the topography was the major determinant of

alignment. The anisotropy of the FFT was further quantified spectrum the long

to short axis index.
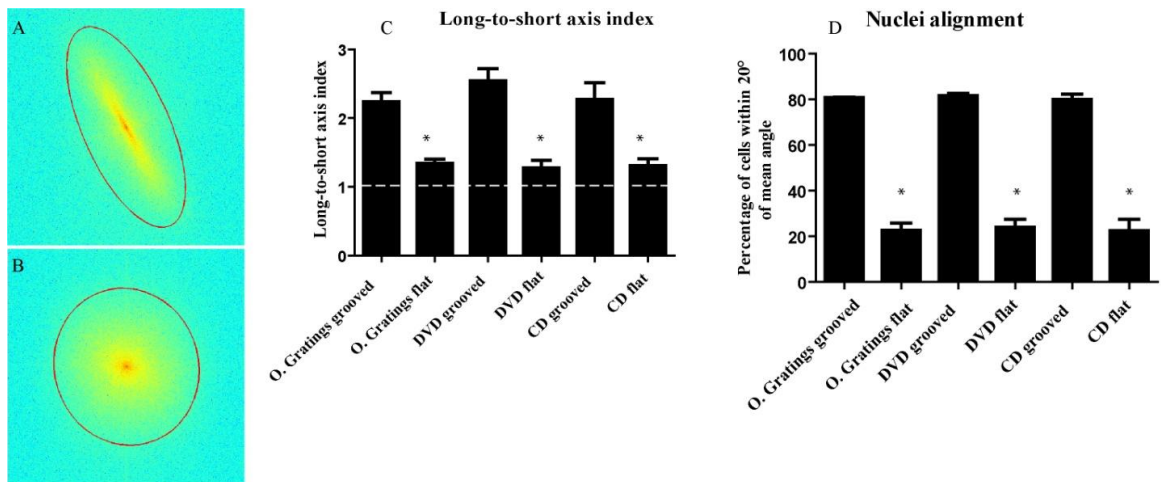


**Figure 20: Quantification of nuclei and cell alignment**. (A-B) shows that the 2D FFT for the aligned cells has an elliptical spectrum while the FFT for the unaligned cells has a circular spectrum. (C) Long-to-short axis index to quantify anisotropy. * indicates $p<0.05$ as compared to flat substrates. (D) Percentage of nuclei that align within 20° of mean nucleus angle. 80% of cells on the grooved substrates fall within this region while about 30% of cells on flat surface fall within the region. * indicates $p<0.05$.

An index of 1 reveals an isotropic (random) distribution while values higher

than 1 shows a preferred direction of alignment of the cells [148]. I observed

that the cells on flat substrates demonstrated an isotropic distribution with

values not significantly higher 1. The cells on the grooved substrates;

however, exhibited anisotropic distribution with values above two (Fig 20C)

further confirming the groove-induced cell alignment. The nucleus alignment

also revealed that while about 80% of the cells on the grooves aligned within

20° of the mean direction, only about 30% of the cells on the flat surfaces were

within this region (Fig 20D). To show the robustness of the CD-R/DVD-R, an

analysis of the cell alignment achieved on different regions of the DVD-R from the center to the edge was carried out (Fig 21).
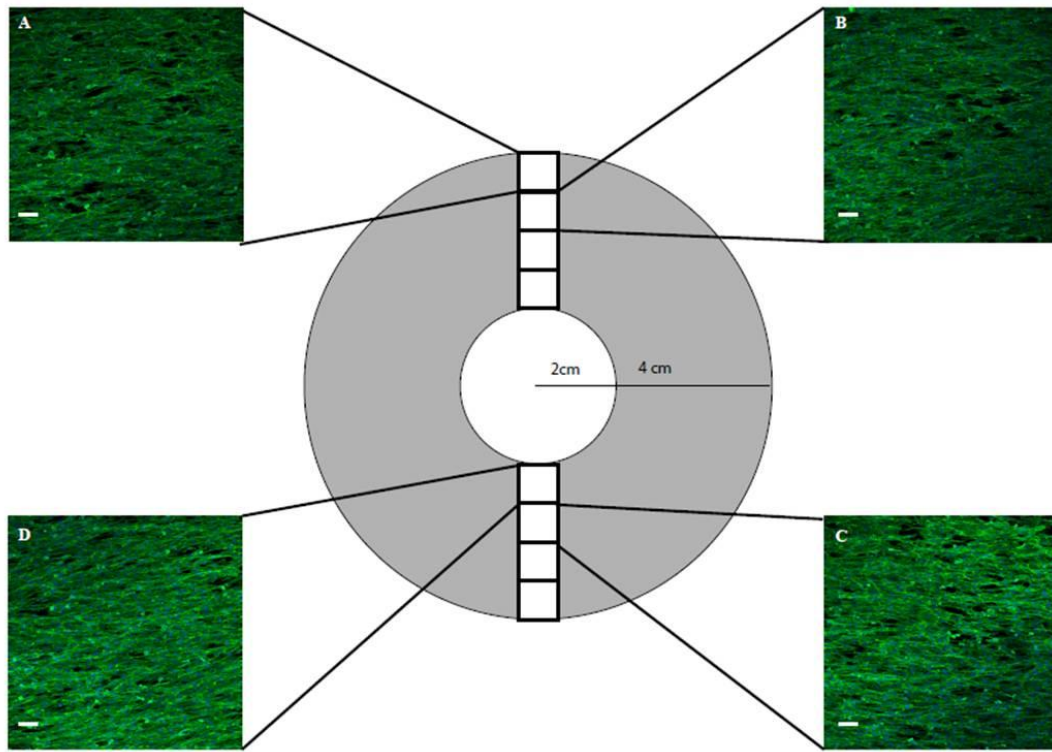


**Figure 21: Cell alignment on different regions of the DVD-R.** Comparative analysis of F-actin and DAPI staining of the cells cultured on different areas of the DVD-R spanning from the centermost (D) to the outermost region (A). Scale bar 100μm.

For this analysis, images were taken at 10X to capture a larger area (1270 X 1270 μm), and both 2D FFT and nucleus alignment algorithms were used to analyze cell alignment. Our results showed that there was no significant difference in the long to short axis ratio (Fig 22A); however, there was a reduction in the percentage of cells that were aligned within 20° for the cells cultured near the center (Fig 22B). The grooves in the DVD-R run in concentric circles, hence the cells closer to the center would sense greater

curvature and a wider angle while the region closer to the edge will sense almost a straight line and a smaller angle.
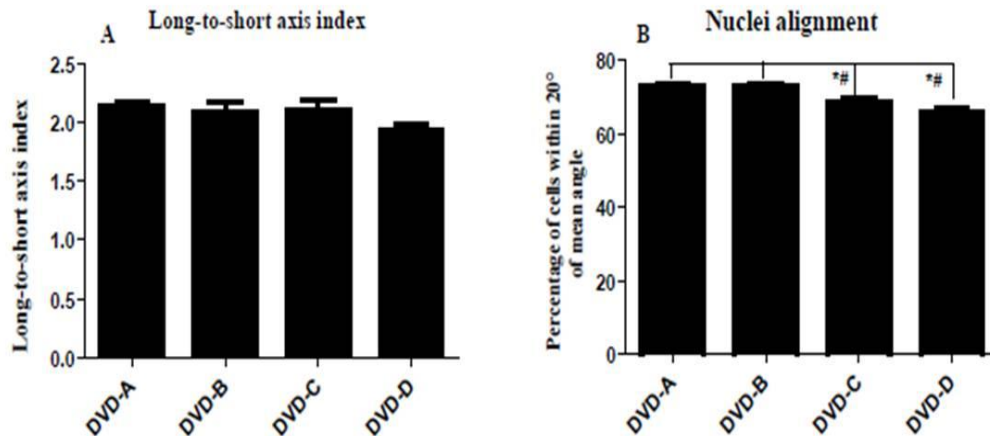


**Figure 22: Quantification of nuclei and cell alignment.** (A) Shows the long-to-short axis index to quantify anisotropy. There was no significant difference across different regions. However, about 6% fewer cells were aligned within 20° of mean nuclei alignment when comparing the innermost (DVD-D) and outermost regions (DVD-A) of the DVD-R (B). * indicates $p<0.05$ as compared to DVD-A, while # indicates $p<0.05$ as compared to DVD-B.

### 3.3.4. H9C2 cell differentiation

Differentiation of H9C2 cells into cardiac lineage was achieved by treating the cells with all-trans retinoic acid as previously reported [158, 159]. Cardiac differentiation is evidenced by an increase in the genes coding for the ventricular isoform of the myosin light chain 2V (MLC-2V) and for sarcomeric proteins such as alpha cardiac actinin, myosin heavy chain and Troponin T. As the cardiomyocytes mature, there is a switch from the beta isoform to the alpha isoform [160, 161]. Other useful markers for cardiac differentiation are the atrial and brain natriuretic peptides (ANP and BNP) participating in the regulation of blood pressure, growth and development of cardiovascular tissue [162]. In our experiment, H9C2 cells show a more

66

differentiated phenotype when cultured on grooved surfaces with a significantly higher expression of alpha cardiac actinin, myosin light chain 2V and Troponin T as compared to the flat surfaces of the optical media (Fig 23A). This was accompanied by a corresponding decrease in the fetal cardiac marker BNP in the cells cultured on grooved surfaces (Fig 23A). There was no increase in the alpha/beta ratio of the myosin heavy chain and no significant difference on both the grooved and flat surfaces (Fig 23B). This relatively low alpha/beta ratio may be a consequence of the absence of the physiological beating phenotype or may be suggestive of a fetal phenotype [161].
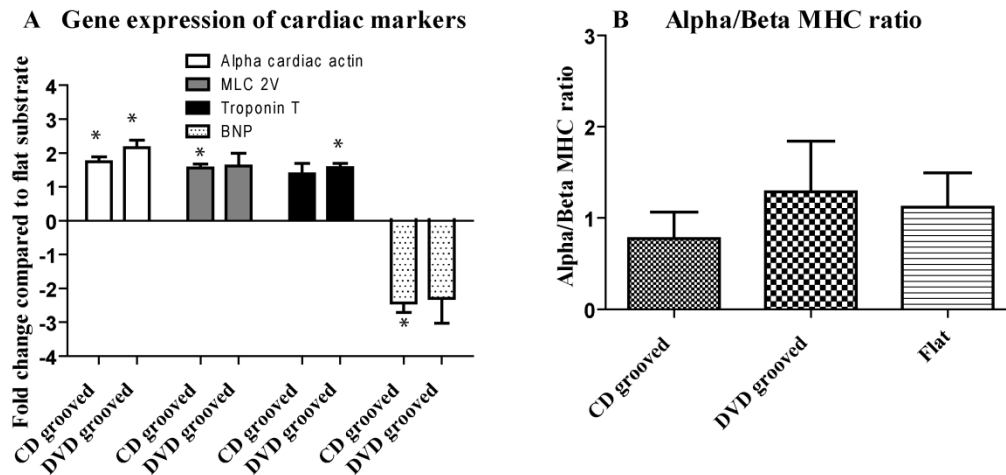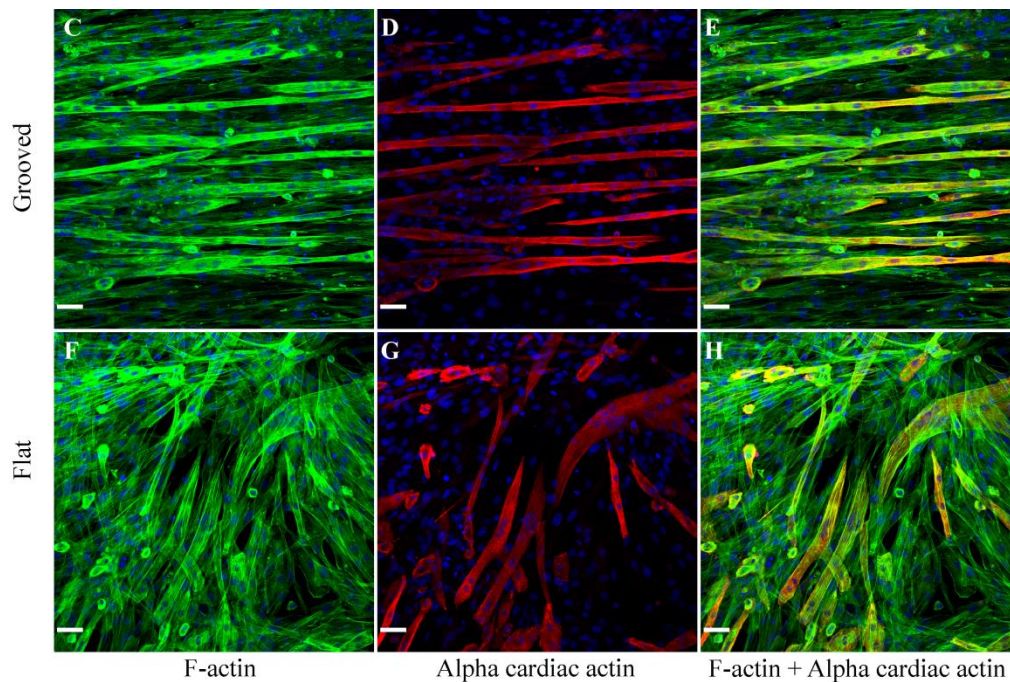
**Figure 23: Cardiac differentiation of H9C2 cells on the optical media**. (A) Gene expression of cardiac specific markers. There was a 1.5-2.5 fold increase in the cardiac specific genes when cultured on grooved substrates.* means $p<0.05$ as compared to flat substrate. (B) Alpha/Beta myosin heavy chain ratio. There was no significant difference in the ratio across all platforms; data are result from 3 independent experiments. (C-H) shows the immunofluorescence images of differentiated H9C2. (C, F) F-actin, (D, G) Alpha cardiac actin and (E, H) merged images of H9C2 cells on grooved and flat surface of the DVD respectively. The cells on the grooved surfaces had formed long thin multinucleated tubes while those on flat surface had broader, shorter and unaligned multinucleated cells. Scale bar 50 μm.

Immunostaining of alpha actinin and F-actin revealed that the H9C2 cells had formed multinucleated cardiomyocytes (Fig 23C-H). Those cultured on grooved substrates had longer, thinner and more organized multinucleated myotubes (Fig 23C-E), while those cultured on the flat surfaces had shorter, broader and more disorganized multinucleated cells (Fig 23F-H). Previous studies on H9C2 differentiation had either been only on flat surfaces or only explored the differentiation of H9C2 into skeletal myotubes. This finding is

68

important considering the fact that recent evidence suggests that the response of H9C2 cells to cardiotoxic drugs differs depending on its differentiation stage [158, 159, 163]. H9C2 cells are widely available and commonly used for study of cardiotoxic drugs; hence further studies would unravel how topographical cues affect cells response to cardiotoxic drugs.

### 3.3.5. C2C12 cell differentiation and maturation

Differentiation of C2C12, a mouse derived myoblast cell line into skeletal muscle was induced by reducing the fetal bovine serum to 1% in the presence of Insulin-selenium as previously reported [19]. The differentiation was assessed by the amount of cells that were stained with the MHC antibody. Our result was in line with previously published result that cell alignment enhances differentiation and maturation of C2C12 cells [19]. The results found that more cells cultured on the side with the grooves were expressing the MHC and forming longer myotubes (Fig 24A-C) when compared to the side without the grooves (Fig 24D-F). To compare the degree of myotube formation between grooved and flat surfaces, I calculated the fusion index that represents the fraction of the total nuclei present within the myotubes (nuclei $\geq$ 2). The index for the cells on grooved surfaces (CD and DVD) was 0.3 and significantly higher than the index for cells cultured on the flat surface, which was about 0.1 (Fig 24G).
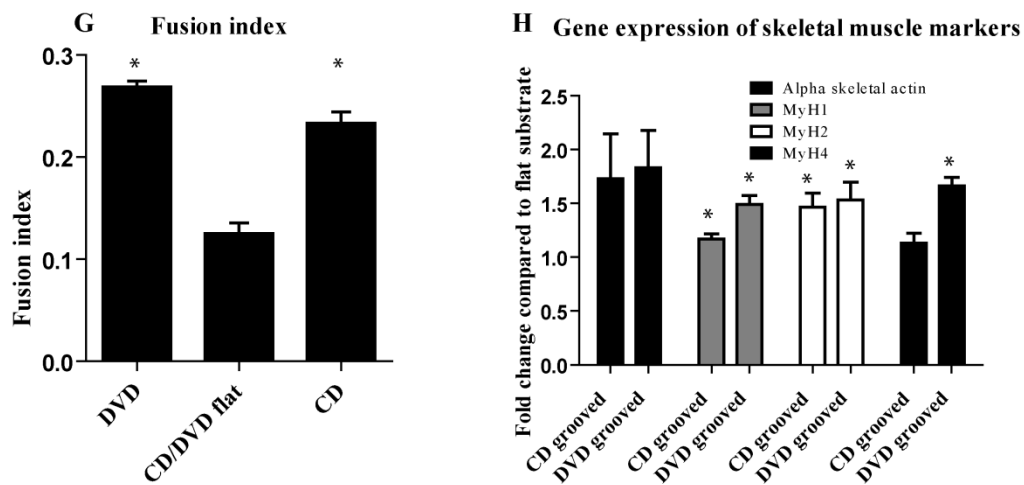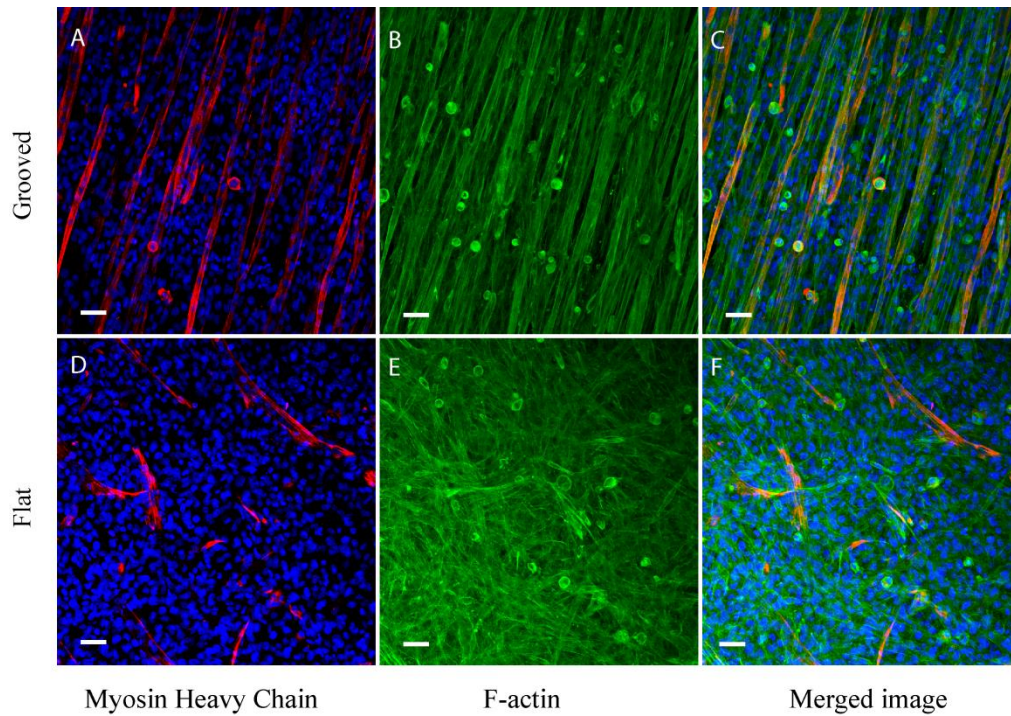
**Figure 24: Differentiation of C2C12 cells on the optical media.** (A-E) shows the Immunofluorescence images of differentiated C2C12 cells. (A, D) corresponds to myosin heavy chain, (B, E) F-actin and (C, E) merged image of C2C12 myotubes on grooved and flat surface respectively. Topographical cues enhance differentiation and maturation of C2C12 cells. Cells on the patterned substrates fused to form longer myotubes. Scale bar 50 μm. (G) shows the fusion index which was calculated by obtaining the fraction of the nuclei within the myotubes (nuclei $\geq$ 2). There was more myotube fusion in cells cultured on the grooved substrates. (H) Shows the gene expression of skeletal muscle markers. There was an increase in the expression of the genes in cells cultured on the grooved substrates. * indicates $p < 0.05$ when compared to flat substrate. Data are results from 4 independent experiments.

RT-PCR of four skeletal muscle genes was performed to assess cell differentiation and maturation. These genes are broadly recognized as important for skeletal muscle development, namely alpha skeletal actinin and the myosin heavy chains 1, 2 and 4 [19]. I observed ~1.5 to 2 fold increase in the expression of these genes in the cells cultured on the grooved surfaces from the control cells cultured on the non-patterned surface (Fig 24H). The up-regulation of MHC 1 and MHC 4 was significantly higher on the DVD-R than on the CD-R possibly due to the groove dimensions, with previous report indicating that nanogroove dimension was more efficient in inducing myoblast formation than microgroove dimensions [155]. Two key events have been identified as important for C2C12 maturation and myotube formation. They are: 1) Exit from mitosis phase into $G_0/G_1$ phase which is usually achieved by serum starvation and 2) End-to-end contact of the cells which fuse for form myotubes. To further understand why nanogrooves enhance C2C12 maturation, a study of the cell cycle phase of the cells at 40-60% confluence and at 80-100% confluence was carried out. Our results show that a higher proportion of cells cultured on the flat surface were in the M phase (Fig 25), while a higher percentage of cells on the grooves were in the $G_0/G_1$ phase (Fig 25). This difference is more pronounced when the cells are less confluent (Fig 25B) as the cells become more confluent and undergo contact inhibition, the difference is reduced (Fig 25A). However, the fact that there are more cells in the G0/G1 on grooved surface suggests that the cells on the grooved surface begin to mature earlier. In addition, from the immunocytochemistry images, there was a better end-to-end contact of cells on the grooved surface. This led to the formation of un-branched and longer myotubes. Both of these

phenomena may explain why cells on the grooves had a higher gene expression
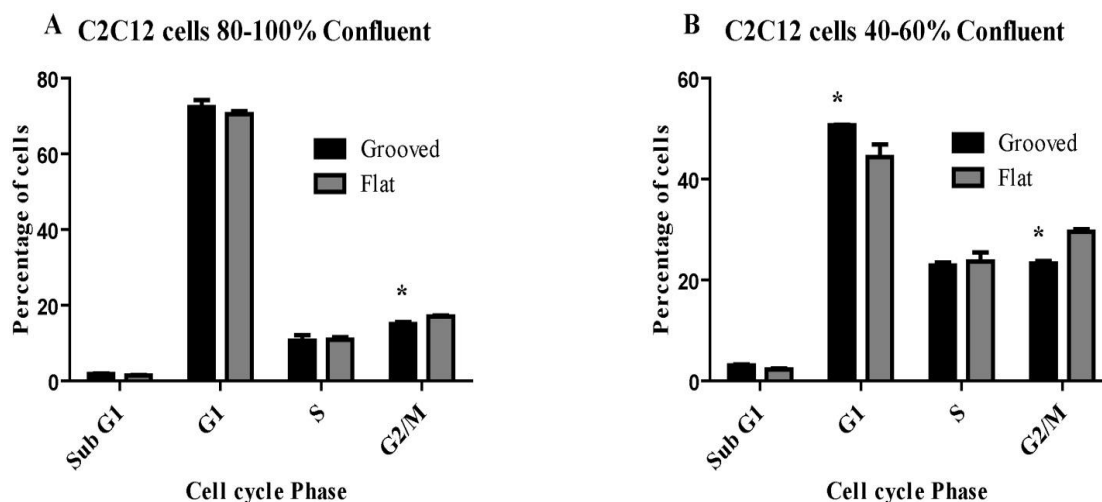


**Figure 25: Cell cycle analysis of C2C12 cells**. A) 80-100% confluence. B) 40-60% confluence. * indicates $p< 0.05$ when compared to flat substrate. Data are results from 3 independent experiments.

### 3.3.6. PC12 cell differentiation

I studied the neurite development and polarity selection in PC12 cells on the optical media coated with 10 μg/ml laminin [164]. The polarity selection of PC12 cells on the optical media is in agreement with previously published data on polystyrene nanogratings produced with nanoimprint lithography [165]. Cells exhibit bipolar morphology when cultured on the gratings, and a multipolar morphology when cultured on flat surface (Fig 26A-D). The effect of topographical cues on polarity selection was dependent on the groove width. There was higher percentage of bipolar cells on the DVD-R (800 nm pitch) than the cells cultured on the CD (1600 nm pitch) (Fig 26E) [165]. Since such topographies can determine the location of the budding

neurites, PC12 cells cultured on optical media can be used to study protein trafficking and neuronal migration that are key events in morphogenesis [39].
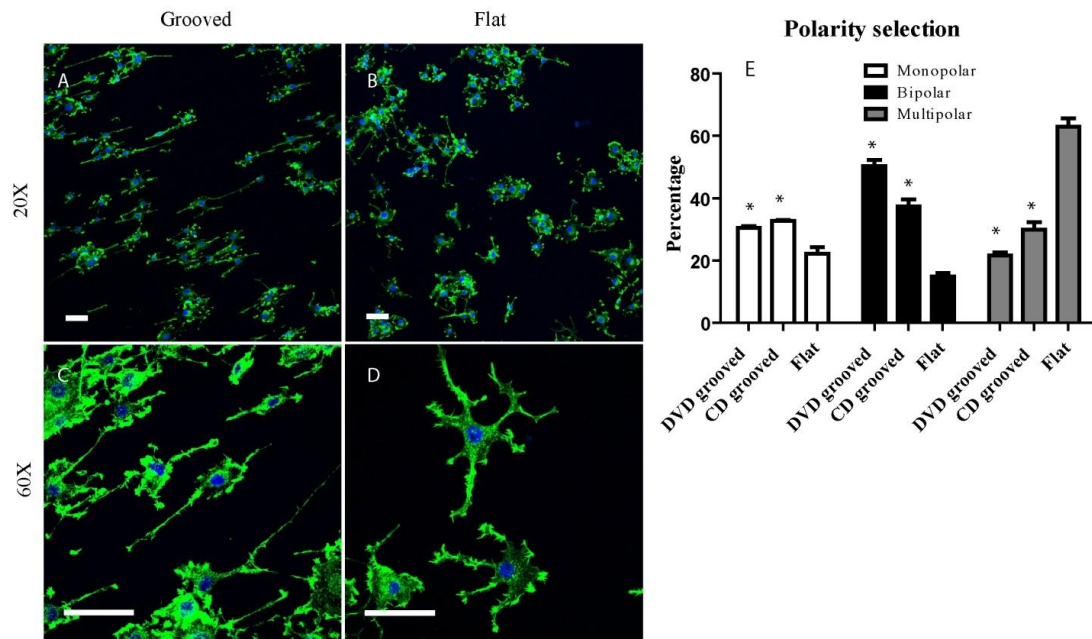


**Figure 26: Polarity selection of PC12 cells on the optical media**. F-actin and DAPI of PC12 cells with 20x magnification (A, B) and 60x magnification (C, D). PC 12 cells on grooved surfaces have predominantly bipolar neurite elongations which align along the direction of the grooves. The cells on flat surfaces have multiple neurite elongation. Scale bar 50 μm. (E) 70-80% of cells on grooved surfaces CD and DVD had either one or only 2 neurite elongations while about 70% of cells on flat surfaces had 3 or more neurite elongations. Only projections longer than the cell soma (5 μm) were considered. * indicates $p<0.05$ as compared to flat substrates.

Substrate topography has been shown to induce an upregulation of neuronal markers in human mesenchymal stem cells or determine the fate of human embryonic stem cells either into neuronal or glial lineage [4, 28]. Topographical cues by nanogratings have been shown to be more effective in determining neurite outgrowth direction, neuronal polarity and neurite-neurite connection than cell-cell stimuli *in vitro* [165]. Neuronal polarity *in vivo* is determined by a series of events preceded by cytoskeletal rearrangement that

leads to activation of signaling pathways, selective protein and organelle trafficking and focal adhesion distribution [40, 41]. Cytoskeletal rearrangement produced by both a gradient of secreted factors and topographical cues provided by glial cells directs neuronal polarity and neuronal migration [39, 42]. Although the mechanism behind neuronal polarity and migration is not yet fully elucidated, researchers have explored the use of physical cues like micro/nanotopographies to induce cytoskeletal rearrangement, neurite development and neuronal migration in neuronal cells [39, 166]. I have demonstrated here that optical media serve as scalable cell alignment substrates with micro-/nano-topography for these studies and applications.

### 3.3.7. Hepatocyte culture on RGD-conjugated optical media

Depending on the cell culture application, various ECM molecules can be used. One of the commonly used ECM molecules is collagen, however, collagen usually forms a gel at 37°C and this obliterates the grooves and ridges which are in nano/microscale dimensions. To avoid this, a cell adhesion peptide Arg-Gly-Asp (RGD) [167] was chemically conjugated to the optical media and rat primary hepatocytes were cultured on the optical media. The RGD ligand on PET has been previously used for hepatocytes culture to maintain a 3D monolayer, and the conjugation procedure has been optimized [168]. After conjugating the RGD on our optical media, the results indicate that the cells attached to the optical media and also aligned along the direction of the grooves (Fig 27). The successful conjugation of the cell adhesion

74

peptide to the optical media means it can be customized to provide support to different cell types.
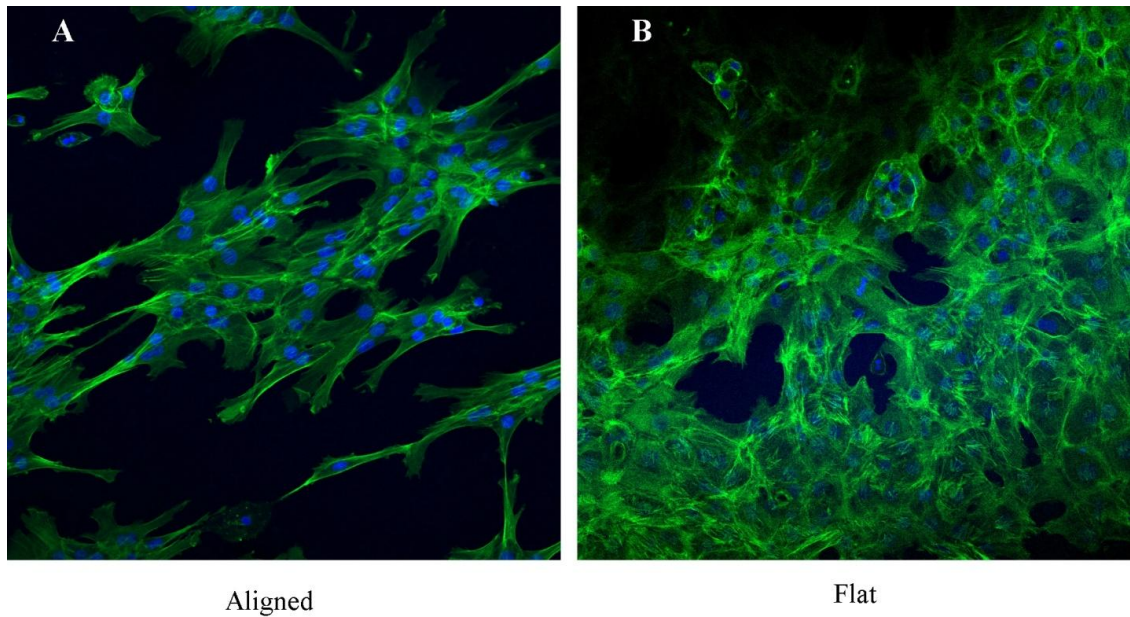


Figure 27: Primary rat hepatocytes culture on PET-RGD. A) Grooved surface. B) Flat surface. Scale bar 100μm

## 3.4. Concluding remarks

Commercially available optical media can serve as scalable cell alignment substrates for applications such as cellular studies or industry-scale drug screening. They are cost effective, versatile for culturing cell types, possess large surface area, and optically transparent suitable for imaging-based assays. With ease of conjugation or coating with specific chemical ligands, the optical media can also be conferred specificity in providing optimal support for different cells. The aligned cells exhibit specific growth and differentiation characteristics in cardiac and skeletal muscle, and neuronal cells that would otherwise be achieved only on topographical features engineered with much

more complex and expensive micro-/ and nano-fabrication techniques. I envision that optical media would henceforth be further exploited to rapidly expand the range of research or industry applications.

**Chapter 4: ENGINEERING SCALABLE 2D AND 3D CELLULAR CONSTRUCTS OF ALIGNED SKELETAL MYOBLASTS IN PDMS MICROFLUIDIC CHIPS EMBEDDED WITH NANOGROOVES**

This chapter deals with the patterning of large surface area PDMS by replica molding, using the optical media as molds. The nanogrooved PDMS obtained from the replica molding is then utilized in microfluidic chips to generate 2D and 3D cellular constructs of aligned skeletal myoblasts. This provides a scalable method for engineering microfluidic chips with embedded nano/microscale cues

## 4.1 Introduction

Microfluidic technologies have been increasingly used for studies such as stem cell differentiation, cell selection, disease modeling and drug screening applications [74, 169]. This is because culturing cells in microfluidic systems permit the use of small quantity of cells and reagents, and can be readily adapted to multiplexed and high throughput assays [169]. In addition, they allow for more precise experimental manipulation of cellular systems, such as spatial patterning of molecules, control over mass transfer regimes, and application of shear stresses [74, 75]. To fully realize the utility of microfluidic cell-based models in biomedical applications, it is important to create a microfluidic cell microenvironment which is conducive for maintaining physiological cellular phenotypes. Earlier developments have focused on the surface modification of microfluidic substrates to facilitate cell attachment [170]. More recently, there has been much emphasis to incorporate

77

3D cellular microenvironment into microfluidics since 3D cell cultures better mimic the *in vivo* environment for more physiological function, differentiation and drug responses [171-173]. Beside 3D cell morphology, cell alignment imposed by the geometry and topography of the cell culture substrate *e.g.,* the extracellular matrix (ECM) is important for maintaining physiological phenotypes and functions, especially in anisotropic cardiac, neuronal and skeletal muscular tissues [45]. Therefore, the incorporation of cell alignment cues in microfluidic platforms is of interest in the customization of microfluidic cell models to better support these specific tissues [174].

Despite the advantages of aligning cells in cultures, there have been relatively few attempts to incorporate engineered features for aligning cells in microfluidic systems [79]. Some researchers achieved aligned monolayer of cells in microfluidic devices by patterning ECM molecules on glass substrates [65, 80]. The alignment was produced by geometrically constraining cell attachment and spreading to only the desired area. The technique can only create aligned monolayer of cells but not 3D cellular constructs in microfluidic chips. The mechanism of eliciting alignment by ECM patterning is different from that of cell alignment *in vivo*, which has been shown to be due to groove-like topographical features of the ECM [10, 113, 175]. Therefore, inducing cell alignment via engineered topographical cues may elicit a cellular phenotype similar to aligned tissues *in vivo* [10].

A major challenge of making topographical cues, such as micro-grooves, a routine feature of microfluidic platforms is the high cost of fabrication of these micro- or nano-topographies. Yang *et al.* proposed a

stitching method to generate large surface areas of micro-grooved substrate. This consists of pre-fabricating micro-grooved substrates using photolithography or electron beam lithography and then stitching them together [79]. Wallin *et al.* used electrospun polymers [85] to create aligned and random patterns in polydimethysiloxane (PDMS) microfluidic chips. However, both methods require costly or specialized photolithography or electrospinning equipment. Alternative methods of producing micro-grooved substrates have been developed, such as micropatterned surfaces ground with abrasives [24] or using metal wrinkles [71]. Although these techniques help to reduce the cost and specialized equipment required, their adaptation into microfluidic cell culture systems has not yet been demonstrated.

Methods for incorporating topographical features into a microfluidic system should also be compatible with the implementation of microfluidic 3D cell culture. To date, cell alignment with micro-patterned ECM or topographical features in microfluidics has only been demonstrated for 2D monolayer cultures [79, 80]. While the generation of aligned 3D cellular constructs have been developed in static bulk cultures, which include stacking of aligned cell sheets [88, 176], encapsulation of cells in hydrogels [86, 161] or culture in scaffold, [87] these methods are not readily implemented in microfluidic systems. The ability to create aligned 3D culture of cells from anisotropic tissues, which require polarity or alignment for proper functioning, [161] will enable one to customize microfluidic cell models of these specific tissues and fully realize their potential in desired applications, such as drug screening.

This chapter reports a cost-effective and scalable method to incorporate micro-topographies into microfluidic chips. Commercially available optical media, which contain micro-grooves of various dimensions that support alignment of cardiac, skeletal and neuronal cell lines, [45] were utilized as molds to transfer the topographical features to a PDMS sheet [135, 137]. These optical media offer a simple and cost effective method to generate large surface area (up to 15 cm x 30 cm) of micro-grooved PDMS substrates, which can be easily incorporated into PDMS microfluidic devices. When coupled with a 3D microfluidic cell culture system, I show that the micro-grooved substrate can align 3D cellular constructs along the orientation of the grooves; and the aligned 3D cellular constructs exhibited improved differentiation of C2C12 myoblast cells into skeletal muscle cells in the microfluidic device.

## 4.2 Material and Methods

### 4.2.1. Pattern transfer from optical media to PDMS

To generate large surface area for the bottom layer, optical media (Vivoalign™ licensed to Bio-Byblos, Taiwan ROC, 8 x 8 cm) and placed into 150 mm cell culture dishes (CORNING, Singapore). The optical media were glued to the bottom of the dish with a double-sided tape, exposing the grooved surface. Subsequently, a mixture of PDMS with curing agent ratio of 10:1 was poured on the surface of the optical media, the mixture was degassed and left to cure in $80^{\circ}C$ for 2 hours.

*4.2.2 Design, fabrication and assembly of microfluidic chip*

The top layer of the microfluidic chip containing the microfluidic network was adapted from a previously developed microfluidic 3D cell culture chip [177]. Briefly, microfluidic channels with a micropillar array were designed using AutoCAD (Autodesk, USA) and L-Edit v10.20 (Tanner Research, USA). The dimensions of the microfluidic channel were 1 cm (length) x 600 µm (width) x 100 µm (height) and had one inlet for cell culture medium, one inlet/cell reservoir and one outlet. An array of 30 µm x 50 µm elliptical micropillars with a gap size of 20 µm was situated in the middle of the microfluidic channel, bounding a cell residence volume that was 1 cm (length) x 200 µm (width) x 100 µm (height) [178]. Silicon templates were fabricated by standard deep reactive ion etching (DRIE) process (Oxford Instruments Plc, UK). The microfluidic channels were then obtained by replica molding polydimethylsiloxane (PDMS) (Dow Corning, USA) on the silicon templates [178].

Both the top layer and bottom layer were subsequently treated with oxygen plasma and subsequently put into an oven at 80$^{\text{o}}$C for another 2 hours. This was to aid a tighter bonding between both PDMS layers. Three different configurations of the bottom layer were used: 1) grooves were arranged to be parallel to the fluidic flow; 2) grooves were perpendicular to the flow; and 3) no grooves on the bottom layer. The microfluidic chips were sterilized by autoclaving and connected to a perfusion circuit as described previously [178]. In addition, PDMS micro-grooved substrates were cut to the size of 24-well plates and were used for monolayer cell culture.

81

*4.2.3 Surface characterization of PDMS micro-groove substrates by Atomic Force Microscopy (AFM)*

AFM samples were prepared by cutting appropriate sizes of the PDMS micro-groove substrates. An atomic force microscope, DI Nanoscope Dimension 3100 (Digital Instruments, USA), was used in tapping mode to identify the groove features on the PDMS substrate.

*4.2.4 Cell culture*

C2C12 is a sub-clone of a murine myoblast and consists of a pure population of myogenic cells that proliferate and differentiate in culture [179]. The cells were obtained from ATCC (USA) and were used at passage number below 20 for this study. Prior to cell seeding, the microfluidic chip was primed by perfusing the following solutions in order: 70% ethanol, DMEM (Gibco®, 31600, Invitrogen, Singapore), PBS and again with DMEM. Each solution was left to run for 20 minutes at 0.5 ml/hr. After the priming step, the bottom layer of the chip was coated with a mixture of 10 μg/ml fibronectin (F1141, Sigma-Aldrich, Singapore) and 1 mg/ml gelatin (G1890, Sigma-Aldrich, Singapore). The solution was added into the cell reservoir and the outlet connected to a syringe pump in withdrawal mode to allow for the solution to flow into the chip. The chips were incubated with the fibronectin-gelatin solution for 2 hours before washing with DMEM. A suspension of C2C12 cells (6 million cells/ml) was introduced into the chip by using a syringe pump to withdraw cells from a cell reservoir. Cells were immobilized three-dimensionally by the micropillar array within the microfluidic chip. Cells were allowed 4 hours to attach before perfusion was initiated at a flow rate of 0.05 ml/hr.

To study the effect of the groove orientation on the cell alignment in the microfluidic chip, cells were cultured for three days in proliferation medium, containing DMEM with 10% Fetal Bovine Serum (FBS) (Gibco®, 16000, Invitrogen, Singapore) and 1% Penicillin-Streptomycin (P4333, Sigma-Aldrich, Singapore). The three different configurations mentioned above were used. For the study of C2C12 cell maturation, the cells were cultured for 3 days in proliferation medium, followed by another 3 days in differentiation medium, which consisted of DMEM, 1% FBS, 1% Penicillin-Streptomycin and 1% insulin-transferrin-sodium selenite (Gibco®, 41400, Invitrogen, Singapore). At the end of the 3 or 6 days culture period, samples were either fixed for immunofluorescence staining or cells were lysed for qPCR analysis. For the maturation experiment, two configurations were compared: a) no grooves and b) grooves parallel to the direction of the fluidic flow.

2D monolayer culture in the microfluidic chip was established by using a low-density cell suspension (1 million/ml) so that the cells cannot be efficiently trapped by the micropillar array. After the cells were introduced into the chip, they were incubated for 4 hours before perfusion culture was initiated.

*4.2.5 Total RNA isolation and gene expression analysis*

Total RNA was harvested and purified with the RNeasy Microkit (74004, Qiagen, Singapore). Cells lysis was performed by perfusing the chip with RLT Plus buffer (1053393, Qiagen, Singapore) at a flow rate of 0.5 ml/hr until a volume of 350 μl was collected. Total RNA was isolated and purified

from the cell lysate according to manufacturer's protocol, and reverse transcribed to cDNA using high capacity RNA to cDNA kit (4387406, Invitrogen, Singapore). A total of 300-600 ng/µl of RNA was obtained from each chip. Previously published primers for C2C12 cells [19] were used for the quantitative PCR and the reactions were performed using the LightCycler® FastStart DNA Master $^{PLUS}$ SYBR Green I (03515869001, Roche, Singapore) in a Roche LightCycler®1.5 carousel based system (Roche, Singapore). Analysis of each gene was performed using the relatively quantitative ΔΔCT method. Transcript levels were first normalized to the housekeeping gene GAPDH and expressed as relative level to that of day 0.

## 4.2.6. Immunofluorescence staining

Cells were fixed, permeabilized and blocked as described previously [178]. Alexa fluor phalloidin 488 (A12379, Invitrogen, Singapore) was used for F-actin visualization and DAPI (D9542, Sigma, Singapore) at 1 µg/ml for nuclei staining. The samples were imaged with a confocal microscope (Olympus FV1000, Japan).

## 4.2.7. Quantification of nuclei and cell orientation

The nuclei alignment angle and elongation ratio (E.R.) was calculated using the ImageJ software (National Institutes of Health, Bethesda, MD, USA,). The nuclei angle alignment is the orientation of the major elliptic axis of the nucleus with respect to the horizontal axis along which the micro-grooves were oriented, [79, 86] while the E.R. is the ratio of the long to short axis of the nucleus [79]. For each sample, images were acquired from three different imaging planes along the height of the microfluidic chip: the bottom

plane, mid plane and top plane, with each plane being 8-12 µm higher than the previous plane [86]. For this analysis, the nuclei alignment angles were normalized to the mean nuclei angle for each sample and the percentage of nuclei within 20º of the mean was calculated [86].

### *4.2.8. 3D image rendering*

3D image rendering of the z-stack confocal images was performed using the Imaris software (Bitplane, Switzerland).

### *4.2.9. Shear stress modeling*

The flow in this study was modeled as the incompressible viscous fluid and governed by Navier-Stokes (NS) equations. The governing equations were discretized in space using finite volume method where a finite set of discrete equations was constructed on unstructured hybrid grids to approximate the NS equations. The computational domain is subdivided into a set of non-overlapping tetrahedral elements. The 3D micro-tissue was modeled as a rectangular block situated at different distances (i.e., 1 µm, 5 µm and 10 µm) from the micropillar array. A modified computational fluid dynamic laminar flow solver in OpenFOAM was used to simulate the flow. The resultant wall shear stress is then calculated

### *4.2.10. Statistical analysis*

Graphs and statistical differences for nuclei alignment, elongation ratio (E.R.) and gene expression were performed using GraphPad Prism 5 (GraphPad Software Inc. California, USA). A one-way analysis of variance followed by bonferroni's multiple comparison tests was employed to compare the nuclei alignment and E.R. across the three configurations of groove

alignment. For the gene expression studies, paired t-test studies were performed comparing flat and grooved for each gene, $p<0.05$ was considered significant.

## 4.3. Results and discussion

### 4.3.1. Fabrication and incorporation of PDMS micro-grooved substrate into microfluidic chips

This chapter reports a simple and scalable method of fabricating a microfluidic chip incorporating topographical features that enabled the alignment of 3D cellular constructs. The chip comprised of a top layer with a microfluidic network optimized for supporting 3D culture of mammalian cells, [178] and a bottom PDMS substrate containing micro-grooves to align cells (Fig. 28A). The top layer consisted of a microfluidic channel which was segregated by a micropillar array into a central cell culture compartment and two flanking perfusion compartments (Fig. 28A). The micropillars permitted 3D trapping of cells during seeding and after perfusion culture; the trapped cells formed a 3D cellular construct with about 3 layers of cells [178]. The bottom PDMS layer was fabricated by simply molding PDMS on a commercial optical media, (Fig 28A) which was pre-imprinted with micro-grooves. These commercial optical media offer a readily available and affordable source of micro-grooved substrates and come in different topographical dimensions, ranging from 500 nm – 2 μm. I have previously demonstrated that the micro-grooves on these commercial optical media can efficiently align multiple cell types, including cardiac, muscular and neuronal cells [45]. The microfluidic chip was assembled by plasma bonding the two

layers together (Fig. 28A). Due to the large surface area of the optical media used, we can achieve an 8 cm x 8 cm PDMS micro-grooved substrate, which can simultaneously be bonded to up to 12 microfluidic chips (Fig. 28B). After bonding both layers by oxygen plasma treatment and heating in an oven, we checked for leakages by setting up the chip and perfusing a colored dye through the channels. There was no evident leakage from any of the chips (Fig. 28B), which indicated the robustness of the method to incorporate micro-grooved substrates into multiple microfluidic chips. This method can produce micro-grooved substrates of considerable larger area than the stitching method proposed by Yang *et al* [79]. Larger scale fabrication can be achieved due to the availability of optical media with even larger footprint.
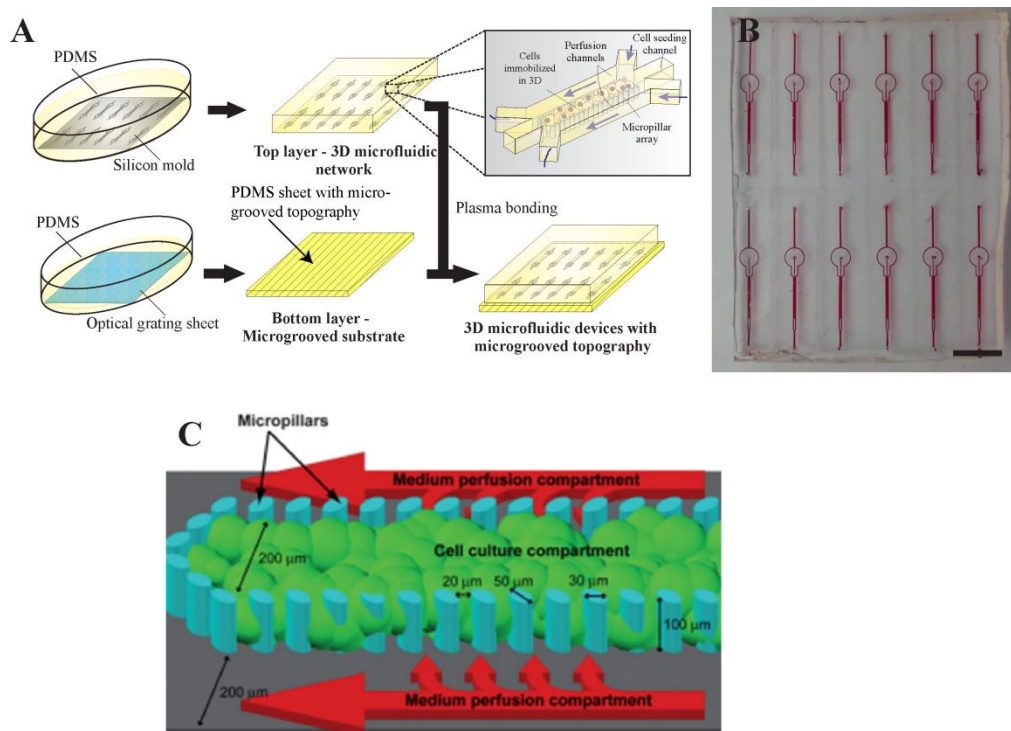


**Figure 28: Incorporating micro-topography into a 3D microfluidic cell culture chip.** (A) Schematic showing the fabrication process of the microfluidic chip. The top layer consisted of a microfluidic channel with a micropillar array to immobilize cells three-dimensionally; while the bottom

layer consisted of a PDMS micro-grooved substrate molded from commercially available optical media. (B) Due to the large surface area of the optical media (15 cm x 30 cm), up to 12 microfluidic chips can be produced simultaneously. Scale bar = 1 cm. (C) Schematic of the microfluidic chip

To determine the fidelity of transferring the topographical features from the optical media to PDMS, AFM images of the PDMS substrate were obtained to assess the grooves. The AFM image showed that the grooves were successfully transferred from the optical media to the PDMS sheet (Fig. 29A). The depth of the PDMS micro-grooves was 225 nm ± 51 nm and the pitch was 2.080 μm ± 0.06 μm. The optical media used as mold had a depth of 282 nm ± 80 nm while the pitch was 2.100 μm 0.05 μm. This represented an 80% fidelity in the transfer of the micro-grooves from the optical media to the PDMS.

B



C
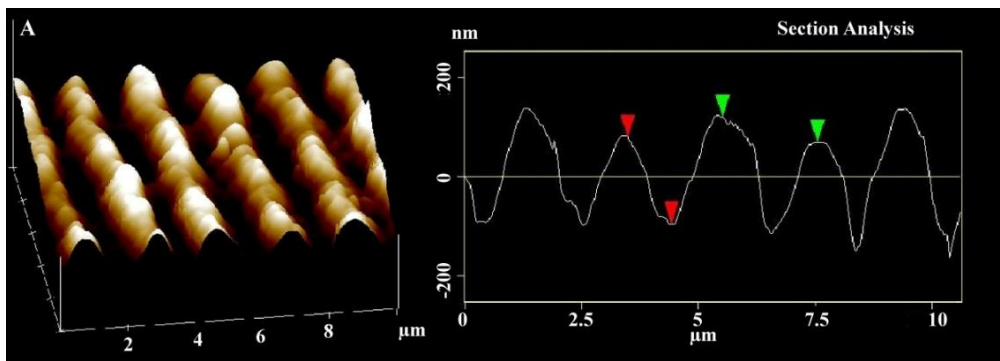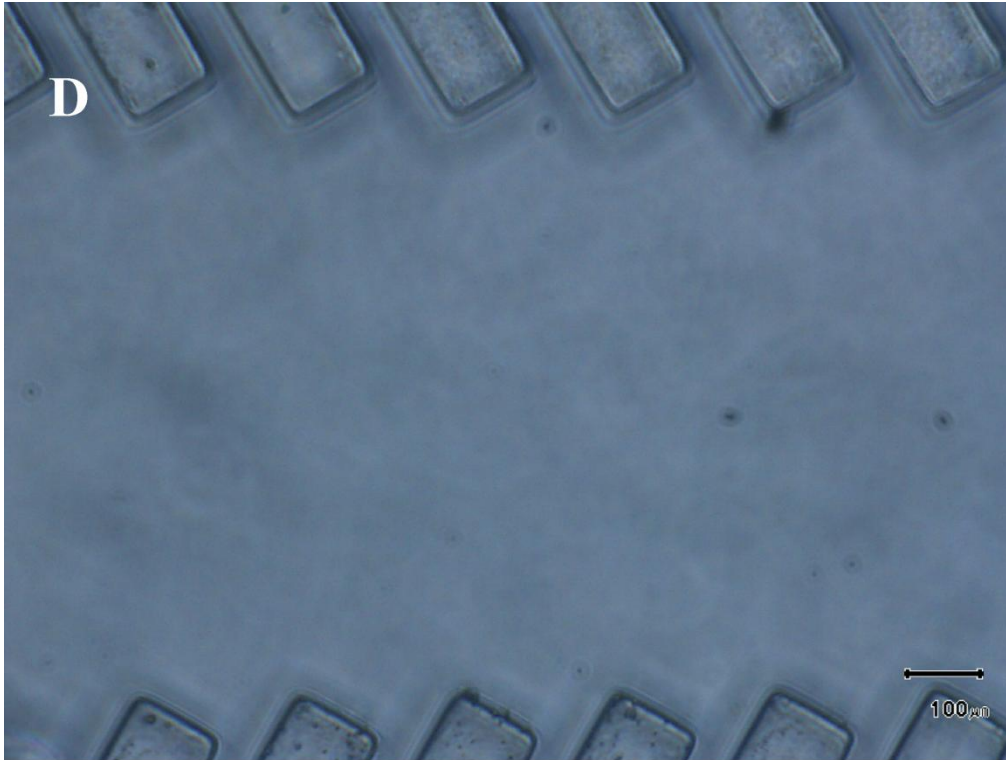
**Figure 29: Characterization of the PDMS micro-groove substrate.** (A) AFM image showing the profile of the PDMS micro-grooved substrate. They maintained the sine wave form of the original commercial optical media. The average depth of the PDMS micro-grooves was $225 \pm 51$ nm and the average pitch was $2.080 \pm 0.06$ μm. (B-D) shows phase contrast images of the microfluidic chips where bottom PDMS substrates were incorporated in three configurations: (B) micro-grooves were parallel to the flow direction, (C) micro-grooves were perpendicular to flow direction and (D) no grooves. Scale bars in (B-D) = 100 μm.

To achieve different configurations of the microfluidic chip, the bottom layer was bonded to the top layer such that the grooves run either parallel (Fig. 29B) or perpendicular to the direction of the flow (Fig. 29C). As a control, chips consisting of a flat PDMS substrate without any grooves were used (Fig. 29D). I validated that the PDMS micro-grooved substrate incorporated into the microfluidic chip could support the attachment and alignment of 2D monolayer of C2C12 cells (Fig. 30). This method provides a

90

simple and robust means to routinely incorporate topographical cues into microfluidic cell culture systems.
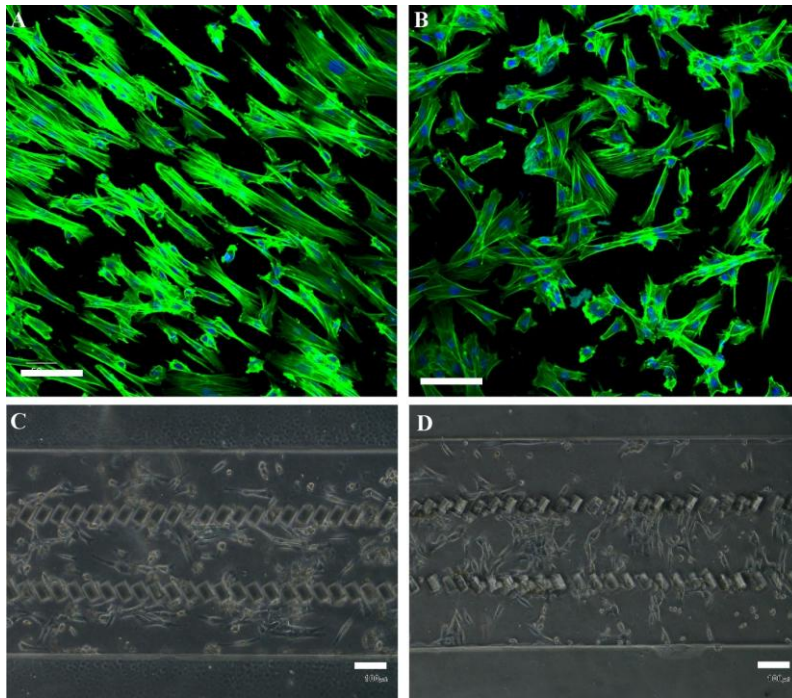


**Figure 30: Monolayer culture of cells on the micro-grooved PDMS substrate**. A) H9C2 cells on microgrooved PDMS. B) H9C2 cells on flat PDMS substrate. C) C2C12 cells cultured in PDMS microfluidic chip with grooves parallel to the flow direction 8 hours after cell seeding. D) Cells cultured with grooves perpendicular to the flow direction

*4.3.2. Alignment of C2C12 myoblast in 2D and 3D cellular constructs*

The alignment of 3D cellular constructs formed from C2C12 mouse myoblasts was examined to determine the topographical effects of the PDMS micro-grooves in the microfluidic chip. During cell seeding, the C2C12 cells were packed three-dimensionally at high density due to the sieving mechanism of the micropillar array. Previous work has validated that various three-dimensionally immobilized cells in this microfluidic chip can maintain high viability for up to 5 days [177, 178, 180]. The C2C12 cells were cultured in

proliferation medium for 3 days to allow remodeling into a 3D cellular construct. Confocal images of fluorescently labeled F-actin revealed that the cells cultured on the flat surface without grooves showed a random orientation of the actin cytoskeleton after 3 days (Fig. 31A-B); however the cells cultured on the grooved substrate were aligned along the direction of the grooves irrespective of their orientation to the flow direction (Fig. 31C-F). An analysis of a 3D confocal optical stack showed that the cell alignment in both the parallel and perpendicular-oriented chips was consistently observed throughout the 15-25 µm thick 3D cellular construct, formed with about 2-3 layer of cells (Fig. 31C,E). The multilayer cell alignment was likely to be a result of layer-by-layer cytoskeletal rearrangement due to the cadherin mediated cell-cell coupling of the C2C12 cells [181]. The bottom layer of the cells, which came in direct contact with the PDMS micro-grooves, could sense the topography and rearranged their cytoskeleton to align along the direction of the groove; the other layers subsequently align on top of the bottom layers. This is in agreement with published literature on the generation of multiple layers of aligned cells in static bulk culture, [182] in which a monolayer of cells was first cultured on micro-patterned polyacrylamide gels and after 2 days, another layer of cells was overlaid on the already existing monolayer. The second layer of the cells aligned along the direction of the first layer of cells, thus forming a double layer of aligned cells.
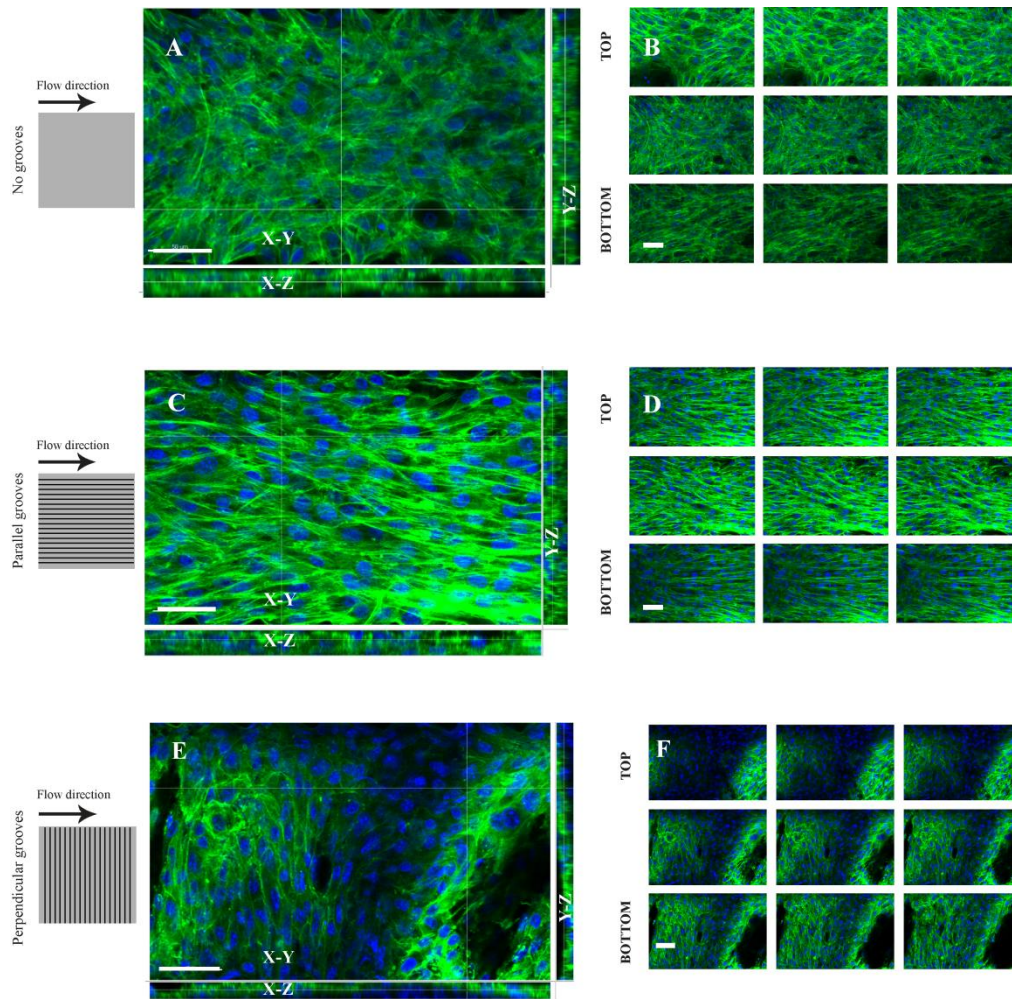
**Figure 31: Alignment of actin cytoskeleton in C2C12 3D myoblast cellular constructs**. C2C12 cells were cultured three-dimensionally for 3 days in proliferation medium with different configurations of the bottom micro-grooved substrates in the microfluidic chip: (A-B) flat surface, (C-D) micro-grooves parallel to flow direction and (E-F) micro-grooves perpendicular to the flow direction. (A,C,E) are the 3D orthogonal views of F-actin and DAPI staining of C2C12 cells. (B,D,F) shows a corresponding selection of individual z-stack images of the C2C12 3D cellular constructs from the bottom to the top of the microfluidic chip. Scale bar = 50 μm.

Cell alignment not only alters the actin cytoskeleton arrangement, it also produces anisotropy in the cell nuclei morphology along the direction of alignment [79, 86]. Hence, I also assessed for cell nuclei morphology and orientation using quantitative image analysis. For each configuration of the

microfluidic chip (*i.e.,* parallel, perpendicular or no grooves), nuclear

measurements were made at 3 different layers of the 3D cellular construct: the

bottom layer in contact with the micro-grooves, the mid-layer and the top

layer furthest from the micro-grooves. The overall alignment of the 3D

cellular construct was taken to be the averaged nuclear measurements from the

3 cell layers.
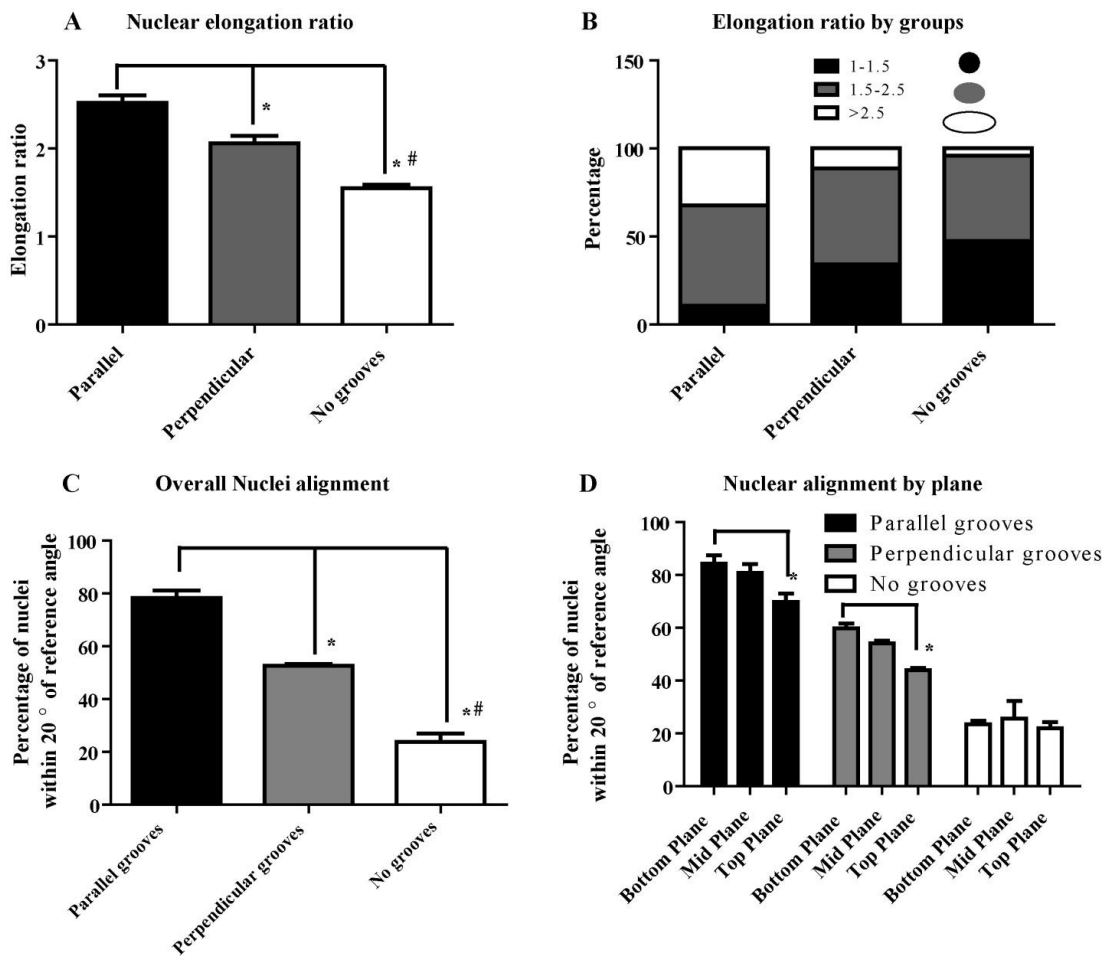


**Figure 32: Quantification of nuclear elongation and alignment in C2C12 3D myoblast cellular constructs.** C2C12 cells were cultured three-dimensionally for 3 days in proliferation medium with different configurations of the bottom micro-grooved substrates before assessing for nuclei morphology and orientation. (A-B) show the nuclear elongation ratio (E.R.). (A) Is the average E.R. of 3D cellular constructs cultured in the three configurations of the micro-grooved substrate. A total of >700 nuclei were analyzed for each configuration. * indicates $p<0.05$ when compared to the chip with parallel grooves, # indicates $p<0.05$ when compared to the chip with

perpendicular grooves. (B) The E.R. of all nuclei in each configuration was binned into 3 groups: $1.0 < E.R. < 1.5$ represents nuclei that are rounded, (ii) $1.5 < E.R. < 2.5$ represents moderately elongated nuclei and (iii) E.R. >2.5 represents very elongated nuclei. (C-D) Show the percentage of nuclei that align to within 20º of the groove direction. (C) Shows the averaged nuclear angle alignment in the 3D cellular constructs. * indicates $p<0.05$ when compared to the chip with parallel grooves, # indicates $p<0.05$ when compared to the chip with perpendicular grooves. (D) Shows the breakdown of the nuclear alignment by imaging planes at different depth of the 3D cellular construct. Three different planes were analyzed (top, middle and bottom) with each plane being about 8-12 μm higher than the previous plane. *indicates $p<0.05$ when compared to the bottom plane.

I calculated the nuclear elongation ratio (E.R.) to study the deformation of the nucleus. This index is a quotient of the long and short axis of the nucleus and is commonly used to assess for nuclear deformation [183]. Nuclear deformation has been shown to alter gene [184] and protein expression, [185] and has been linked to differentiation of progenitor cells and commitment into a particular lineage [186]. An E.R close to one shows a more rounded nuclear morphology while values higher than 1 tend towards an anisotropic ellipse. The average nuclear E.R. of C2C12 3D cellular constructs cultured in different topographical configurations is shown in Fig. 32A. It was much higher for the cells cultured on the parallel grooves, followed by cells on the perpendicular grooves and lowest on cells cultured without grooves. These differences were found to be a result of variations in the proportion of nuclei exhibiting different extent of deformation across the 3 configurations. A breakdown of the overall nuclear E.R. in the C2C12 3D cellular constructs was performed by binning the E.R. of approximately 700 nuclei from each configuration into 3 groups, representative of (1) round nuclei ($1.0 < E.R. < 1.5$), (2) moderately elongated nuclei ($1.5 < E.R. < 2.5$) and (3) very elongated

nuclei (E.R. > 2.5) (Fig. 32B). The results show that the proportion of cells with moderately elongated nuclei in all the 3 configurations was approximately the same, with 48% (no grooves), 55% (perpendicular grooves) and 57% (parallel grooves) falling into this category. However, there was a significant difference in the proportion of cells with round or very elongated nuclei across the 3 configurations. ~50% of the cells cultured without grooves had round nuclei (group 1), while only 35% and 10% of the cells on the perpendicular and parallel grooves respectively were in this group. The reverse was the case for the proportion of cells with very elongated nucleus (group 3), with about 2% (no grooves), 10% (perpendicular grooves) and 33% (parallel grooves) of the cells falling into this group. To determine if these observed differences were due to variability in the transmission of alignment cues across the thickness of the 3D cellular construct, the degree of elongation was investigated in three planes. The results showed that ~38% and 22% of the nuclei in the bottom layer of the parallel and perpendicular chips respectively had a ratio of > 2.5 (group 3). This percentage was reduced in the top layer, with the reduction being more evident in the perpendicular chips (from 22% to 6%) than in the parallel chip (from 38% to 33%). This suggests that transmission of alignment cue was dependent on the distance a cell in the 3D cellular construct from the micro-grooves (Fig. 33).
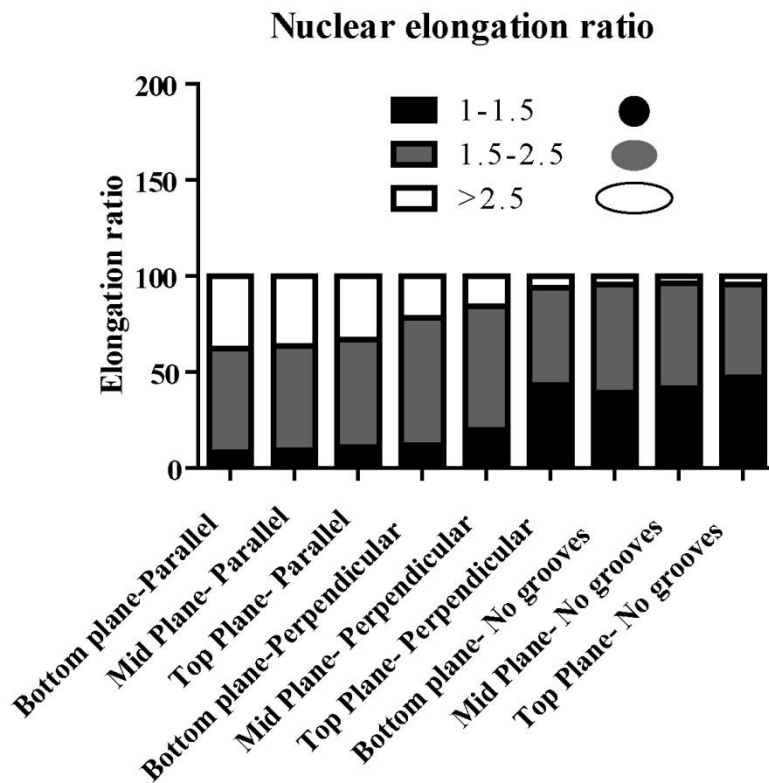
**Figure 33: Nuclear elongation ratio by plane**. The cells nearest to the grooves had a higher elongation ratio for both the cells cultured on the parallel (38% with >2.5 and 54% with 1.5-2.5) and perpendicular grooves (22% with >2.5 and 66% with 1.5-2.5). This ratio reduced in the top layer especially for the cells in the perpendicular chip (6% with >2.5 and 51% with 1.5-2.5) while the parallel grooves reduced but at a lower rate (33% with >2.5 and 56% with 1.5-2.5). The cells cultured on the chips with no grooves had similar orientation. The slight increase in the bottom layer may be due to the effect of the flow on the cells.

To quantitatively measure the extent to which nuclear elongation within the C2C12 3D cellular construct was directed by the PDMS micro-grooves, I determined the direction of cell nuclei orientation. For the chips with micro-grooves oriented parallel to the flow direction, 78% of the nuclei were correctly aligned to within 20º from the orientation of the micro-grooves. For 3D cellular constructs cultured on the perpendicular grooves, 53% of the cells were correctly aligned; while correct alignment for cells on a flat

substrate was about 20% (Fig. 32C). This suggests that the direction along which nuclear deformation occurs was indeed dependent on micro-grooves since nuclear alignment in both parallel and perpendicular configurations were significantly higher than that of the flat substrate configuration. A breakdown of the top, mid and bottom planes for each configuration again revealed that the percentage of nuclei alignment along the micro-grooves reduced from the bottom layer (which was in direct contact with the micro-grooves) to the top layer for both the parallel and perpendicular grooves. However, there was no significant change for the chips with flat surface (Fig. 32D). For the parallel and perpendicular grooves, the strongest layer was the plane nearest to the bottom, which came in direct contact with the PDMS micro-grooves (82% for parallel and 60% for perpendicular) while the top layer was the weakest (70% for parallel and 42% for perpendicular) (Fig. 32D). This further buttresses the fact that the grooves were the key determinant of the alignment.

Both the actin cytoskeleton and nuclear deformation results collectively demonstrated that alignment of 3D myoblast cellular constructs could be achieved by incorporating micro-grooves into the 3D microfluidic chip. Cell alignment was the most efficient in the parallel configuration, where I observed the highest extent of nuclear deformation and alignment along the micro-grooves (Fig. 32A, C). In the perpendicular configuration, even though the actin cytoskeleton was aligned along the micro-grooves, the transmission of the cytoskeletal alignment to nuclear deformation was significantly lower than that in the parallel configuration (Fig. 32A, C), which suggests that other factors in addition to topography can also modulate cell alignment in the

98

microfluidic chip. One of such factors is the shear stress by the fluid flow. Using fluid simulation, I estimated that cells at the periphery of the 3D cellular construct experienced shear stress ranging from 0.3 to 15 dynes/cm$^2$ depending on how far they were away from the micro-pillar array (Fig. 34). This range of shear has been reported to produce cell alignment [106, 187]. Therefore, in the parallel configuration, in addition to alignment cues provided from the micro-grooves, the shear stress provided synergistic cue to align the entire 3D cellular construct. However, in the perpendicular configuration, this shear stress could act antagonistically to the alignment cues from the micro-grooves, causing cytoplasm and nuclear spreading, [79] thereby reducing both the nuclear E.R. and the percentage of cells aligned along the micro-groove orientation. Another possible explanation is the geometry of the microfluidic channel. Aubin *et al* [86] showed that even in the absence of flow, when cells with an innate tendency to align (such as C2C12 and fibroblasts) are encapsulated in a gel with high aspect ratio (50 μm wide x 150 μm long), the cells align along the direction of the long axis. This alignment reduces as the width of the channel increases, thereby decreasing the aspect ratio of the gel strip. Similarly, when the C2C12 cells were trapped within the 200 μm x 1 cm 3D microfluidic compartment, they may experience similar geometrical aspect ratio and tend to align along the long axis. The presence of the perpendicular grooves therefore has to compete against the flow direction and the shape of the cell compartment in the chip in aligning the cells.
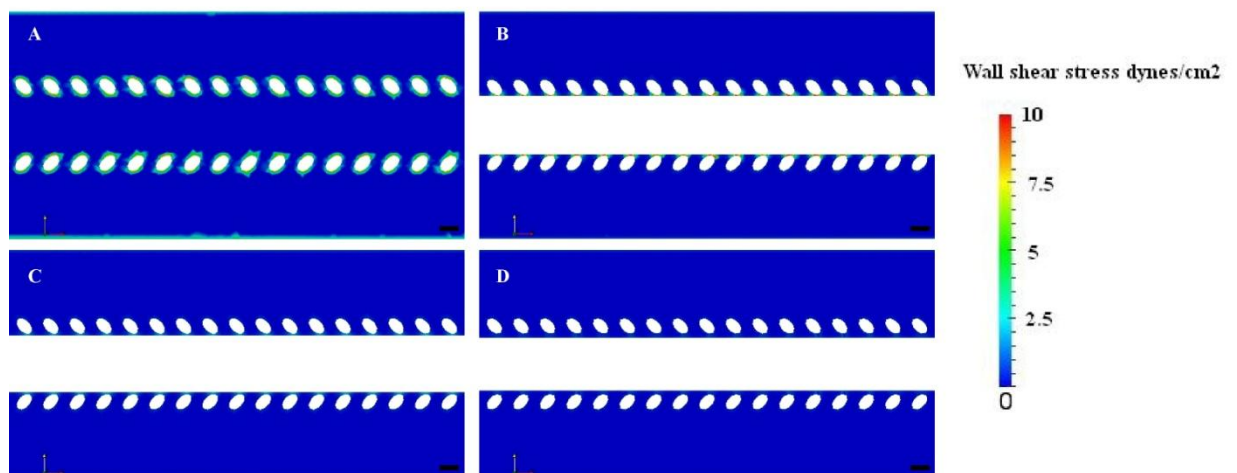
**Figure 34: Shear stress simulation**. A) The fluid shear stress simulation of the chip without cells. B) With cells at 1 μm. C) 5 μm. D) and 10 μm. The cells at the edge experience a range of "0.3 dynes to 15dynes/cm2" depending on the distance to the pillars. Scale bar 50 μm

*4.3.3. Enhancement of differentiation in aligned 3D myoblast cellular constructs*

3D culture has been shown to better mimic the *in vivo* environment and hence represents a more physiologically model for *in vitro* studies [179, 188]. To determine the importance of alignment to a 3D myoblast cellular construct in the microfluidic chip, further investigation into the cells' ability to differentiate into skeletal muscle was carried out. C2C12 cells were seeded into 2 configurations (*i.e.,* flat substrate and parallel grooves) of the microfluidic chip and cultured in proliferation medium for 3 days to allow cells to remodel into a 3D myoblast cellular constructs. Differentiation into skeletal muscle was initiated by perfusing with differentiation medium for 3 days.
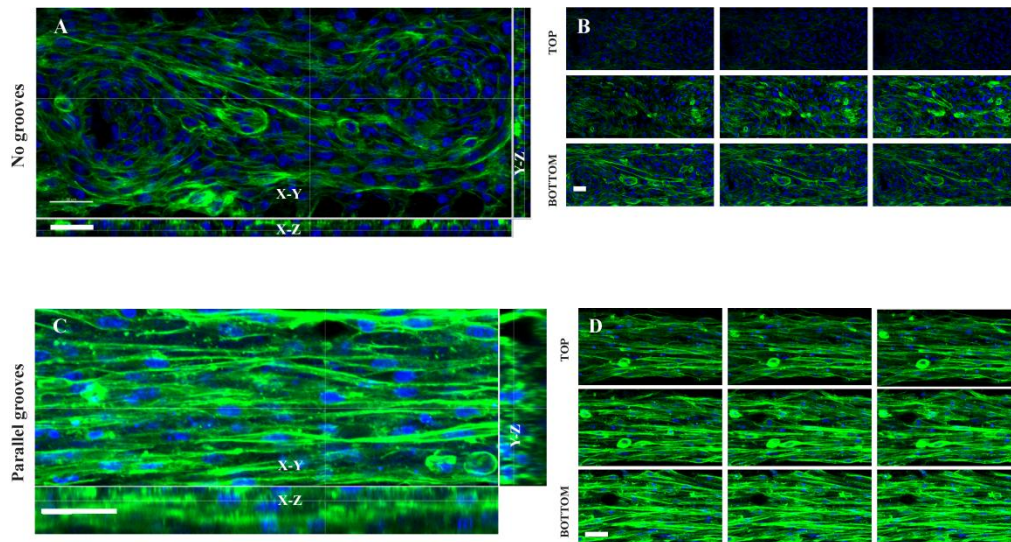
**Figure 35: Morphology of nascent myotubes after differentiation of C2C12 3D myoblast cellular constructs.** C2C12 cells in the microfluidic chips were first cultured for 3 days in proliferation medium to form the 3D myoblast cellular construct, before switching to differentiation medium for 3 days. (A,C) show the 3D orthogonal view of F-actin and DAPI staining of C2C12 cells in the chips after 6 days of perfusion culture using two configurations of the micro-grooved substrate in the microfluidic chips. The configurations were: (A) chips with no grooves, and (C) chips with parallel grooves. (B,D) show a corresponding selection of individual z-stack images of the C2C12 nascent myotubes. They belong to (B) chips with no grooves and (D) chips with parallel grooves. Scale bars = 50 µm.

I first used immunocytochemistry to analyze myotube formation in the 3D cellular construct. Myotube formation is a good indicator of skeletal myocyte's maturation and is enhanced by cessation of proliferation and end-to-end contacts between myoblast [19]. Immunostaining results showed that both the cells on the grooved and flat substrates had started fusing (Fig. 35A-D) with the alignment facilitating a better end-to-end contact of the myoblasts (Fig. 35C-D).
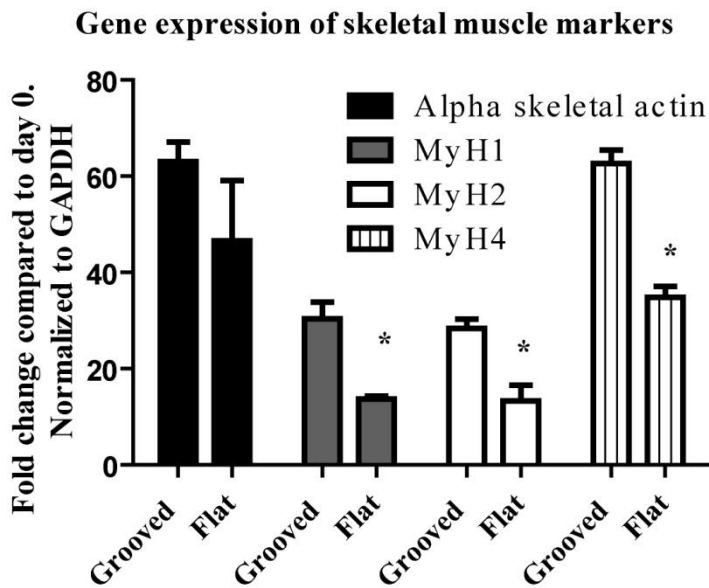
**Figure 36: Gene expression of skeletal gene markers**. C2C12 cells were perfusion cultured for 3 days in proliferation medium and 3 days in differentiation medium before assessing the expression of skeletal gene markers. There was a 1.5-2 fold increase in the gene expression of skeletal muscle markers especially the myosin heavy chains when cultured in chips with grooves. * indicates $p < 0.05$ when compared to flat substrate. Data are average ± S.D. of 3 independent experiments.

I also examined the expression levels of 4 skeletal muscle genes, which are key components of the sarcomere in the skeletal muscle and are used as indicators of myoblast maturation into skeletal muscle [19]. Gene expression results indicated that the 3D myoblast cellular construct cultured on the micro-grooved substrate had a significantly higher expression of the skeletal genes, especially the myosin heavy chains 1, 2 and 4 (Fig. 36). These genes are important for the skeletal muscle development and form part of the contractile apparatus. This result is in agreement with a large number of published literature that shows that alignment enhances myotube formation and maturation of C2C12 cells in both 2D [19] and 3D [189].

C2C12 cells have been used widely as a model to study the development of skeletal muscle and cell alignment since they possess intrinsic potential to align both *in vivo* and *in vitro* [86]. They are also valuable as cell models to study effects of drugs on skeletal muscle contraction, [190] insulin induced glucose metabolism of muscle cells, [190] and muscle regeneration [191]. Engineering 3D cellular constructs of skeletal muscle can therefore serve as platform for drug screening or to better understand the role of skeletal muscle in glucose homeostasis especially in type 2 diabetes.

## 4.4. Concluding remarks

This chapter has demonstrated a cost-effective and scalable method to incorporate micro-topographical cues into microfluidic chips by employing optical media as molds to transfer micro-grooves onto a PDMS substrate, which can be plasma bonded to PDMS microfluidic devices. The large surface area of these optical media makes it scalable for larger-scale production and greatly reduces cost associated with fabricating micro-topography for cell culture applications. By incorporating the micro-topographical cues into a 3D microfluidic chip, aligned 3D myoblast cellular constructs can be obtained. These cells aligned along the direction of the micro-grooves when they were oriented either parallel or perpendicular to the direction of microfluidic flow. The efficiency of cell alignment differed between the 2 configurations due to synergistic or antagonistic modulation by fluid shear stresses. The alignment enhanced maturation of the 3D myoblast cellular constructs into skeletal muscle as it facilitated end-to-end contact of the myoblasts and enhanced the expression of skeletal muscle genes. This will help to improve the biological

performance of tissue-on-chips for drug testing and disease modeling applications.

*Part of the work has been reproduced by permission of the royal society of chemistry <u>Scalable alignment of three-dimensional cellular constructs in a microfluidic chip</u>

# CHAPTER 5: DEVELOPING A HIGH THROUGHPUT *IN VITRO* PLATFORM FOR PHYSIOLOGICAL AND PHARMACOLOGICAL STUDY OF NEONATAL RAT CARDIOMYOCYTES

This chapter highlights the importance of drug induced cardiotoxicity as one of the leading causes of drug withdrawals, and details the importance of *in vitro* platforms in drug development. It then explores the utility of the biomimetic platform to restore cardiomyocyte morphology, enhance their function and increase their potential for drug screening applications. Due to the large surface area of the optical media, they can be scaled up for medium to high-throughput screening.

## 5.1 Introduction

Cardiotoxic drugs can lead to adverse effects on the heart; such as contractile dysfunction, arrhythmias, change in blood pressure and ischemia [192]. These toxic effects are at times life-threatening and constitute one of the major causes of drug withdrawals during the clinical development phases. Of the approximately 35–40% of drugs withdrawn from the market due to pharmacological safety [51, 52], cardiovascular related toxicities was one of the leading cause, making up about 19% of the withdrawn drugs. A significant proportion of these toxicities are due to functional and dose-dependent effects, with about half of the 19% causing arrhythmias [192]. The fact that several cardiac as well as noncardiac drugs have been withdrawn from the market due to cardiovascular toxic effects in humans, although no toxic effects was observed in animals [52, 53, 193], has led the pharmaceutical regulatory

authorities to extend requirements on cardiotoxicity testing [192]. In a meeting held on 23 July 2013, led by the US Food and Drug Administration (FDA), the FDA-sponsored Cardiac Safety Research Consortium and the non-profit Health and Environmental Sciences Institute (HESI), laid out a new set of regulations for cardiotoxic drug assessment [194]. One of the major aspects of the new scheme deals with electrophysiological assessment using the right cell type (human stem cell-derived cardiomyocytes). In summary, the regulation addresses the following issues: 1) Choice of the right cell type - human stem cell-derived cardiomyocytes. 2) Culture conditions that mimic *in vivo* conditions and enhance maturation 3) Use of the right predictive assays and 4) Taking advantage of both *in silico* models and high throughput in vitro models to reduce the cost of drug development

With respect to choosing the right cell type, currently, Chinese hamster ovary (CHO) cells over expressed with HERG ion channels are used to test effect of drugs on ion channels, however, they propose using human cardiac cells for assessing drug induced arrhythmias. These cells which can be derived from embryonic stem cells or induced pluripotent stem cells have all the important ion channels and also maintain a beating phenotype *in vitro* making it a more physiological model. Although these cells hold a great promise for the future of drug testing, one major drawback of current human stem cell-derived cardiomyocytes is their lack of functional maturation *in vitro* [194]. The functional maturation of cardiomyocytes is evidenced in the panel of proteins being expressed as the cells transit from embryonic to adult stage. Some of the important changes include: a switch of the contractile protein

106

from alpha MHC to beta MHC, an increase in expression of the L-type calcium current channel (up to 3 fold), additional expression of inwardly rectifying potassium channel, a switch of the dominant mode of intracellular calcium release from IP3R to RyR and the expression of cardiac specific sodium channel [72, 195]. The mitochondria also increase in mass with changes in mitochondrial ultrastructure as evidenced by greater number of closely packed cistae and more electron-dense matrix [163]. To address this issue numerous sets of culture conditions have been proposed to enhance maturation and to mimic the native tissue more closely [192].

The selection of a suitable species and cell culture condition by replicating key *in vivo* environment is crucial for drug development [192]. In the case of cardiotoxicity, the heart has a complex hierarchical organization of the molecular, electrical, topographical and mechanical signal and it would be ideal for *in vitro* models to factor in all these signals [196]. While it is currently not feasible for *in vitro* models to exactly match the native tissue, certain physiological parameters have been shown to be important for different *in vitro* applications. Hence, instead of attempting to mimic the entire complexity of the organ, a reasonable goal would be to replicate the tissue-specific architecture and a subset of most relevant functions in a way predictable of human physiology [196]. One of such important physiological parameters is cardiac anisotropy. Native ventricular cardiomyocytes (VCMs) are aligned in a highly organized fashion such that electrical conduction is anisotropic for coordinated contractions. Restoring this alignment *in vitro* has been shown to restore *in vivo* like conduction velocity and to be a more

accurate model for prediction of drug induced arrhythmias (the most common manifestation of drug induced cardiotoxicity) [73]. In addition, cardiac cell alignment *in vitro* has been shown to restore other structural and functional properties of the native VCM such as sarcomeric organization [10], length to width ratio [197], calcium handling [72], and gap junctional protein distribution [10]. Alignment also enhances maturation [198], and force of contraction [65] in cultured cardiomyocytes. Consequently platforms that factor in cardiac cell alignment *in vitro* would be useful for efficacious drug discovery and development [73].

Choosing the right set of predictive assays *in vitro* would also help increase the potential of *in vitro* platforms for drug screening. Although arrhythmias are the most common manifestation of drug induced cardiotoxicity, and the most commonly tested, companies and scientists recognize the importance of other types of cardiotoxicity in drug safety testing [194]. In an internal study of roughly 1,000 compounds that had failed at various stages in discovery, AstraZeneca found that only about 25% had a direct impact on cardiac electrophysiology (pro-arrhythmias). The rest affected functional and structural aspects of the cells, such as mitochondrial activity and calcium homeostasis which are fundamental aspects of the biology of cardiomyocytes [194]. Hence it is proposed that more than one assay be used to reflect the key players in drug induced cardiotoxicity [194]. Patch clamp method is still currently used as one the most sensitive methods to detect changes to the ion channels, however, it requires expert skills, specialized equipment and most importantly it is low throughput [64]. Viable

alternatives for predicting drug induced cardiotoxicity include the use of multi electrode array, calcium imaging and mitochondrial toxicity kits [64]. These assays can be scaled up for high throughput assessment and are useful for the early stages of drug discovery [64]. The multi electrode array detects field potential of a group of cells and can be used to assess the effects of drugs on the field potential duration [199, 200]. Although this is not as sensitive as the patch clamp, the field potential duration correlates to the action potential duration measured by patch clamp and hence serves similar purpose [199, 200]. It is also easier to manipulate and can be scaled up especially for high throughput measurement [199, 200]. Another important assay for cardiotoxicity is calcium flux. Calcium is a very important ion for the cardiac function. It is the principal ion in charge of the excitation-contraction coupling of the heart. Excitation–contraction coupling is a well-described, fundamental property by which a cardiomyocyte's ionic (excitation) properties tightly coordinate its mechanical (contractile) function [201]. The process starts with the opening of voltage gated L-type calcium channels following membrane depolarization. The transient opening of these channels allows a small amount of calcium to flow into the cell through dihydropyridine receptors that are strategically localized in close spatial proximity to the sarcoplasmic reticulum. This calcium entry initiates a positive feedback process of calcium-induced calcium release in the sarcoplasmic reticulum through ryanodine receptors, which form functional units with surface voltage gated L-type calcium channels, resulting in myofilament contraction [202]. Alterations in calcium homeostasis in the cardiac cell have been shown to affect the membrane potential due to deleterious effects on the sodium-calcium exchanger, and

have also been implicated in the pathogenesis of arrhythmias and contractile dysfunction [60]. It can therefore be said that cardiac toxicity presenting as mitochondrial toxicity, cardiac contractile failure, myocardial ischemic events, and cardiac arrhythmias may in part be due to changes in intracellular calcium homeostasis and hence calcium flux measurement is a key assay for cardiotoxicity drug screening [60]. Calcium can be measured by fluorescent probes and thus direct visualization of Ca2+ dynamics in cardiomyocytes is emerging as an ideal *in vitro* high throughput model for assessing drug-induced cardiotoxicity because it integrates the electrophysiological and signaling events leading to muscle contraction. Dynamic calcium changes have been validated for predicting arrhythmias and contractile dysfunction in a number of cardiotoxic drugs [64], it can be used to assess beating rates and hence can be used to study the drugs that have chronotropic effects on cardiac cells [57].

In summary the current trend in predicting drug induced cardiotoxicity is geared towards developing a cost-effective high throughput platform with the relevant culture conditions, appropriate cell type and one or more predictive assays that gives a holistic readout of the necessary end points for assessing drug induced cardiotoxicity. This study shows that commercially available optical media integrated into 48-96 well plates can be used as high throughput platforms for the study of drug induced cardiotoxicity using neonatal rat ventricular cardiomyocytes. The commercially available media induce cell alignment which in turn restores *in vivo* like cylindrical morphology, sarcomeric organization, gap junctional protein distribution and

110

calcium handling of the cardiomyocytes. The platform is amenable to multi electrode array and calcium imaging and by using these assays; we show both positive and negative chronotropic effects of paradigm drugs to the cardiomyocytes. Although neonatal rat cardiomyocytes have been used, this platform can also be used for human induced pluripotent stem cell-derived cardiomyocytes.

## 5.2 Materials and methods

### 5.2.1 Cardiomyocyte isolation

Hearts were removed from 1- to 2-day-old neonatal Sprague-Dawley rats and placed in calcium and magnesium free HBSS (Sigma, Singapore H4891-10X1L) buffer on ice. The atria were removed and the ventricles were washed several times with cold HBSS buffer. The ventricles were subsequently minced with dissecting scissors. The cells were incubated first with 1mg/ml trypsin for 2 hours and then dissociated at 37°C with a collagenase type 2 at 0.8 mg/ml (Worthington Biochemical) in HBSS for 5 serial incubations at 30-min periods for each digestion. During the digestion, triturating the tissue through a 1ml pipette tip mechanically disrupted the tissue. The cells released after the first digestion were discarded (fibroblast and debris-rich mixture), whereas the cells from subsequent digestions were added to 25 ml of DMEM and kept on ice. After final collection, the cells were filtered through a 100 um sieve and pelleted by centrifugation (150 g for 5 min at room temperature). The supernatant was discarded, and cells were re-suspended in complete medium and pelleted again at 150g for 5 minutes. After the second centrifugation, the supernatant was discarded, the cells were re-

suspended in DMEM and the resulting cell mixture was preplated twice for 45 mins each in a 37°C $CO_2$ incubator to plate out the fibroblasts. The remaining enriched myocytes were then plated at high density (100,000 cells/cm$^2$) and cultured in DMEM with 10% FBS for 2 days before switching to DMEM with 1%FBS (maintenance medium). The optical media was prepared as explained previously [45]. A solution of fibronectin (10ug/ml) and gelatin (1mg/ml) was used to coat the optical media for 1 hour at 37°C before cell culture.

### 5.2.2 Calcium imaging

Neonatal rat ventricular myocytes were incubated with 5µm Fluo-4 AM (Invitrogen) and pluronic F-127 (0.1%; Invitrogen) for 30 minutes at 37°C. Myocytes were subsequently washed three times in Tyrode solution (Sigma Singapore, T2145-10X1L) to remove dye residues and incubated in DMEM for 15 minutes to de-esterify. The experimental dish was mounted on the stage of an upright Zeiss LSM510 confocal microscope (Carl Zeiss) and myocytes were observed through a 60x water immersion objective. Line scanning was performed at suitable regions with the myocytes spontaneously beating. A 488-nm wavelength laser was used to excite the dye, and signal was collected at 515 nm. The scanning line was oriented transversely, across the width of the cell and away from the nucleus to monitor the cytosolic component of the calcium transients in high temporal resolution (500 Hz). Fluorescence signals were analyzed using Olympus software and Excel. Peak and decay times are defined as the time for the calcium signal to reach its peak value and then decay by 50%, respectively. To minimize the toxicity of Fluo-4, experiments were conducted within 1 hour after dye loading.

*5.2.3 Determination of Cell length, width, length to width ratio and sarcomere length*

Confocal images of cultured cardiomyocytes were taken with a Zeis microscope. Cell length and width were quantified using ImageJ (National Institute of Health). Myocytes were measured along their long axis to determine cell lengths whereas the width of cells was defined as the length along the perpendicular axis with respect to the major. On average, approximately 200 cells were analyzed per condition. Cells selected for measurements were as intact as possible

*5.2.4 Western Blot*

Protein measurements using Western blot were carried out with cell lysate after 7 days in culture. A mixture of RIPA (Radio-immunoprecipitation Assay) buffer (Sigma, Singapore R0278) and protease inhibitor (100:1) was added to the cell culture after discarding the medium. The cell lysate obtained was centrifuged at 14,000 rpm for 15 mins. Protein content was determined using Bradford assay (Biorad) and equal amounts of protein samples (40mg) were separated on a 10% SDS–PAGE in 1X Tris Glycine, and transferred onto a 0.22mm nitrocellulose membrane overnight in 1X Tris-buffered saline (TBS) with 10% methanol. To ascertain equal loading and transfer efficiency, the membranes were stained with Ponceau S. The Ponceau S stain was washed off the membrane and was placed in blocking buffer (2% skimmed milk prepared in 1XTBS with 0.01% Tween 20 (1TBST) for 1 h at room temperature with shaking. The membrane was subsequently washed 3 times in 0.05% TBST and treated with mouse anti N-Cadherin 1:750 (BD Biosciences

Singapore 610921), Mouse anti Connexin 43 1:1,000 (Merck Singapore MAB 3067), Mouse anti SERCA 1:750 (Sigma Singapore S1314), Mouse anti GAPDH 1:1,000 (Santa Cruz Singapore SC 59540), Mouse anti Troponin T 1:1000 (Thermo Scientific Singapore MS-295-PO) all diluted in 0.01% TBST for 2 h at RT. After the primary antibody incubation, the membranes were washed 3 times in 0.05 % TBST and treated with goat anti-mouse IgG-HRP (Santa Cruz sc-2005) 1:10,000 in blocking buffer, for 1 h at RT. The membrane was developed using SuperSignal West Pico Chemiluminescent solution (Thermo Scientific) and the band intensity was measured using ImageJ (WS Rasband, National Institutes of Health, Bethesda, MD).

*5.2.5 RNA isolation, cDNA synthesis and qPCR analysis*

Cells were lysed using RLT buffer from Qiagen (Qiagen, Singapore, cat no 79216). Cell lysate was collected and RNA isolation was done and total RNA was reverse transcribed to cDNA according to manufacturer's protocol. Custom designed primers were used for the quantitative PCR and the reactions were performed using both Roche lightcycler and Bio-Rad real time system. Analysis of each gene was performed using the quantitative $\Delta\Delta CT$ method. Transcript levels were first normalized to the house keeping gene GAPDH and expressed as relative level to that on the flat surface.

*5.2.6 Immunocytochemistry*

Cells were fixed with 3.7% PFA for 10 minutes at 37ºC, permeabilized with 0.1% Triton-X 100/PBS for 30 minutes at room temperature and blocked with 2% bovine serum albumin for 2hours at room temperature. Washing after

each step was performed by using 0.1% triton-x 100/PBS three times at 10 minutes each.

All incubations with primary antibodies were done overnight at 4ºC. Primary antibody concentrations were as follows: 1:200 for mouse anti alpha sarcomeric actinin (A7811, Sigma, Singapore), 1:200 for rabbit anti connexin 43 (clone MY32, M4276, Sigma, Singapore), 1:200 for mouse anti N Cadherin (BD Biosciences Singapore 610921), 1:200 mouse anti Vinculn. After primary incubation, samples were washed three times as explained above and incubated with secondary antibodies for 1hr at room temperature. The dilution used for secondary antibody was 1:250 Alexa Fluor® 546 Donkey anti mouse IgG (H+L) (A100436, Invitrogen, Singapore). Alexa fluor phalloidin 488 (A12379, Invitrogen, Singapore) was added during the secondary antibody incubation for F-actin visualization. The samples were washed three times and counter stained with DAPI (D9542, Sigma, Singapore) at 1μg/ml for 10 minutes at room temp. After washing, the samples were mounted and imaged with a confocal microscope.

### 5.2.7 Drug treatment

Verapamil a calcium channel blocker and Isoproterenol an adrenergic agonist were used to assess drug response. 1000x Verapamil stocks in DMSO were prepared to a concentration of 0.75 mg/ml while 100x Isoproterenol stocks were prepared in distilled water to a concentration of 0.75 μM.

### 5.2.8 Statistical Analysis

Statistical differences were performed using Graphpad prism 5 (GraphPad Software Inc. California, USA). Paired t-test studies were

performed comparing cells cultured on the flat surface to cells cultured on the grooved surface for morphometric analysis (cell length, width, length to width ratio), gene expression and western blot. $p<0.05$ was considered significant.

## 5.3 Results and discussion

### 5.3.1 Cardiomyocyte alignment on grooved optical media

Rat neonatal ventricular cardiomyocytes were isolated and cultured on the optical media. Cells were allowed to attach for one day in plating medium containing 10% FBS. Unattached cells were removed and the medium replaced with plating medium for another 24hrs. This is to allow for some proliferation of the neonatal rat cardiomyocytes. From third day onwards, the cells are maintained in maintenance medium containing 1% FBS. This has been shown to reduce fibroblasts overgrowth and to enhance cardiomyocyte maturation. After 7 days in culture, the cells are either fixed for immunocytochemistry or lysed for both western blot and RT-PCR experiments. Fig. 37 shows that the cells on the grooved surface had a predominantly spindle shape with a more uniform orientation (Fig. 37A-B) while those on the flat surface were pleomorphic without any particular direction or orientation (Fig 37C-D). There was also a more uniform and aligned sarcomeric structure in the cells on the grooved substrate (Fig 37A).
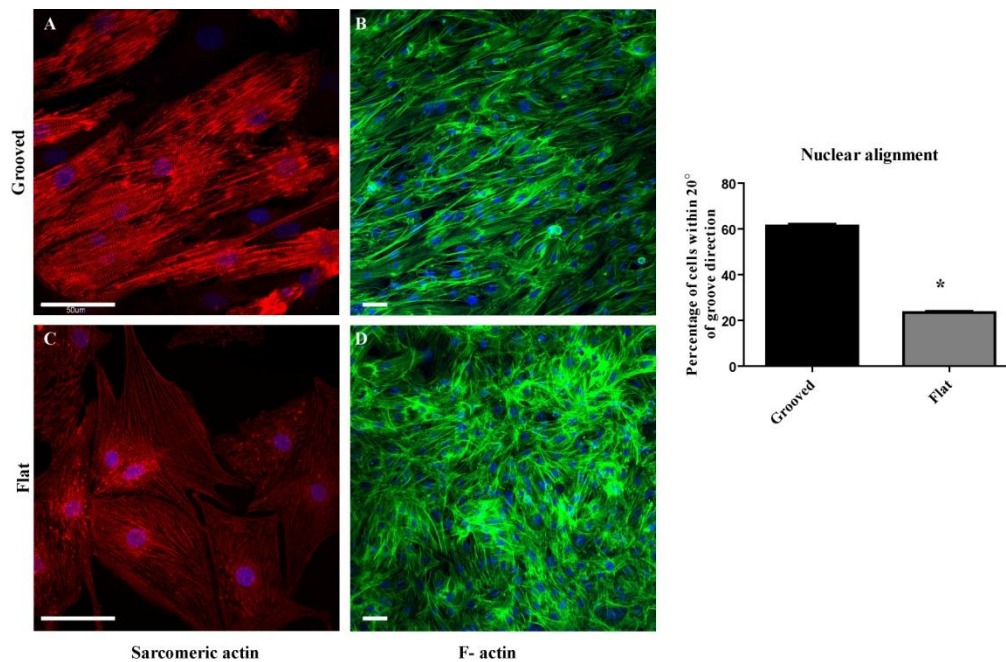
**Figure 37: Cardiomyocyte alignment and sarcomeric structure**. Alpha sarcomeric actinin for cells on: A) grooved surface and C) flat surface. F-actin staining for cells on: B) grooved surface and D) flat surface. E) Nuclei alignment, more than 60% of cells on the grooved surface align within 20° of groove direction. * indicates *p*< 0.05 when comparing grooved to flat surface. Scale bar 50μm.

An analysis of nuclear orientation revealed that cells on the grooved surface had about 60-70% of the nuclei within 20° of the groove direction (Fig 37E). This value was significantly higher than the cells on the flat surface. These results are consistent with numerous published results on the effect of grooves on cell alignment [45]. Grooves have been shown to be biomimetic in inducing alignment of cardiomyocytes *in vitro* as the collagen fibers in the myocardium are arranged in such a way that they form grooves and ridges. Cardiomyocyte cell alignment *in vitro* is hence a desired feature for cardiac tissue engineering.

*5.3.2 Morphometric analysis*

Cell length, width, length to width ratio and sarcomeric structure were analyzed. Our results showed that cells cultured on the grooved surface were longer and thinner with a higher aspect ratio than cells cultured on flat surfaces which were shorter and broader (Fig. 38A). The aspect ratio of cells cultured on the grooved surface ranged from 5:1 to 6:1, while those cultured on flat surface was about 2:1 (Fig. 38B). Cardiomyocytes' shape is important for its ultimate function and this relationship has been studied both in vivo and *in vitro* [197]. The heart actively remodels its architecture in response to physiological and pathological changes. A number of cardiomyopathies are known to manifest with altered aspect ratio of the cardiomyocytes, these changes lead to reduced contractile function of the heart [69]. Healthy ventricles have an aspect ratio of 6-7:1. This ratio can increase or decrease depending on the pathology [197]. In an interesting study, Kuo et al used fibronectin patterning to engineer cardiomyocytes with aspect ratios of 1:1, 3:1, 5:1, 7:1 9:1 and 11:1 [197]. Their results revealed that the cells with healthy aspect ratio 5-7:1 exerted the greatest tractional force and had better contractility along the longitudinal axis [197]. They also showed that cells with this aspect ratio had a better calcium handling apparatus as the peak and decay time was considerably lower than cells with either very high or very low aspect ratio [197].
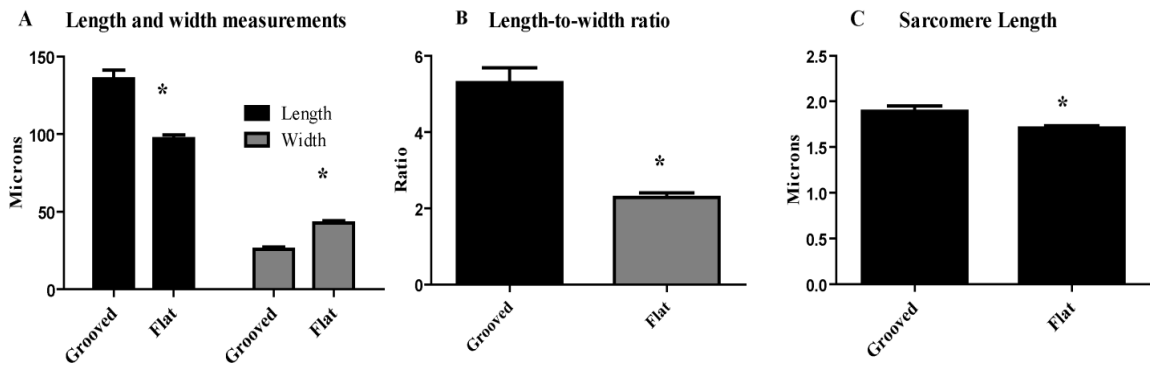
**Figure 38: Morphometric analysis of the cardiomyocytes on both sides of the optical media**. A) Length and width measurements. Cells on the grooved surface were longer and thinner. B) Length-to-width ratio. Cells on the grooved surface had a higher length-to-width ratio. C) Sarcomere length. Cells on the grooved surface had a more mature sarcomere as evidenced by the longer sarcomeres. * indicates $p<0.05$ when comparing grooved to flat surface.

Furthermore, I assessed the sarcomere length in cells cultured on both flat and grooved surfaces. Sarcomere length is a good indicator of the cardiomyocytes mechanical function [203]. A sarcomere is the functional unit of cardiomyocytes containing both the thick and thin filaments. The mean sarcomere length is defined as the spatial fundamental period of repeating patterns of sarcomeres in a microscopy image of a cardiomyocyte [204]. Sarcomere length is an indicator of cell maturation. Our results indicate that the cells on the grooved surface had a longer sarcomere length (Fig. 38C), this suggests better mechanical function as it would lead to higher contractile force amplitudes [205].

*5.3.3 Cell-substrate and Cell-Cell communication*

Gap junctions provide a low-resistance pathway for propagation of electric signals such that the heart can beat synchronously. In the heart

connexin 43 are the principal gap junction proteins [206]. In early life, the gap junctions are uniformly distributed, aligning along the perimeter of the cardiomyocytes. As the cardiac cells mature into adult heart, the gap junctions localize principally at the end of the cells and to a lesser extent along the sides of the cardiomyocytes [206, 207]. Immunostaining of connexin 43 indicates that the gap junctions (GJ) of the cardiomyocytes on the grooves were arranged along the perimeter of the cardiomyocytes parallel to the grooves as opposed to the random orientation on flat surfaces (Fig. 39A-B). This disposition of the GJ will ensure an anisotropic propagation of action potentials as is present *in vivo* [73]. It also reduces the possibility of re-entrant arrhythmias which is more common in conditions where the CX-43 is disorganized [73].

N-Cadherin, a cell-cell contact protein also plays a role in cardiomyocytes structure. It is the major transmembrane constituent of the adherens junction, highly expressed in the heart and principally localized to intercalated disks [208]. It has been proposed that this molecule is necessary for myofibril organization [209]. N-Cadherin is also important for mechanosensing, polarization, differentiation of the cardiomyocytes and transmission of contractile forces across the cardiac tissue [210]. In hypertrophic cardiomyopathies, the ordered arrangement of the N-cadherin is lost leading to a severe disarray of the N-cadherin localization and expression; this disarray may lead to arrhythmias in the cardiomyocytes [208].
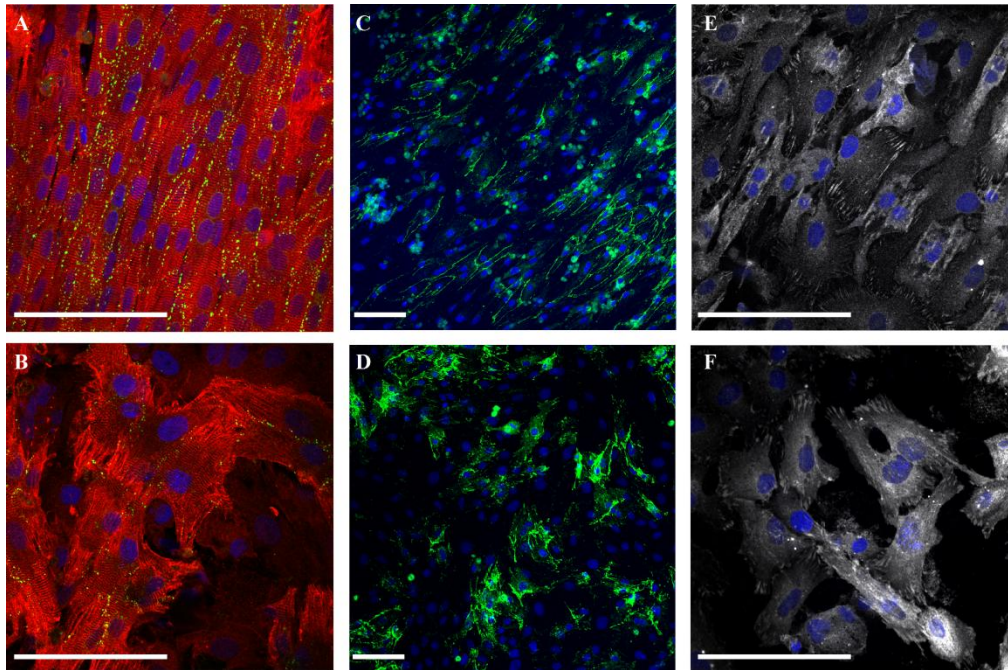
**Figure 39: Cell-cell and cell-substrate interactions**. Cells on the grooved surface: A) Connexin 43, C) N-Cadherin, E) Vinculin. Cells on the flat surface: B) Connexin 43, D) N-Cadherin, F) Vinculin. Scale bar 100μm.

This suggests that the spatial organization of the N-Cadherin protein is important for proper functioning of the cardiomyocytes. Our results indicate that cells cultured on the grooved substrates have a more organized spatial disposition of the N-cadherin molecules (Fig. 39C-D). This disposition is similar to what is seen *in vivo*; in contrast, the random disposition of the N-cadherin on flat substrates resembles that seen in cardiac "disarray".

Cell-ECM interactions play a role in assembly, re-arrangement and maintenance of cardiomyocyte architecture, and vinculin is one of the key focal adhesion molecules required for cardiomyocytes cell-ECM interaction. These cell-ECM adhesion sites serve as nucleation sites for the assembly of myofibrils [211]. In addition, the vinculin/Sarcomeric actinin/ F-actin

121

association is crucial for stabilization of the myofibrils [212] The ordered orientation of the vinculin hence plays a role in sarcomere alignment as the myofibrils follow the focal adhesion complexes. This would in turn lead to a directional arrangement of the sarcomeric proteins [213]. Our results indicate that the vinculin/focal adhesion plaques are also aligned along the direction of the grooves and this forms a basis for a more ordered arrangement of the myofibrils within the cardiomyocytes (Fig. 39E-F).

*5.3.4 Gene and Protein expression*

Using qRT-PCR, I assessed expression of cardiac-specific structural genes in cells cultured on both grooved and flat substrates after 7 days in culture. The genes assayed were: Alpha cardiac actin, Troponin T, and Myosin light chain 2V (MLC2v). Though the cells cultured on grooved substrates showed slightly higher patterns of gene expression, there wasn't a significant difference except for MLC 2V and troponin T (Fig 40A). The western blot revealed similar results showing no significant difference across both substrates (Fig 40 B-C). These results are similar to previous studies comparing grooved and flat substrates [72]. It seems that the major differences in function found in neonatal rat cardiomyocytes on grooved substrates are predominantly due to the structural reorganization of its contractile and cell-cell communication proteins. The sarcomeric alignment produced as a result of structural reorganization ensures better force of contraction, faster anisotropic propagation of action potential, better calcium handling apparatus and reduced excitation threshold [72, 214].
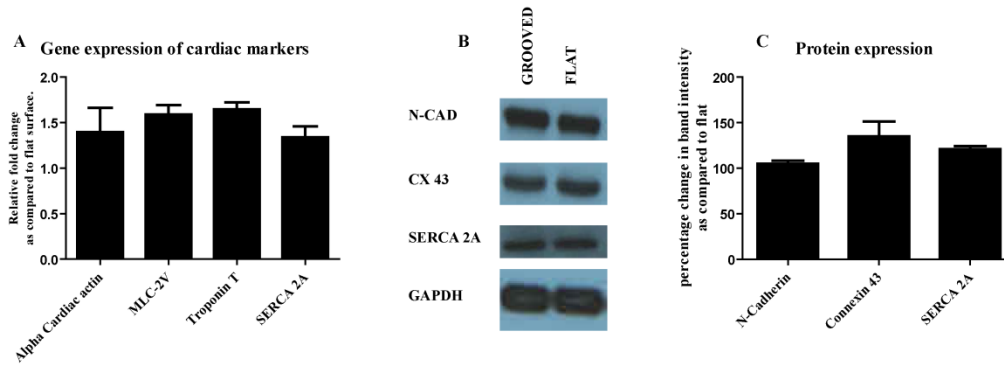
**Figure 40**: **Gene and protein expression.** A) Gene expression of cardiac specific markers. There was about 1.5 fold increase in the cardiac specific genes when cultured on grooved substrates.* means *p*<0.05 as compared to flat substrate. B) Representative western blot bands. C) Relative band intensity of western blot bands.

*5.3.5 Calcium transients*

In cardiomyocytes, contraction begins by the opening of the voltage-sensitive L-type Ca2$^+$ channels (Ca$_v$1.2) on the sarcolemma, this influx of calcium into the cytoplasm triggers the opening of the ryanodine receptors (RyR), which results in a significant Ca2$^+$ release, in a process of Ca2$^+$-induced Ca2$^+$ release (CICR) [215]. The calcium binds to the troponin and causes a conformational change in the tropomyosin which subsequently leads to contraction [215]. A better calcium handling apparatus as evidenced by faster time to peak and faster time to decay is characteristic of more matured cells *in vitro* [72]. In the heart, it has also been shown that prolonged mechanical unloading of the heart leads to an altered calcium handling. Neonatal rat ventricular cardiomyocytes cultured on grooved substrates had a shorter time to 50% transient decay than cells cultured on the flat substrates (Fig 41B). This finding is also in line with previously published literature [72]. Fig 41A shows a characteristic calcium flux tracing.
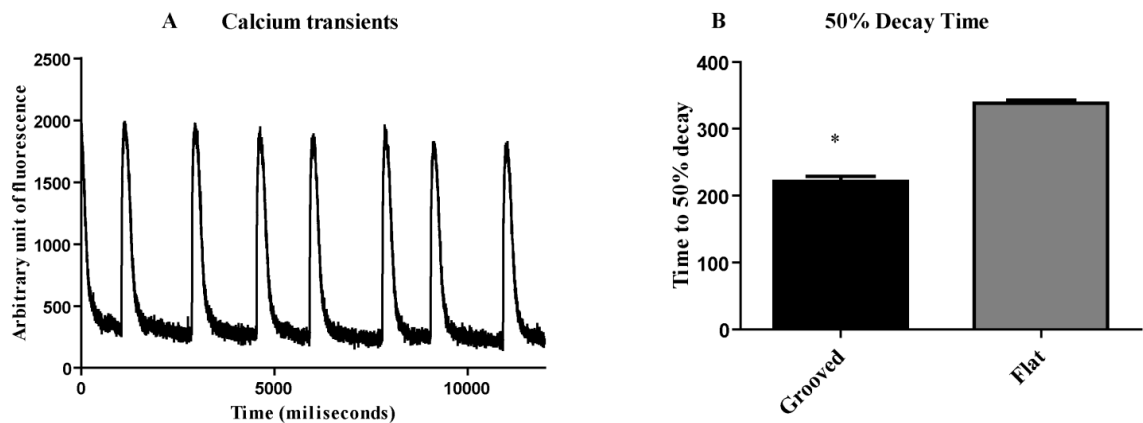
**Figure 41: Calcium imaging**. A) Representative calcium flux measurement on grooved surfaces. B) Time taken to 50% decay of fluorescence intensity. Cells on grooved surface have a faster time to fluorescence decay. * indicates $p<0.05$ when comparing grooved to flat surfaces.

One of the possible reasons for this finding is the co-localization of the $Ca_v1.2$ and RyR which may be enhanced in cells cultured on grooved substrates [72]. In ventricular myocytes, the spatial relationship between the L-type $Ca2^+$ channel and RyR has been shown to enhance the CICR [215]. Other possible causes explaining the more mature calcium handling apparatus of the cells on the grooved substrate are an enhanced expression of the channels and proteins involved in calcium cycling and an increase in diastolic calcium found in such cells at higher frequencies [72, 216]. The findings in our gene expression studies do not support the theory and I didn't study the diastolic calcium content in the cells.

*5.3.6 Pharmacological studies*

To study the utility of our platform for drug screening, we tested 2 paradigm drugs: Verapamil a calcium channel blocker (negative ionotrope and chronotrope) and Isoproterenol (positive chronotrope). A number of assays

have been identified as important for cardiotoxicity drug screening. Of these

assays, scientists have highlighted three important parameters: Alterations in

cell membrane and mitochondrial membrane potential, Alterations in calcium

homeostasis, and ATP depletion [67]. In view of this, two assays were chosen:

Multi-electrode array (High throughput membrane potential assessment) and

Fluo-4am (calcium imaging) and show that our platform can be used for these

assays *in vitro*.
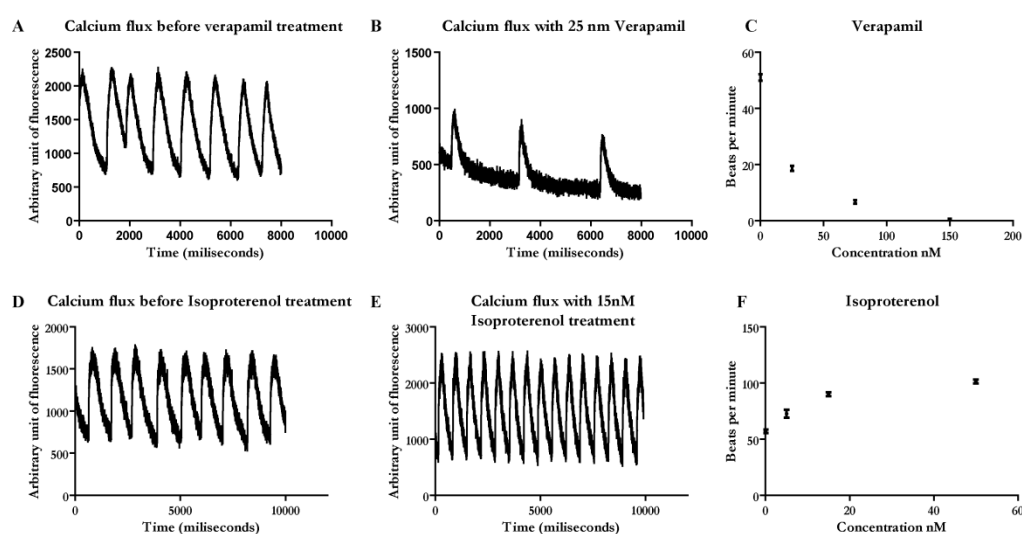


**Figure 42**: **Drug response using calcium imaging.** A) Calcium flux before treatment with verapamil. B) Calcium flux after treatment with verapamil.

Using calcium transients, our results indicate that the NRVM respond

to calcium channel blockers by a reduction in beating rate (Fig 42 A-B). There

was a dose dependent reduction in beating rate upon treatment with verapamil

(Fig 42 C). Conversely, there was an increase in beating rate when the NRVM

were treated with Isoproterenol which is a positive chronotrope (Fig 42 D-F).

Besides using the calcium transients as a read out, we also used the MEA to

assess beating rate of the NRVM. Preliminary results with the MEA show that

our platform can be used for the readings (Fig 43). In addition, video of the

beating cardiomyocytes before and after addition of verapamil was captured.

Video 2 and 3
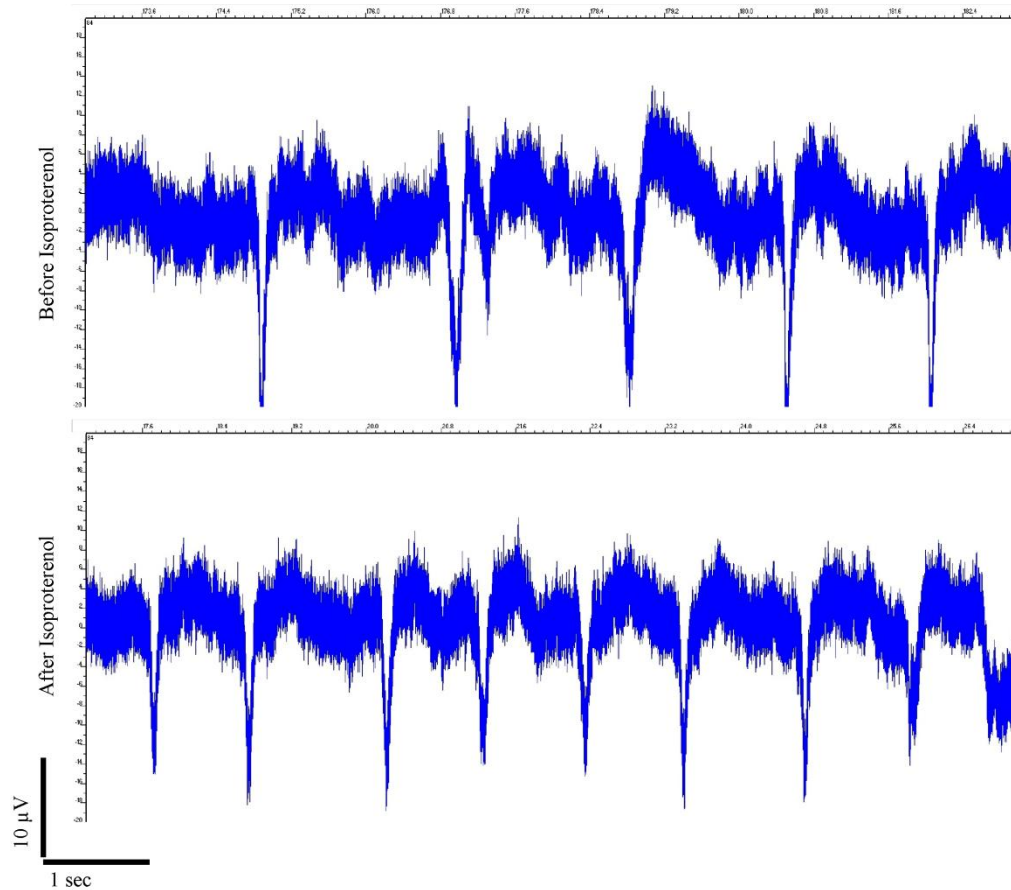


**Figure 43: Multi electrode array (MEA) reading from cells on the optical media**. Before and after drug treatment with Isoproterenol. Our platform can be used with the MEA.

The versatility of the optical media means it can be manipulated and

used for bio-imaging applications such as calcium imaging as well as multi

electrode array. In addition, because of the large surface area of these optical

media, they can be scaled up to 48 and 96 well plates and used for high

throughput studies.

126

## 5.4 Concluding remarks

I have reported the development of a high throughput platform for cardiotoxicity screening using optical media. I previously showed that these optical media are cost effective and support cell culture of different cells. Here we show that this platform allows the culture and functional maturation of NRVM. In addition we show that the platform is amenable for various assays such as calcium flux readings. Experiments are ongoing using multi electrode array for pharmacological studies with the platform. Our platform is ideal for a cost effective, high throughput platform for preclinical screening of cardiotoxic drugs.

# CHAPTER 6: CONCLUSIONS AND DIRECTIONS FOR FUTURE RESEACRH

## 6.1 Final conclusions

This thesis has covered the use of cost effective, commercially available optical media as substrates for aligning cells in culture to be used for various tissue engineering purposes. I have shown that these optical media substrates can be used either directly for cell culture or as molds for patterning large surface area PDMS.

- In the first instance, I showed that cardiac, neuronal and skeletal muscle cell lines attach, proliferate and align on these optical media substrates. The alignment enhanced maturation of both the skeletal and cardiac muscle cell line while inducing a bipolar morphology in the neuronal cell line.

- Moving forward, I explored the use of these optical media substrates as molds for large scale patterning of PDMS through soft lithography. These PDMS substrates with micro/nanogrooves were subsequently used for cell culture or as bottom layers for 3D microfluidic chip. I showed a synergistic effect of both fluid shear stress and micro/nano grooves in forming an aligned 3D cellular constructs.

- Finally the use of these substrates as platforms for the study of drug induced cardiotoxicity was explored. I not only showed the beneficial effects of alignment on cardiomyocytes but I also show the amenability of this platform to important assays necessary for the study of drug induced cardiotoxicity.

**6.2 Recommendations for future research**

*6.2.1 Cell alignment for basic research.*

Cell alignment has been shown to affect morphology, gene and protein expression in many cell types. One unexplored field is to study the effect of cell alignment on cell cycle, understanding the effect of alignment on this basic cell function can help researchers understand how to manipulate the cells for various studies. Cell cycle understanding will be useful for modulating proliferation, cell passaging and cell differentiation. To the best of our knowledge, we are the first to show that cell alignment in C2C12 increases the percentage of cells in the G0/G1 phase while reducing the percentage of cells in the M phase. Expanding this study to other cell types would be insightful. Another area to explore with the commercially available optical media would be mechanobiology studies. Currently we are studying the importance of kinectin in regulating cell shape by culturing kinectin knock-down cells on the optical media. Preliminary data suggests that kinectin knock-down cells do not elongate and align as efficiently as cells with kinectin. In addition, scientists have been interested in exploring the importance of mechanotransduction in inducing stem cell differentiation on various topographies [124]. These commercially available optical media can serve as cost effective platforms for these studies and make it accessible for all labs.

*6.2.2 Cell alignment for stem cell differentiation*

Numerous studies have explored the importance of alignment in stem cell differentiation, especially for the neuronal, skeletal and cardiac muscle lineages [3]. Recently, a paper reported that topography was very efficient for

the generation of human induced pluripotent stem cells [5]. This technology can be exploited for these studies. Due to the ubiquitous nature of these commercially available optical media, and its low cost, they can be used for large scale expansion and differentiation. They could especially be useful for countries without advanced infrastructure and technology.

*6.2.3 Optical media as molds for large scale soft lithography*

We have already shown that these substrates can be used as cost effective molds for patterning PDMS through soft lithography. Our next step would be to develop pump-free microfluidic chips with micro/nano grooves for drug testing applications. In addition, we hope to study the effects of stiffness and topography on cell function and differentiation. To do this we would use the optical media to pattern PDMS of different stiffness and culture embryonic stem cells to evaluate differentiation and maturation.

# ANNEXES

## 7.1 Primers for Rat

| Name | Sequence |
|---|---|
| Potassium voltage-gated channel, subfamily Q, member 1 | F-TGAGTCCGGCCGGGCATCGAGT |
| | R-GCCCGCTGGGAGTGCAAAGA |
| Potassium voltage-gated channel, subfamily H (eag-related), member 2 | F-CGCTACCGAACCATTAGCAAG |
| | R-GTGCTATGATTTCCCGGTCAC |
| Potassium voltage-gated channel, Isk-related subfamily, member 1 | F-TGCCCTCGCTGTGGCAGGAA |
| | R-TCGGAGCTGGGACCTACGAGC |
| Potassium voltage-gated channel, Isk-related subfamily, gene 2 | F-AACAGCCGAACAACAGGCGCT |
| | R-TGGTACGGGTCCTGGGAGTGC |
| Caveolin 3 | F-TCCGCACCTTCTGCAACCCG |
| | R-AGCCTTCCCTTCGCAGCACC |
| Adrenergic receptor, beta 2 | F-AGCGACTTCTTGCTGGCACCC |
| | R-CCCACGCTTCGTCCCGTTCC |
| Troponin T | F-GCGGAAGAGTGGGAAGAGACA |
| | R-CCACAGCTCCTTGGCCTTCT |
| Alpha cardiac actin | F-ATGATGCTCCCAGAGCTGTC |
| | R-TGTCGTCCCAGTTGGTGATA |
| Alpha skeletal actin | F-TGCGGGGATCCATGAGACCACC |
| | R-TGCATGCGGTCAGCGATACCG |
| Alpha myosin heavy chain | F-AAGCACTTGAAGAACGCCCAA |

| | R-CGATGTTCTCCTTCAGGTCGTC |
|---|---|
| Connexin 43 | F-CAAGGTCCAAGCCTACTCCAC |
| | R-ATTTTCACCTTGCCGTGCTCT |
| Sarcoplasmic reticulum calcium ATPase | F-CCTGTCGGCATGCACCGACG |
| | R-GACCCAGACCACCAGGGGCATA |
| Beta Myosin heavy chain | F-TGGCACCGTGGACTACAATA |
| | TACAGGTGCATCAGCTCCAG |
| Brain natriuretic peptide | F-AGACAGCGCCTTCCGGATCCA |
| | R-CCCGTCACAGCCCAAGCGAC |

**7.2.1 Time lapse video of H9C2 alignment on the optical media**

**7.2.2 Cardiomyocyte beating on grooved and flat surface. Cells on the grooved surface maintain a faster and more synchronized beating than cells on the flat surface**

**7.2.3 Cardiomyocytes beating before (A) and after (B) drug treatment. There is a reduction in beating rate after addition of verapamil**

# REFERENCES

[1] Li Y, Huang G, Zhang X, Wang L, Du Y, Lu TJ, et al. Engineering cell alignment in vitro. Biotechnology Advances. 2014;32:347-65.

[2] Lee MR, Kwon KW, Jung H, Kim HN, Suh KY, Kim K, et al. Direct differentiation of human embryonic stem cells into selective neurons on nanoscale ridge/groove pattern arrays. Biomaterials. 2010;31:4360-6.

[3] Yim EK, Leong KW. Significance of synthetic nanostructures in dictating cellular response. Nanomedicine : nanotechnology, biology, and medicine. 2005;1:10-21.

[4] Yim EK, Pang SW, Leong KW. Synthetic nanostructures inducing differentiation of human mesenchymal stem cells into neuronal lineage. Experimental cell research. 2007;313:1820-9.

[5] Downing TL, Soto J, Morez C, Houssin T, Fritz A, Yuan F, et al. Biophysical regulation of epigenetic state and cell reprogramming. Nature materials. 2013;12:1154-62.

[6] Diop-Frimpong B, Chauhan VP, Krane S, Boucher Y, Jain RK. Losartan inhibits collagen I synthesis and improves the distribution and efficacy of nanotherapeutics in tumors. Proceedings of the National Academy of Sciences of the United States of America. 2011;108:2909-14.

[7] Kissa K, Herbomel P. Blood stem cells emerge from aortic endothelium by a novel type of cell transition. Nature. 2010;464:112-5.

[8] Gokhin DS, Fowler VM. A two-segment model for thin filament architecture in skeletal muscle. Nature reviews Molecular cell biology. 2013;14:113-9.

[9] Pacary E, Martynoga B, Guillemot F. Crucial first steps: the transcriptional control of neuron delamination. Neuron. 2012;74:209-11.

[10] Kim DH, Lipke EA, Kim P, Cheong R, Thompson S, Delannoy M, et al. Nanoscale cues regulate the structure and function of macroscopic cardiac tissue constructs. Proceedings of the National Academy of Sciences of the United States of America. 2010;107:565-70.

[11] Etemad-Moghadam B, Guo S, Kemphues KJ. Asymmetrically distributed PAR-3 protein contributes to cell polarity and spindle alignment in early C. elegans embryos. Cell. 1995;83:743-52.

[12] Chew SY, Mi R, Hoke A, Leong KW. The effect of the alignment of electrospun fibrous scaffolds on Schwann cell maturation. Biomaterials. 2008;29:653-61.

[13] Hoehme S, Brulport M, Bauer A, Bedawy E, Schormann W, Hermes M, et al. Prediction and validation of cell alignment along microvessels as order principle to restore tissue architecture in liver regeneration. Proceedings of the National Academy of Sciences of the United States of America. 2010;107:10371-6.

[14] Jeong SI, Kwon JH, Lim JI, Cho SW, Jung Y, Sung WJ, et al. Mechano-active tissue engineering of vascular smooth muscle using pulsatile perfusion bioreactors and elastic PLCL scaffolds. Biomaterials. 2005;26:1405-11.

[15] Friedl P, Sahai E, Weiss S, Yamada KM. New dimensions in cell migration. Nature reviews Molecular cell biology. 2012;13:743-7.

[16] Scott CW, Peters MF, Dragan YP. Human induced pluripotent stem cells and their use in drug discovery for toxicity testing. Toxicology letters. 2013;219:49-58.

[17] Wang PY, Yu HT, Tsai WB. Modulation of alignment and differentiation of skeletal myoblasts by submicron ridges/grooves surface structure. Biotechnology and bioengineering. 2010;106:285-94.

[18] Dang JM, Leong KW. Myogenic Induction of Aligned Mesenchymal Stem Cell Sheets by Culture on Thermally Responsive Electrospun Nanofibers. Advanced materials. 2007;19:2775-9.

[19] Ricotti L, Polini A, Genchi GG, Ciofani G, Iandolo D, Vazao H, et al. Proliferation and skeletal myotube formation capability of C2C12 and H9c2 cells on isotropic and anisotropic electrospun nanofibrous PHB scaffolds. Biomedical materials. 2012;7:035010.

[20] Huang NF, Lee RJ, Li S. Engineering of aligned skeletal muscle by micropatterning. American journal of translational research. 2010;2:43-55.

[21] Sun Y, Duffy R, Lee A, Feinberg AW. Optimizing the structure and contractility of engineered skeletal muscle thin films. Acta biomaterialia. 2013;9:7885-94.

[22] Pennisi CP, Olesen CG, de Zee M, Rasmussen J, Zachar V. Uniaxial cyclic strain drives assembly and differentiation of skeletal myocytes. Tissue engineering Part A. 2011;17:2543-50.

[23] Tanaka T, Hattori-Aramaki N, Sunohara A, Okabe K, Sakamoto Y, Ochiai H, et al. Alignment of Skeletal Muscle Cells Cultured in Collagen Gel by Mechanical and Electrical Stimulation. International Journal of Tissue Engineering. 2014;2014:5.

[24] Shimizu K, Fujita H, Nagamori E. Alignment of skeletal muscle myoblasts and myotubes using linear micropatterned surfaces ground with abrasives. Biotechnology and bioengineering. 2009;103:631-8.

[25] Zhao Y, Zeng H, Nam J, Agarwal S. Fabrication of skeletal muscle constructs by topographic activation of cell alignment. Biotechnology and bioengineering. 2009;102:624-31.

[26] Cui X, Gao G, Qiu Y. Accelerated myotube formation using bioprinting technology for biosensor applications. Biotechnology letters. 2013;35:315-21.

[27] Yang HS, Ieronimakis N, Tsui JH, Kim HN, Suh KY, Reyes M, et al. Nanopatterned muscle cell patches for enhanced myogenesis and dystrophin expression in a mouse model of muscular dystrophy. Biomaterials. 2014;35:1478-86.

[28] Ankam S, Suryana M, Chan LY, Moe AA, Teo BK, Law JB, et al. Substrate topography and size determine the fate of human embryonic stem cells to neuronal or glial lineage. Acta biomaterialia. 2013;9:4535-45.

[29] Brook GA, Plate D, Franzen R, Martin D, Moonen G, Schoenen J, et al. Spontaneous longitudinally orientated axonal regeneration is associated with the Schwann cell framework within the lesion site following spinal cord compression injury of the rat. Journal of neuroscience research. 1998;53:51-65.

[30] Guenard V, Kleitman N, Morrissey TK, Bunge RP, Aebischer P. Syngeneic Schwann cells derived from adult nerves seeded in semipermeable guidance channels enhance peripheral nerve regeneration. The Journal of

neuroscience : the official journal of the Society for Neuroscience. 1992;12:3310-20.

[31] Ribeiro-Resende VT, Koenig B, Nichterwitz S, Oberhoffner S, Schlosshauer B. Strategies for inducing the formation of bands of Bungner in peripheral nerve regeneration. Biomaterials. 2009;30:5251-9.

[32] Miller C, Shanks H, Witt A, Rutkowski G, Mallapragada S. Oriented Schwann cell growth on micropatterned biodegradable polymer substrates. Biomaterials. 2001;22:1263-9.

[33] Thompson DM, Buettner HM. Oriented Schwann cell monolayers for directed neurite outgrowth. Annals of biomedical engineering. 2004;32:1120-30.

[34] Curtis A, Wilkinson C. Topographical control of cells. Biomaterials. 1997;18:1573-83.

[35] Laulicht B, Gidmark NJ, Tripathi A, Mathiowitz E. Localization of magnetic pills. Proceedings of the National Academy of Sciences of the United States of America. 2011;108:2252-7.

[36] Lietz M, Dreesmann L, Hoss M, Oberhoffner S, Schlosshauer B. Neuro tissue engineering of glial nerve guides and the impact of different cell types. Biomaterials. 2006;27:1425-36.

[37] Bozkurt A, Deumens R, Beckmann C, Olde Damink L, Schugner F, Heschel I, et al. In vitro cell alignment obtained with a Schwann cell enriched microstructured nerve guide with longitudinal guidance channels. Biomaterials. 2009;30:169-79.

[38] Zhang Y, Luo H, Zhang Z, Lu Y, Huang X, Yang L, et al. A nerve graft constructed with xenogeneic acellular nerve matrix and autologous adipose-derived mesenchymal stem cells. Biomaterials. 2010;31:5312-24.

[39] Ferrari A, Cecchini M, Degl Innocenti R, Beltram F. Directional PC12 cell migration along plastic nanotracks. IEEE transactions on bio-medical engineering. 2009;56:2692-6.

[40] Horton AC, Ehlers MD. Neuronal polarity and trafficking. Neuron. 2003;40:277-95.

[41] Tahirovic S, Bradke F. Neuronal polarity. Cold Spring Harbor perspectives in biology. 2009;1:a001644.

[42] Yokota Y, Gashghaei HT, Han C, Watson H, Campbell KJ, Anton ES. Radial glial dependent and independent dynamics of interneuronal migration in the developing cerebral cortex. PloS one. 2007;2:e794.

[43] Flemming RG, Murphy CJ, Abrams GA, Goodman SL, Nealey PF. Effects of synthetic micro- and nano-structured surfaces on cell behavior. Biomaterials. 1999;20:573-88.

[44] Martinez E, Engel E, Planell JA, Samitier J. Effects of artificial micro- and nano-structured surfaces on cell behaviour. Annals of anatomy = Anatomischer Anzeiger : official organ of the Anatomische Gesellschaft. 2009;191:126-35.

[45] Anene-Nzelu CG, Choudhury D, Li H, Fraiszudeen A, Peh KY, Toh YC, et al. Scalable cell alignment on optical media substrates. Biomaterials. 2013;34:5078-87.

[46] Piccini JP, Whellan DJ, Berridge BR, Finkle JK, Pettit SD, Stockbridge N, et al. Current challenges in the evaluation of cardiac safety during drug

development: translational medicine meets the Critical Path Initiative. American heart journal. 2009;158:317-26.

[47] Adams CP, Brantner VV. Estimating the cost of new drug development: is it really 802 million dollars? Health affairs. 2006;25:420-8.

[48] Steinmetz KL, Spack EG. The basics of preclinical drug development for neurodegenerative disease indications. BMC neurology. 2009;9 Suppl 1:S2.

[49] Elliott NT, Yuan F. A review of three-dimensional in vitro tissue models for drug discovery and transport studies. Journal of pharmaceutical sciences. 2011;100:59-74.

[50] Terstappen GC, Schlupen C, Raggiaschi R, Gaviraghi G. Target deconvolution strategies in drug discovery. Nature reviews Drug discovery. 2007;6:891-903.

[51] Kola I, Landis J. Can the pharmaceutical industry reduce attrition rates? Nature reviews Drug discovery. 2004;3:711-5.

[52] Lasser KE, Allen PD, Woolhandler SJ, Himmelstein DU, Wolfe SM, Bor DH. Timing of new black box warnings and withdrawals for prescription medications. JAMA : the journal of the American Medical Association. 2002;287:2215-20.

[53] Lexchin J. Drug withdrawals from the Canadian market for safety reasons, 1963-2004. CMAJ : Canadian Medical Association journal = journal de l'Association medicale canadienne. 2005;172:765-7.

[54] Stummann TC, Beilmann M, Duker G, Dumotier B, Fredriksson JM, Jones RL, et al. Report and recommendations of the workshop of the European Centre for the Validation of Alternative Methods for Drug-Induced Cardiotoxicity. Cardiovascular toxicology. 2009;9:107-25.

[55] Fermini B, Fossa AA. The impact of drug-induced QT interval prolongation on drug discovery and development. Nature reviews Drug discovery. 2003;2:439-47.

[56] Bottino D, Penland RC, stamps A, Traebert M, Dumotier B, Georgiva A, et al. Preclinical cardiac safety assessment of pharmaceutical compounds using an integrated systems-based computer model of the heart. Progress in biophysics and molecular biology. 2006;90:414-43.

[57] Sirenko O, Crittenden C, Callamaras N, Hesley J, Chen YW, Funes C, et al. Multiparameter in vitro assessment of compound effects on cardiomyocyte physiology using iPSC cells. Journal of biomolecular screening. 2013;18:39-53.

[58] Sanguinetti MC, Tristani-Firouzi M. hERG potassium channels and cardiac arrhythmia. Nature. 2006;440:463-9.

[59] Wible BA, Hawryluk P, Ficker E, Kuryshev YA, Kirsch G, Brown AM. HERG-Lite: a novel comprehensive high-throughput screen for drug-induced hERG risk. Journal of pharmacological and toxicological methods. 2005;52:136-45.

[60] Gwathmey JK, Tsaioun K, Hajjar RJ. Cardionomics: a new integrative approach for screening cardiotoxicity of drug candidates. Expert opinion on drug metabolism & toxicology. 2009;5:647-60.

[61] Kim MJ, Lee SC, Pal S, Han E, Song JM. High-content screening of drug-induced cardiotoxicity using quantitative single cell imaging cytometry on microfluidic device. Lab on a chip. 2011;11:104-14.

[62] Remiao F, Carmo H, Carvalho F, Bastos ML. The study of oxidative stress in freshly isolated Ca(2+)-tolerant cardiomyocytes from the adult rat. Toxicology in vitro : an international journal published in association with BIBRA. 2001;15:283-7.

[63] Zordoky BN, Anwar-Mohamed A, Aboutabl ME, El-Kadi AO. Acute doxorubicin cardiotoxicity alters cardiac cytochrome P450 expression and arachidonic acid metabolism in rats. Toxicology and applied pharmacology. 2010;242:38-46.

[64] Cerignoli F, Charlot D, Whittaker R, Ingermanson R, Gehalot P, Savchenko A, et al. High throughput measurement of Ca(2)(+) dynamics for drug risk assessment in human stem cell-derived cardiomyocytes by kinetic image cytometry. Journal of pharmacological and toxicological methods. 2012;66:246-56.

[65] Grosberg A, Alford PW, McCain ML, Parker KK. Ensembles of engineered cardiac tissues for physiological and pharmacological study: heart on a chip. Lab on a chip. 2011;11:4165-73.

[66] Kaneko T, Kojima K, Yasuda K. An on-chip cardiomyocyte cell network assay for stable drug screening regarding community effect of cell network size. The Analyst. 2007;132:892-8.

[67] Pointon A, Abi-Gerges N, Cross MJ, Sidaway JE. Phenotypic profiling of structural cardiotoxins in vitro reveals dependency on multiple mechanisms of toxicity. Toxicological sciences : an official journal of the Society of Toxicology. 2013;132:317-26.

[68] Sengupta PP, Krishnamoorthy VK, Korinek J, Narula J, Vannan MA, Lester SJ, et al. Left ventricular form and function revisited: applied translational science to cardiovascular ultrasound imaging. Journal of the American Society of Echocardiography : official publication of the American Society of Echocardiography. 2007;20:539-51.

[69] Heineke J, Molkentin JD. Regulation of cardiac hypertrophy by intracellular signalling pathways. Nature reviews Molecular cell biology. 2006;7:589-600.

[70] Grayson WL, Martens TP, Eng GM, Radisic M, Vunjak-Novakovic G. Biomimetic approach to tissue engineering. Seminars in cell & developmental biology. 2009;20:665-73.

[71] Luna JI, Ciriza J, Garcia-Ojeda ME, Kong M, Herren A, Lieu DK, et al. Multiscale biomimetic topography for the alignment of neonatal and embryonic stem cell-derived heart cells. Tissue engineering Part C, Methods. 2011;17:579-88.

[72] Rao C, Prodromakis T, Kolker L, Chaudhry UA, Trantidou T, Sridhar A, et al. The effect of microgrooved culture substrates on calcium cycling of cardiac myocytes derived from human induced pluripotent stem cells. Biomaterials. 2013;34:2399-411.

[73] Wang J, Chen A, Lieu DK, Karakikes I, Chen G, Keung W, et al. Effect of engineered anisotropy on the susceptibility of human pluripotent stem cell-derived ventricular cardiomyocytes to arrhythmias. Biomaterials. 2013;34:8878-86.

[74] Inamdar NK, Borenstein JT. Microfluidic cell culture models for tissue engineering. Current opinion in biotechnology. 2011;22:681-9.

[75] Meyvantsson I, Beebe DJ. Cell culture models in microfluidic systems. Annual review of analytical chemistry. 2008;1:423-49.

[76] Sia SK, Whitesides GM. Microfluidic devices fabricated in poly(dimethylsiloxane) for biological studies. Electrophoresis. 2003;24:3563-76.

[77] Berthier E, Young EW, Beebe D. Engineers are from PDMS-land, Biologists are from Polystyrenia. Lab on a chip. 2012;12:1224-37.

[78] Gribova V, Crouzier T, Picart C. A material's point of view on recent developments of polymeric biomaterials: control of mechanical and biochemical properties. J Mater Chem. 2011;21:14354-66.

[79] Yang Y, Kulangara K, Sia J, Wang L, Leong KW. Engineering of a microfluidic cell culture platform embedded with nanoscale features. Lab on a chip. 2011;11:1638-46.

[80] Tourovskaia A, Figueroa-Masot X, Folch A. Differentiation-on-a-chip: a microfluidic platform for long-term cell culture studies. Lab on a chip. 2005;5:14-9.

[81] Anene-Nzelu CG, Peh KY, Fraiszudeen A, Kuan YH, Ng SH, Toh YC, et al. Scalable alignment of three-dimensional cellular constructs in a microfluidic chip. Lab on a chip. 2013;13:4124-33.

[82] Klauke N, Smith GL, Cooper J. Stimulation of single isolated adult ventricular myocytes within a low volume using a planar microelectrode array. Biophysical journal. 2003;85:1766-74.

[83] Yang M, Zhang X. Electrical assisted patterning of cardiac myocytes with controlled macroscopic anisotropy using a microfluidic dielectrophoresis chip. Sensors and Actuators A: Physical. 2007;135:73-9.

[84] Hallfors N, Khan A, Dickey MD, Taylor AM. Integration of pre-aligned liquid metal electrodes for neural stimulation within a user-friendly microfluidic platform. Lab on a chip. 2013;13:522-6.

[85] Wallin P, Zanden C, Carlberg B, Hellstrom Erkenstam N, Liu J, Gold J. A method to integrate patterned electrospun fibers with microfluidic systems to generate complex microenvironments for cell culture applications. Biomicrofluidics. 2012;6:24131.

[86] Aubin H, Nichol JW, Hutson CB, Bae H, Sieminski AL, Cropek DM, et al. Directed 3D cell alignment and elongation in microengineered hydrogels. Biomaterials. 2010;31:6941-51.

[87] Engelmayr GC, Jr., Cheng M, Bettinger CJ, Borenstein JT, Langer R, Freed LE. Accordion-like honeycombs for tissue engineering of cardiac anisotropy. Nature materials. 2008;7:1003-10.

[88] Lam MT, Huang YC, Birla RK, Takayama S. Microfeature guided skeletal muscle tissue engineering for highly organized 3-dimensional free-standing constructs. Biomaterials. 2009;30:1150-5.

[89] Isenberg BC, Tsuda Y, Williams C, Shimizu T, Yamato M, Okano T, et al. A thermoresponsive, microtextured substrate for cell sheet engineering with defined structural organization. Biomaterials. 2008;29:2565-72.

[90] Detrait E, Lhoest JB, Knoops B, Bertrand P, van den Bosch de Aguilar P. Orientation of cell adhesion and growth on patterned heterogeneous polystyrene surface. Journal of neuroscience methods. 1998;84:193-204.

[91] Rehfeldt F, Engler AJ, Eckhardt A, Ahmed F, Discher DE. Cell responses to the mechanochemical microenvironment--implications for regenerative

medicine and drug delivery. Advanced drug delivery reviews. 2007;59:1329-39.

[92] Pang Y, Wang X, Lee D, Greisler HP. Dynamic quantitative visualization of single cell alignment and migration and matrix remodeling in 3-D collagen hydrogels under mechanical force. Biomaterials. 2011;32:3776-83.

[93] Kaunas R, Nguyen P, Usami S, Chien S. Cooperative effects of Rho and mechanical stretch on stress fiber organization. Proceedings of the National Academy of Sciences of the United States of America. 2005;102:15895-900.

[94] Neidlinger-Wilke C, Grood ES, Wang J-C, Brand RA, Claes L. Cell alignment is induced by cyclic changes in cell length: studies of cells grown in cyclically stretched substrates. Journal of orthopaedic research : official publication of the Orthopaedic Research Society. 2001;19:286-93.

[95] Wang JH, Goldschmidt-Clermont P, Wille J, Yin FC. Specificity of endothelial cell reorientation in response to cyclic mechanical stretching. Journal of biomechanics. 2001;34:1563-72.

[96] Foolen J, Deshpande VS, Kanters FM, Baaijens FP. The influence of matrix integrity on stress-fiber remodeling in 3D. Biomaterials. 2012;33:7508-18.

[97] Xu F, Moon SJ, Emre AE, Turali ES, Song YS, Hacking SA, et al. A droplet-based building block approach for bladder smooth muscle cell (SMC) proliferation. Biofabrication. 2010;2:014105.

[98] Gupta V, Grande-Allen KJ. Effects of static and cyclic loading in regulating extracellular matrix synthesis by cardiovascular cells. Cardiovascular research. 2006;72:375-83.

[99] Chen C, Krishnan R, Zhou E, Ramachandran A, Tambe D, Rajendran K, et al. Fluidization and resolidification of the human bladder smooth muscle cell in response to transient stretch. PloS one. 2010;5:e12035.

[100] Crouchley CM, Barron V, Punchard M, O'Cearbhaill E, Smith T. Development of a co-culture system for tissue engineered vascular grafts. Bio-medical materials and engineering. 2008;18:291-4.

[101] Hsu HJ, Lee CF, Kaunas R. A dynamic stochastic model of frequency-dependent stress fiber alignment induced by cyclic stretch. PloS one. 2009;4:e4853.

[102] Rahimi N, Molin DG, Cleij TJ, van Zandvoort MA, Post MJ. Electrosensitive polyacrylic acid/fibrin hydrogel facilitates cell seeding and alignment. Biomacromolecules. 2012;13:1448-57.

[103] Shyu K-G. Cellular and molecular effects of mechanical stretch on vascular cells and cardiac myocytes. Clinical Science. 2009;116:377-89.

[104] Lee AA, Graham DA, Dela Cruz S, Ratcliffe A, Karlon WJ. Fluid shear stress-induced alignment of cultured vascular smooth muscle cells. Journal of biomechanical engineering. 2002;124:37-43.

[105] Liu SQ, Tang D, Tieche C, Alkema PK. Pattern formation of vascular smooth muscle cells subject to nonuniform fluid shear stress: mediation by gradient of cell density. American journal of physiology Heart and circulatory physiology. 2003;285:H1072-80.

[106] Hahn C, Wang C, Orr AW, Coon BG, Schwartz MA. JNK2 promotes endothelial cell alignment under flow. PloS one. 2011;6:e24338.

[107] Tzima E, del Pozo MA, Shattil SJ, Chien S, Schwartz MA. Activation of integrins in endothelial cells by fluid shear stress mediates Rho-dependent cytoskeletal alignment. The EMBO journal. 2001;20:4639-47.

[108] Lim JY, Donahue HJ. Cell sensing and response to micro- and nanostructured surfaces produced by chemical and topographic patterning. Tissue engineering. 2007;13:1879-91.

[109] Singhvi R, Kumar A, Lopez GP, Stephanopoulos GN, Wang DI, Whitesides GM, et al. Engineering cell shape and function. Science. 1994;264:696-8.

[110] Geisse NA, Sheehy SP, Parker KK. Control of myocyte remodeling in vitro with engineered substrates. In vitro cellular & developmental biology Animal. 2009;45:343-50.

[111] Ratner BD. Surface modification of polymers: chemical, biological and surface analytical challenges. Biosensors & bioelectronics. 1995;10:797-804.

[112] Chen CS, Mrksich M, Huang S, Whitesides GM, Ingber DE. Geometric control of cell life and death. Science. 1997;276:1425-8.

[113] Au HT, Cheng I, Chowdhury MF, Radisic M. Interactive effects of surface topography and pulsatile electrical field stimulation on orientation and elongation of fibroblasts and cardiomyocytes. Biomaterials. 2007;28:4277-93.

[114] Shao S, Zhou S, Li L, Li J, Luo C, Wang J, et al. Osteoblast function on electrically conductive electrospun PLA/MWCNTs nanofibers. Biomaterials. 2011;32:2821-33.

[115] Hronik-Tupaj M, Kaplan DL. A review of the responses of two- and three-dimensional engineered tissues to electric fields. Tissue engineering Part B, Reviews. 2012;18:167-80.

[116] Roach P, Parker T, Gadegaard N, Alexander MR. Surface strategies for control of neuronal cell adhesion: A review. Surface Science Reports. 2010;65:145-73.

[117] Sun S, Titushkin I, Cho M. Regulation of mesenchymal stem cell adhesion and orientation in 3D collagen scaffold by electrical stimulus. Bioelectrochemistry. 2006;69:133-41.

[118] Histed MH, Bonin V, Reid RC. Direct activation of sparse, distributed populations of cortical neurons by electrical microstimulation. Neuron. 2009;63:508-22.

[119] Tandon V, Zhang B, Radisic M, Murthy SK. Generation of tissue constructs for cardiovascular regenerative medicine: from cell procurement to scaffold design. Biotechnol Adv. 2013;31:722-35.

[120] Radisic M, Park H, Shing H, Consi T, Schoen FJ, Langer R, et al. Functional assembly of engineered myocardium by electrical stimulation of cardiac myocytes cultured on scaffolds. Proceedings of the National Academy of Sciences of the United States of America. 2004;101:18129-34.

[121] Ramon-Azcon J, Ahadian S, Estili M, Liang X, Ostrovidov S, Kaji H, et al. Dielectrophoretically aligned carbon nanotubes to control electrical and mechanical properties of hydrogels to fabricate contractile muscle myofibers. Advanced materials. 2013;25:4028-34.

[122] Brunette DM. Fibroblasts on micromachined substrata orient hierarchically to grooves of different dimensions. Experimental cell research. 1986;164:11-26.

[123] Ohara PT, Buck RC. Contact guidance in vitro. A light, transmission, and scanning electron microscopic study. Experimental cell research. 1979;121:235-49.

[124] Yim EK, Darling EM, Kulangara K, Guilak F, Leong KW. Nanotopography-induced changes in focal adhesions, cytoskeletal organization, and mechanical properties of human mesenchymal stem cells. Biomaterials. 2010;31:1299-306.

[125] del Campo A, Arzt E. Fabrication approaches for generating complex micro- and nanopatterns on polymeric surfaces. Chemical reviews. 2008;108:911-45.

[126] Rebollar E, Frischauf I, Olbrich M, Peterbauer T, Hering S, Preiner J, et al. Proliferation of aligned mammalian cells on laser-nanostructured polystyrene. Biomaterials. 2008;29:1796-806.

[127] Tan JY, Wen JC, Shi WH, He Q, Zhu L, Liang K, et al. Effect of microtopographic structures of silk fibroin on endothelial cell behavior. Molecular medicine reports. 2013;7:292-8.

[128] Dumond JJ, Mahabadi KA, Yee YS, Tan C, Fuh JY, Lee HP, et al. High resolution UV roll-to-roll nanoimprinting of resin moulds and subsequent replication via thermal nanoimprint lithography. Nanotechnology. 2012;23:485310.

[129] Kim MS, Kim AY, Jang KJ, Kim JH, Kim JB, Suh KY. Effect of nanogroove geometry on adipogenic differentiation. Nanotechnology. 2011;22:494017.

[130] Ahn SH, Guo LJ. Large-area roll-to-roll and roll-to-plate nanoimprint lithography: a step toward high-throughput application of continuous nanoimprinting. ACS nano. 2009;3:2304-10.

[131] Rajnicek A, Britland S, McCaig C. Contact guidance of CNS neurites on grooved quartz: influence of groove dimensions, neuronal age and cell type. Journal of cell science. 1997;110 ( Pt 23):2905-13.

[132] Parker NW, Brodie AD, McCoy JH. A high throughput NGL electron beam direct-write lithography system. P Soc Photo-Opt Ins. 2000;3997:713-20.

[133] Grossman WEL. The optical characteristics and production of diffraction gratings: A quantitative explanation of their experimental qualities with a description of their manufacture and relative merits. Journal of Chemical Education. 1993;70:741.

[134] Emmelius M, Pawlowski G, Vollmann HW. Materials for Optical Data Storage. Angewandte Chemie International Edition in English. 1989;28:1445-71.

[135] Vernon RB, Gooden MD, Lara SL, Wight TN. Microgrooved fibrillar collagen membranes as scaffolds for cell support and alignment. Biomaterials. 2005;26:3131-40.

[136] Chowdhury D, Paul A, Chattopadhyay A. Patterning Design in Color at the Submicron Scale. Nano letters. 2001;1:409-12.

[137] Gil ES, Park SH, Marchant J, Omenetto F, Kaplan DL. Response of human corneal fibroblasts on silk film surface patterns. Macromolecular bioscience. 2010;10:664-73.

[138] Du Y, Han R, Wen F, Ng San San S, Xia L, Wohland T, et al. Synthetic sandwich culture of 3D hepatocyte monolayer. Biomaterials. 2008;29:290-301.

[139] Ramazani SAA, Mousavi SA, Seyedjafari E, Poursalehi R, Sareh S, Silakhori K, et al. Polycarbonate surface cell's adhesion examination after Nd:YAG laser irradiation. Mat Sci Eng C-Bio S. 2009;29:1491-7.

[140] Kenar H, Kose GT, Hasirci V. Tissue engineering of bone on micropatterned biodegradable polyester films. Biomaterials. 2006;27:885-95.

[141] Lee CH, Shin HJ, Cho IH, Kang YM, Kim IA, Park KD, et al. Nanofiber alignment and direction of mechanical strain affect the ECM production of human ACL fibroblast. Biomaterials. 2005;26:1261-70.

[142] Wang PY, Yu J, Lin JH, Tsai WB. Modulation of alignment, elongation and contraction of cardiomyocytes through a combination of nanotopography and rigidity of substrates. Acta biomaterialia. 2011;7:3285-93.

[143] Bursac N, Parker KK, Iravanian S, Tung L. Cardiomyocyte cultures with controlled macroscopic anisotropy: a model for functional electrophysiological studies of cardiac muscle. Circulation research. 2002;91:e45-54.

[144] Xia L, Sakban RB, Qu Y, Hong X, Zhang W, Nugraha B, et al. Tethered spheroids as an in vitro hepatocyte model for drug safety screening. Biomaterials. 2012;33:2165-76.

[145] Menard C, Pupier S, Mornet D, Kitzmann M, Nargeot J, Lory P. Modulation of L-type calcium channel expression during retinoic acid-induced differentiation of H9C2 cardiac cells. The Journal of biological chemistry. 1999;274:29063-70.

[146] Meng F, Hlady V, Tresco PA. Inducing alignment in astrocyte tissue constructs by surface ligands patterned on biomaterials. Biomaterials. 2012;33:1323-35.

[147] Williams C, Xie AW, Yamato M, Okano T, Wong JY. Stacking of aligned cell sheets for layer-by-layer control of complex tissue structure. Biomaterials. 2011;32:5625-32.

[148] Frisch KE, Duenwald-Kuehl SE, Kobayashi H, Chamberlain CS, Lakes RS, Vanderby R, Jr. Quantification of collagen organization using fractal dimensions and Fourier transforms. Acta histochemica. 2012;114:140-4.

[149] Joy A, Cohen DM, Luk A, Anim-Danso E, Chen C, Kohn J. Control of surface chemistry, substrate stiffness, and cell function in a novel terpolymer methacrylate library. Langmuir : the ACS journal of surfaces and colloids. 2011;27:1891-9.

[150] Kearns V, Mistry A, Mason S, Krishna Y, Sheridan C, Short R, et al. Plasma polymer coatings to aid retinal pigment epithelial growth for transplantation in the treatment of age related macular degeneration. Journal of materials science Materials in medicine. 2012;23:2013-21.

[151] Ni M, Zimmermann PK, Kandasamy K, Lai W, Li Y, Leong MF, et al. The use of a library of industrial materials to determine the nature of substrate-dependent performance of primary adherent human cells. Biomaterials. 2012;33:353-64.

[152] Gonzalez RJ, Tarloff JB. Evaluation of hepatic subcellular fractions for Alamar blue and MTT reductase activity. Toxicology in vitro : an international journal published in association with BIBRA. 2001;15:257-9.

[153] Anoopkumar-Dukie S, Carey JB, Conere T, O'Sullivan E, van Pelt FN, Allshire A. Resazurin assay of radiation response in cultured cells. The British journal of radiology. 2005;78:945-7.

[154] Bettinger CJ, Zhang Z, Gerecht S, Borenstein JT, Langer R. Enhancement of In Vitro Capillary Tube Formation by Substrate Nanotopography. Advanced materials. 2008;20:99-103.

[155] Huang NF, Patel S, Thakar RG, Wu J, Hsiao BS, Chu B, et al. Myotube assembly on nanofibrous and micropatterned polymers. Nano letters. 2006;6:537-42.

[156] Mih JD, Marinkovic A, Liu F, Sharif AS, Tschumperlin DJ. Matrix stiffness reverses the effect of actomyosin tension on cell proliferation. Journal of cell science. 2012;125:5974-83.

[157] Wang Y, Wang G, Luo X, Qiu J, Tang C. Substrate stiffness regulates the proliferation, migration, and differentiation of epidermal cells. Burns : journal of the International Society for Burn Injuries. 2012;38:414-20.

[158] Branco AF, Pereira SL, Moreira AC, Holy J, Sardao VA, Oliveira PJ. Isoproterenol cytotoxicity is dependent on the differentiation state of the cardiomyoblast H9c2 cell line. Cardiovascular toxicology. 2011;11:191-203.

[159] Pereira SL, Ramalho-Santos J, Branco AF, Sardao VA, Oliveira PJ, Carvalho RA. Metabolic remodeling during H9c2 myoblast differentiation: relevance for in vitro toxicity studies. Cardiovascular toxicology. 2011;11:180-90.

[160] Ng WA, Grupp IL, Subramaniam A, Robbins J. Cardiac myosin heavy chain mRNA expression and myocardial function in the mouse heart. Circulation research. 1991;68:1742-50.

[161] Tiburcy M, Didie M, Boy O, Christalla P, Doker S, Naito H, et al. Terminal differentiation, advanced organotypic maturation, and modeling of hypertrophic growth in engineered heart tissue. Circulation research. 2011;109:1105-14.

[162] Cameron VA, Ellmers LJ. Minireview: natriuretic peptides during development of the fetal heart and circulation. Endocrinology. 2003;144:2191-4.

[163] Comelli M, Domenis R, Bisetto E, Contin M, Marchini M, Ortolani F, et al. Cardiac differentiation promotes mitochondria development and ameliorates oxidative capacity in H9c2 cardiomyoblasts. Mitochondrion. 2011;11:315-26.

[164] Tomaselli KJ, Damsky CH, Reichardt LF. Interactions of a neuronal cell line (PC12) with laminin, collagen IV, and fibronectin: identification of integrin-related glycoproteins involved in attachment and process outgrowth. The Journal of cell biology. 1987;105:2347-58.

[165] Cecchini M, Bumma G, Serresi M, Beltram F. PC12 diiierentiation on biopolymer nanostructures. Nanotechnology. 2007;18.

[166] Haq F, Anandan V, Keith C, Zhang G. Neurite development in PC12 cells cultured on nanopillars and nanopores with sizes comparable with filopodia. International journal of nanomedicine. 2007;2:107-15.

[167] Tashiro K, Sephel GC, Greatorex D, Sasaki M, Shirashi N, Martin GR, et al. The RGD containing site of the mouse laminin A chain is active for cell attachment, spreading, migration and neurite outgrowth. Journal of cellular physiology. 1991;146:451-9.

[168] Du Y, Chia SM, Han R, Chang S, Tang H, Yu H. 3D hepatocyte monolayer on hybrid RGD/galactose substratum. Biomaterials. 2006;27:5669-80.

[169] Neuzi P, Giselbrecht S, Lange K, Huang TJ, Manz A. Revisiting lab-on-a-chip technology for drug discovery. Nature reviews Drug discovery. 2012;11:620-32.

[170] Tan W, Desai TA. Microfluidic patterning of cells in extracellular matrix biopolymers: effects of channel size, cell type, and matrix composition on pattern integrity. Tissue engineering. 2003;9:255-67.

[171] Abbott A. Cell culture: biology's new dimension. Nature. 2003;424:870-2.

[172] Chen AA, Underhill GH, Bhatia SN. Multiplexed, high-throughput analysis of 3D microtissue suspensions. Integrative biology : quantitative biosciences from nano to macro. 2010;2:517-27.

[173] Jang KJ, Suh KY. A multi-layer microfluidic device for efficient culture and analysis of renal tubular cells. Lab on a chip. 2010;10:36-42.

[174] Huh D, Torisawa YS, Hamilton GA, Kim HJ, Ingber DE. Microengineered physiological biomimicry: organs-on-chips. Lab on a chip. 2012;12:2156-64.

[175] Oakley C, Brunette DM. The sequence of alignment of microtubules, focal contacts and actin filaments in fibroblasts spreading on smooth and grooved titanium substrata. Journal of cell science. 1993;106 ( Pt 1):343-54.

[176] Shimizu T, Yamato M, Isoi Y, Akutsu T, Setomaru T, Abe K, et al. Fabrication of pulsatile cardiac tissue grafts using a novel 3-dimensional cell sheet manipulation technique and temperature-responsive cell culture surfaces. Circulation research. 2002;90:e40.

[177] Toh YC, Lim TC, Tai D, Xiao G, van Noort D, Yu H. A microfluidic 3D hepatocyte chip for drug toxicity testing. Lab on a chip. 2009;9:2026-35.

[178] Toh YC, Zhang C, Zhang J, Khong YM, Chang S, Samper VD, et al. A novel 3D mammalian cell perfusion-culture system in microfluidic channels. Lab on a chip. 2007;7:302-9.

[179] Grabowska I, Szeliga A, Moraczewski J, Czaplicka I, Brzoska E. Comparison of satellite cell-derived myoblasts and C2C12 differentiation in two- and three-dimensional cultures: changes in adhesion protein expression. Cell biology international. 2011;35:125-33.

[180] Ong SM, Zhang C, Toh YC, Kim SH, Foo HL, Tan CH, et al. A gel-free 3D microfluidic cell culture system. Biomaterials. 2008;29:3237-44.

[181] Tanaka K, Sato K, Yoshida T, Fukuda T, Hanamura K, Kojima N, et al. Evidence for cell density affecting C2C12 myogenesis: possible regulation of myogenesis by cell-cell communication. Muscle & nerve. 2011;44:968-77.

[182] Engler AJ, Griffin MA, Sen S, Bonnemann CG, Sweeney HL, Discher DE. Myotubes differentiate optimally on substrates with tissue-like stiffness: pathological implications for soft or stiff microenvironments. The Journal of cell biology. 2004;166:877-87.

[183] Nagaoka U, Uchihara T, Iwabuchi K, Konno H, Tobita M, Funata N, et al. Attenuated nuclear shrinkage in neurones with nuclear inclusions of SCA1 brains. Journal of neurology, neurosurgery, and psychiatry. 2003;74:597-601.

[184] Li Y, Chu JS, Kurpinski K, Li X, Bautista DM, Yang L, et al. Biophysical regulation of histone acetylation in mesenchymal stem cells. Biophysical journal. 2011;100:1902-9.

[185] Thomas CH, Collier JH, Sfeir CS, Healy KE. Engineering gene expression and protein synthesis by modulation of nuclear shape. Proceedings of the National Academy of Sciences of the United States of America. 2002;99:1972-7.

[186] Pajerowski JD, Dahl KN, Zhong FL, Sammak PJ, Discher DE. Physical plasticity of the nucleus in stem cell differentiation. Proceedings of the National Academy of Sciences of the United States of America. 2007;104:15619-24.

[187] Dolan JM, Meng H, Singh S, Paluch R, Kolega J. High fluid shear stress and spatial shear stress gradients affect endothelial proliferation, survival, and alignment. Annals of biomedical engineering. 2011;39:1620-31.

[188] Rhim C, Lowell DA, Reedy MC, Slentz DH, Zhang SJ, Kraus WE, et al. Morphology and ultrastructure of differentiating three-dimensional mammalian skeletal muscle in a collagen gel. Muscle & nerve. 2007;36:71-80.

[189] Hosseini V, Ahadian S, Ostrovidov S, Camci-Unal G, Chen S, Kaji H, et al. Engineered contractile skeletal muscle tissue on a microgrooved methacrylated gelatin substrate. Tissue engineering Part A. 2012;18:2453-65.

[190] Ghaemmaghami AM, Hancock MJ, Harrington H, Kaji H, Khademhosseini A. Biomimetic tissues on a chip for drug discovery. Drug discovery today. 2012;17:173-81.

[191] Kelc R, Trapecar M, Vogrin M, Cencic A. Skeletal muscle-derived cell cultures as potent models in regenerative medicine research. Muscle & nerve. 2013;47:477-82.

[192] Mandenius CF, Steel D, Noor F, Meyer T, Heinzle E, Asp J, et al. Cardiotoxicity testing using pluripotent stem cell-derived human cardiomyocytes and state-of-the-art bioanalytics: a review. Journal of applied toxicology : JAT. 2011;31:191-205.

[193] Redfern WS, Carlsson L, Davis AS, Lynch WG, MacKenzie I, Palethorpe S, et al. Relationships between preclinical cardiac electrophysiology, clinical QT interval prolongation and torsade de pointes for a broad range of drugs: evidence for a provisional safety margin in drug development. Cardiovascular research. 2003;58:32-45.

[194] Chi KR. Revolution dawning in cardiotoxicity testing. Nature reviews Drug discovery. 2013;12:565-7.

[195] Maltsev VA, Wobus AM, Rohwedel J, Bader M, Hescheler J. Cardiomyocytes differentiated in vitro from embryonic stem cells developmentally express cardiac-specific genes and ionic currents. Circulation research. 1994;75:233-44.

[196] Cimetta E, Godier-Furnemont A, Vunjak-Novakovic G. Bioengineering heart tissue for in vitro testing. Current opinion in biotechnology. 2013;24:926-32.

[197] Kuo PL, Lee H, Bray MA, Geisse NA, Huang YT, Adams WJ, et al. Myocyte shape regulates lateral registry of sarcomeres and contractility. The American journal of pathology. 2012;181:2030-7.

[198] Nunes SS, Miklas JW, Liu J, Aschar-Sobbi R, Xiao Y, Zhang B, et al. Biowire: a platform for maturation of human pluripotent stem cell-derived cardiomyocytes. Nature methods. 2013;10:781-7.

[199] Matsa E, Rajamohan D, Dick E, Young L, Mellor I, Staniforth A, et al. Drug evaluation in cardiomyocytes derived from human induced pluripotent stem cells carrying a long QT syndrome type 2 mutation. European heart journal. 2011;32:952-62.

[200] Pradhapan P, Kuusela J, Viik J, Aalto-Setala K, Hyttinen J. Cardiomyocyte MEA data analysis (CardioMDA)--a novel field potential data analysis software for pluripotent stem cell derived cardiomyocytes. PloS one. 2013;8:e73637.

[201] Bers DM. Cardiac excitation-contraction coupling. Nature. 2002;415:198-205.

[202] Bers DM. Calcium fluxes involved in control of cardiac myocyte contraction. Circulation research. 2000;87:275-81.

[203] Bub G, Camelliti P, Bollensdorff C, Stuckey DJ, Picton G, Burton RA, et al. Measurement and analysis of sarcomere length in rat cardiomyocytes in situ and in vitro. American journal of physiology Heart and circulatory physiology. 2010;298:H1616-25.

[204] Peterson P, Kalda M, Vendelin M. Real-time determination of sarcomere length of a single cardiomyocyte during contraction. American journal of physiology Cell physiology. 2013;304:C519-31.

[205] Zhang D, Shadrin IY, Lam J, Xian HQ, Snodgrass HR, Bursac N. Tissue-engineered cardiac patch for advanced functional maturation of human ESC-derived cardiomyocytes. Biomaterials. 2013;34:5813-20.

[206] Motlagh D, Hartman TJ, Desai TA, Russell B. Microfabricated grooves recapitulate neonatal myocyte connexin43 and N-cadherin expression and localization. Journal of biomedical materials research Part A. 2003;67:148-57.

[207] Matsuda T, Fujio Y, Nariai T, Ito T, Yamane M, Takatani T, et al. N-cadherin signals through Rac1 determine the localization of connexin 43 in cardiac myocytes. Journal of molecular and cellular cardiology. 2006;40:495-502.

[208] Matsuda T, Takahashi K, Nariai T, Ito T, Takatani T, Fujio Y, et al. N-cadherin-mediated cell adhesion determines the plasticity for cell alignment in response to mechanical stretch in cultured cardiomyocytes. Biochemical and biophysical research communications. 2005;326:228-32.

[209] Luo Y, Radice GL. Cadherin-mediated adhesion is essential for myofibril continuity across the plasma membrane but not for assembly of the contractile apparatus. Journal of cell science. 2003;116:1471-9.

[210] Chopra A, Tabdanov E, Patel H, Janmey PA, Kresh JY. Cardiac myocyte remodeling mediated by N-cadherin-dependent mechanosensing. American journal of physiology Heart and circulatory physiology. 2011;300:H1252-66.

[211] Lin ZX, Holtzer S, Schultheiss T, Murray J, Masaki T, Fischman DA, et al. Polygons and adhesion plaques and the disassembly and assembly of myofibrils in cardiac myocytes. The Journal of cell biology. 1989;108:2355-67.

[212] Lu MH, DiLullo C, Schultheiss T, Holtzer S, Murray JM, Choi J, et al. The vinculin/sarcomeric-alpha-actinin/alpha-actin nexus in cultured cardiac myocytes. The Journal of cell biology. 1992;117:1007-22.

[213] Terai M, Komiyama M, Shimada Y. Myofibril assembly is linked with vinculin, alpha-actinin, and cell-substrate contacts in embryonic cardiac myocytes in vitro. Cell motility and the cytoskeleton. 1989;12:185-94.

[214] Feinberg AW, Alford PW, Jin H, Ripplinger CM, Werdich AA, Sheehy SP, et al. Controlling the contractile strength of engineered cardiac muscle by hierarchal tissue architecture. Biomaterials. 2012;33:5732-41.

[215] Ibrahim M, Al Masri A, Navaratnarajah M, Siedlecka U, Soppa GK, Moshkov A, et al. Prolonged mechanical unloading affects cardiomyocyte excitation-contraction coupling, transverse-tubule structure, and the cell surface. FASEB journal : official publication of the Federation of American Societies for Experimental Biology. 2010;24:3321-9.

[216] Yin L, Bien H, Entcheva E. Scaffold topography alters intracellular calcium dynamics in cultured cardiomyocyte networks. American journal of physiology Heart and circulatory physiology. 2004;287:H1276-85.

```
        1              2                  3
     PAYMENT         REVIEW          CONFIRMATION
```

## Step 3: Order Confirmation

**Thank you for your order!** A confirmation for your order will be sent to your account email address. If you have questions about your order, you can call us at +1.855.239.3415 Toll Free, M-F between 3:00 AM and 6:00 PM (Eastern), or write to us at info@copyright.com. This is not an invoice.

**Confirmation Number: 11170389**
**Order Date: 03/24/2014**

If you paid by credit card, your order will be finalized and your card will be charged within 24 hours. If you choose to be invoiced, you can change or cancel your order until the invoice is generated.

### Payment Information

Chukwuemeka G. Anene-Nzelu
a0066305@nus.edu.sg
+65 84398504
Payment Method: n/a

### Order Details

#### Biomaterials

| | |
|---|---|
| **Order detail ID:** | 64561084 |
| **Order License Id:** | 3355230392578 |
| **Article Title:** | Scalable cell alignment on optical media substrates |
| **Author(s):** | Anene-Nzelu, Chukwuemeka G. ; et al |
| **DOI:** | 10.1016/J.BIOMATERIALS.2013.03.0? |
| **Date:** | Jan 01, 2013 |
| **ISSN:** | 1878-5905 |
| **Publication Type:** | e-Journal |
| **Volume:** | 34 |
| **Issue:** | 21 |
| **Start page:** | 5078 |
| **Publisher:** | PERGAMON |
| **Author/Editor:** | Biological Engineering Society |

**Permission Status:** ✅ Granted

| | |
|---|---|
| **Permission type:** | Republish or display content |
| **Type of use:** | reuse in a thesis/dissertation |
| **Number of pages** | 10 |
| **Portion** | full article |
| **Format** | both print and electronic |
| **Are you the author of this Elsevier article?** | Yes |
| **Will you be translating?** | No |
| **Title of your thesis/dissertation** | Cost effective and scalable topography-induced cell alignment for tissue engineering applications |
| **Expected completion date** | Jul 2014 |
| **Elsevier VAT number** | GB 494 6272 12 |

**Note:** This item will be invoiced or charged separately through CCC's **RightsLink** service. More info          **$ 0.00**

**This is not an invoice.**

**Total order items: 1**                                                          **Order Total: $ 0.00**

# Technology Disclosure Form

## SECTION 1: TECHNOLOGY DISCLOSURE DETAILS

| | |
|---|---|
| RI Technology Disclosure No | **IBN-303**<br>**Lead Scientist: Prof Hanry Yu** |
| (1) Title of Technology | **Gratings-on-a-Dish – Processing of Large-Area, Low-Cost Diffraction Gratings (Holographic Gratings and Optical Discs CD/DVD) for Cell Culture/Cell Alignment** |
| (2) Keywords relating to your technology (5-10 keywords) | Diffraction gratings, holographic gratings, CD/DVD, cell culture platform, cell alignment, and cell orientation. |
| (3) Indicate the category in which your technology falls under | ☐ Drug and Gene Delivery<br>☒ Cell and Tissue Engineering<br>☐ Biodevices and Diagnostics<br>☐ Pharmaceuticals Synthesis and Green Chemistry |
| (4) Brief summary of your technology<br><br>Attach also a detailed description of your technology. | Cell alignment is a robust process in response to topographical cues regardless of the materials of the grooved substrates and dimensions of the grooves within a certain range. However, the creation of large area grooved substrates (especially nanogrooves) presents a technological challenge, involves expensive instrumentation, is time-consuming and is not easily available to most of the labs for cell-based screening or research applications. We surveyed grooved surface materials and devices that are commercially used in non-biomedical areas *and discovered a class of inexpensive materials (diffraction gratings) that* are commercially available with topographically aligned structures that are within the range of parameters that might allow cell culture and effective alignments. In fact, compact disc (CD) and digital versatile disc (DVD) are perhaps the most commonly used examples of diffraction gratings. *We propose that the surface of the commercially available diffraction gratings (optical discs like CDs/DVDs and holographic gratings) can be directly utilized to culture cells and align them for various applications when the materials are properly processed.*<br><br>Our innovation includes the sequence of processing steps to make the gratings amenable for culturing cells. The processed gratings are subsequently cut into smaller pieces and incorporated into the cell culture wells/dishes. This novel way of utilizing commercially available gratings as a cell culture platform ("gratings-on-a-dish") would open up ways for large-scale adoption of aligned cells for biomedical research and development.<br><br>Please refer to the attached manuscript for details. |

| (5) Key technical features (excluding advantages such as cost, efficiency). | Processing the diffraction gratings to make them biocompatible and use them for aligning/orienting cells for various biomedical applications. |
|---|---|

## SECTION 2: INTELLECTUAL PROPERTY ASSESSMENT

|  | Date & Details |
|---|---|
| (1) Conception of Invention  Attach relevant pages of your lab notebook. | July 7, 2011 |
| (2) Public Disclosure | March 28, 2012  The PhD Thesis of Deepak Choudhury (Drug Toxicity Testing on Chips) has been submitted to NUS NGS for correction on March 28, 2012. All non-disclosure agreements of the proposed thesis examiners have been collected and attached herewith. |

|  | RI Ref No: | Patent / Appl. Title |
|---|---|---|
| (3) Related RI's Patents/Applications /TDs |  |  |

| (4) Prior Art  Provide references to what you consider to be the closest published work (inc. your own).  Provide the details in separate sheets if necessary. | a. Cell alignment on grooved surfaces<br> • Hot embossing – Charest, J.L., et al., Combined microscale mechanical topography and chemical patterns on polymer cell culture substrates. Biomaterials, 2006, 27(11): p. 2487-2494.<br> • Nanoimprint lithography – Chou, S.Y., Krauss, P.R., and Renstrom, P.J., Imprint lithography with 25-nanometer resolution. Science, 1996, 272(5258): p. 85-87.<br> • Laser irradiation – Rebollar, E., et al., Proliferation of aligned mammalian cells on laser-nanostructured polystyrene. Biomaterials, 2008, 29(12): p. 1796-1806.<br><br>All these methods involve costly equipments, lot of processing steps and highly-skilled workforce to operate.<br><br>b. Use of CD/DVDs/holographic gratings/phonograph records to transfer patterns on polymers<br> • Patterning using CD/DVD – Chowdhury, D., Paul, A., and Chattopadhyay, A., Patterning design in color at the submicron scale. Nano Letters, 2001, 1(8): p. 409-412.<br> • Mukherjee, R., et al., Soft lithography meets self-organization: |

Institute of
Bioengineering and
Nanotechnology
A*STAR

*Innovations for Tomorrow*

CONFIDENTIAL

| | |
|---|---|
| | Some new developments in meso-patterning. Bulletin of Materials Science, 2008, 31(3): p. 249-261. |
| | • Patterning using holographic gratings/phonograph records – Vernon, R.B., et al., Microgrooved fibrillar collagen membranes as scaffolds for cell support and alignment. Biomaterials, 2005, 26(16): p. 3131-3140. |
| | • Gil, E.S., et al., Response of human corneal fibroblasts on silk film surface patterns. Macromolecular Bioscience, 2010, 10(6): p. 664-673. |
| | The authors demonstrated the usage of gratings to pattern various polymers, but they did not note the possibility of culturing cells on those gratings. |
| | c. Cell culture vessel having interior ridges, US Patent No.: 5272084, O' Connell, D.M., and Paris M.S., Cell culture vessels having interior ridges and method for cultivating cells in same. 1991, Corning Inc., New York, USA. |
| | This patent is different from our invention. It does not involve any usage of commercially available gratings (CD/DVDs/holographic gratings). The dimension of the ridges covered is only in microscale. Our innovation covers from nanoscale to microscale. The range of responses elicited from nanotopography is thought to be greater, and the effects produced on cells can range from subtle to strong (see Ref. 47 of manuscript attached). |
| **(5) Novelty / Non-obviousness** <br><br> Highlight the novelty and non-obviousness of your technology disclosure in view of prior art in which you have cited. <br><br> Provide the details in separate sheets if necessary. | Since the surface of the gratings contain other layers of materials (chemicals and dyes in the case of optical discs) and is non-sterile, <u>it has not been obvious to consider culturing cells on the gratings directly</u>. In this regard, our innovation includes the sequence of processing steps to make the gratings amenable for culturing cells. <br><br> The processed gratings are subsequently cut into smaller pieces and incorporated into the cell culture wells/dishes <br><br> The advantages of the diffraction gratings for cell culture are as follows: <br><br> a.   The micro-nano grooves on the gratings can simulate biomechanical cues of the extracellular matrix materials around the cell. <br><br> b.   They could be utilized for cell culture on large surface areas (e.g. the holographic gratings we have used are in the form of 6"x12" sheets or 6"x200" rolls). In contrast, other methods involve: <br> • laser irradiation – petri dish of up to 6 cm in diameter, <br> • hot embossing – mold silicon of 4" in diameter, <br> • electron beam lithography – 5 mm x 5 mm block of quartz. <br><br> c. |

Institute of
Bioengineering and
Nanotechnology
A∗STAR

Innovations for Tomorrow

CONFIDENTIAL

- CD/DVD is <S$1 a piece (e.g. ~60 cents for an Imation CD-R).
- Holographic grating ~S$8 (Edmund Optics, holographic diffraction film) for a 6"x12" sheet (one holographic grating can be used for ~7 24-well plates).

d. These commercially available gratings are ready-to-use with faster, easier and fewer processing steps for cell culture.

e. They do not require costly clean-room equipment and lengthy protocols.

f. They are transparent substrates and hence convenient to image.

g. Small labs, or start-up companies with less capital can utilize the gratings for elaborate biological studies.

h. The used CDs/DVDs, which are discarded as waste and pose an environmental concern, can be recycled for the proposed usage.

| (6) Does this technology arise out of a collaboration? If yes, list the collaborators and provide details | Yes, please refer to Section 4. |
|---|---|

## SECTION 3: COMMERCIAL ASSESSMENT

| (1) List the top 5 organizations that may be interested in this invention or working in the similar field. Please also provide contacts if any. | We can license our IP to an interested company who can leverage on this to develop a library of relevant gratings (or use already available gratings) for various cell culture applications. We foresee that our innovation would be interesting for three categories of clients: |
|---|---|

a. Companies manufacturing diffraction gratings, e.g. Jovin Yvon, Edmund Optics, Holographix, Thor Labs, Lightsmyth manufacture gratings of varying groove-depth and different groove designs (plane-ruled, sinusoidal, psuedosinusoidal, concave, ellipsoids, saw-toothed, etc.) for various applications such as telecommunication, encoding, lasers, spectroscopy. They would be eager to acquire this IP, which would enable them to move into biotech applications.

b. Companies developing cell culture-ware, e.g. Millipore, Becton Dickinson (BD), Corning and Thermo Scientific, make cell culture dishes and plates. However, none of them provide à cell culture surface that has a groove on it. They would be interested in this new application.

c. Companies manufacturing CDs and DVDs, e.g. Moser Baer, Verbatim, and Imation would be interested to find out a biological application to the optical storage devices, which they manufacture in bulk.

Institute of
Bioengineering and
Nanotechnology
A∗STAR

*Innovations for Tomorrow*

CONFIDENTIAL

Competitors: None at present.

Market size: The academic/industry laboratories doing cell culture, tissue engineering, mechanobiology, drug testing and stem cell differentiation etc. would be interested in this gratings-on-a-dish platform.

a. Cell culture products (Report by BCC Research, July 2010)
   - Media, Sera, Reagents – from $2.3 billion in 2009 to an estimated $3.9 billion by 2015.

b. Cell-based assays (Report by BCC Research, May 2011)
   - Drug targets and lead profiling – from $6.2 billion in 2010 to $10.8 billion in 2015.
   - ADME (absorption, distribution, metabolism, and excretion) testing -from $1.5 billion in 2010 to $3 billion by 2015.

c. *In vitro* toxicity (predictive toxicity) (Report by BCC Research, Sept. 2010)
   - Cosmetic and personal care safety screening – $702 million and is expected to reach $1.3 billion by 2015.
   - Pharmaceuticals segment – $424 million in 2010 to $976 million by 2015.

d. Tissue engineering – (Report by Market Publishers Ltd, Feb. 2012)
   - Estimated to value at US$11 billion in 2012, the global market for tissue engineering is expected to reach US$27 billion by 2018.

e. Stem cells and regenerative medicine (Report by Global Industry Analysts Inc., Oct. 2010)
   - Global regenerative medicine market to reach US$1.4 Billion by 2015.

Biological studies possible on the diffraction gratings:

a. Large-area gratings for micro-tissue formation (cell sheets)

b. Cell remodelling for drug testing
   - Isolated cardiomyocytes/neurons from the animal models can again regain their morphology and functionality on the gratings.

c. Human embryonic/mesenchymal stem cells differentiation
   - to neuronal cell lineage with or without growth factor,
   - to osteoprogenitor differentiation.

d. Cell proliferation and recombinant protein production
   - Zhu, B.S., et al., Effects of laser-modified polystyrene substrate on CHO cell growth and alignment. Journal of Biomedical Materials Research Part B-Applied Biomaterials, 2004, 70B(1): p.

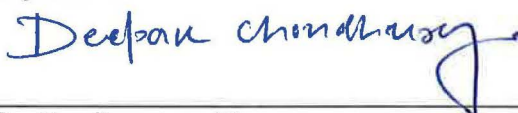Institute of
Bioengineering and
Nanotechnology
A∗STAR

*Innovations for Tomorrow*

CONFIDENTIAL

| | |
|---|---|
| | 43-48. Chinese Hamster Ovary (CHO) have been shown to proliferate better on the gratings of certain aspect ratios, one could potentially leverage on this to increase the therapeutic protein production from this robust cell line. |
| (2) Does the technology possess disadvantages or limitations? Can they be overcome and how? | The technology involves simple processing steps to make the diffraction gratings biocompatible for cell culture/cell orientation. We do not see any particular disadvantages in applying this technology. |
| (3) How can the technology be traced? Please elaborate. | It would be difficult to determine if someone makes use of the diffraction gratings in academic lab settings (although still traceable if it is published or presented). However, it is easy to trace if some company sells the processed or unprocessed diffraction gratings for cell culture applications. |
| (4) How can the technology be worked around? | As explained in section 2 (clause 4) there are other ways of producing grooved structures for cell culture. However, all these methods involve costly equipments, skilled work force and hence not readily available for mass use. Our technology would open up avenues for research labs and start-ups that would be in a position to use our device. |
| (5) Indicate the level of development. | ☐ No data<br><br>☐ Simulation results available<br><br>☒ Experimental results available<br><br>☐ Animal models created<br><br>☐ Prototype built<br><br>☐ Others, Please Highlight: |

**Institute of Bioengineering and Nanotechnology**
A·STAR
*Innovations for Tomorrow*

## SECTION 4: INVENTORS' DETAILS AND CONTRIBUTIONS

I/We hereby declare that we are the inventors for the technology.
(Note: An inventor means the actual deviser of the invention. A person is <u>NOT</u> an inventor if he/she

- Only helps to implement the invention
- Only financially contribute or sponsor the work
- Employs or manages the actual deviser/devisers of the invention )

---

1. Family name: Choudhury
   Given name: Deepak

Country of Permanent Residency: Singapore
Citizenship: Indian
Resident of Singapore during Invention: Yes

Email: deepakc@ibn.a-star.edu.sg
Tel: 9150-6967
Employer: Institute of Bioengineering and Nanotechnology

State aspect and percentage of contribution:
Conceptualization of the invention and establishing the proof-of-concept (30%)

Signature:

---

2. Family name: Anene-Nzelu
   Given name: Chukwuemeka

Country of Permanent Residency: Nigeria
Citizenship: Nigerian
Resident of Singapore during Invention: Yes

Email: anene_nzeluc@nus.edu.sg
Tel: 8439-8504
Employer: National University of Singapore

State aspect and percentage of contribution:
Establishing the proof-of-concept (10%)

Signature:

---

3. Family name: Yu
   Given name: Hanry

Country of Permanent Residency:
Citizenship: Singaporean
Resident of Singapore during Invention: Yes

Email: hyu@ibn.a-star.edu.sg
Tel: 6824-7103
Employer: Institute of Bioengineering and Nanotechnology

State aspect and percentage of contribution:
Conceptualization of the invention and establishing the proof-of-concept (30%)

Signature:

---

4. Family name: Toh
   Given name: Yi-Chin

Country of Permanent Residency:
Citizenship: Singaporean
Resident of Singapore during Invention: Yes

Email: yctoh@ibn.a-star.edu.sg
Tel: 6824-7161
Employer: Institute of Bioengineering and Nanotechnology

State aspect and percentage of contribution:
Conceptualization of the invention (10%)

Signature:

---

| | |
|---|---|
| 5. Family name: Leo<br>    Given name: Hwa Liang<br><br>Country of Permanent Residency:<br>Citizenship: Singaporean<br>Resident of Singapore during Invention: Yes<br><br>Email: bielhl@nus.edu.sg<br>Tel: 6516-5608<br>Employer: National University of Singapore<br><br><br>State aspect and percentage of contribution:<br>Conceptualization of the invention (10%)<br><br>Signature: | 6. Family name: Ng<br>    Given name: Sum Huan<br><br>Country of Permanent Residency:<br>Citizenship: Singaporean<br>Resident of Singapore during Invention: Yes<br><br>Email: shng@simtech.a-star.edu.sg<br>Tel: 6793-8382<br>Employer: Singapore Institute of<br>Manufacturing Technology<br><br>State aspect and percentage of contribution:<br>Conceptualization of the invention (10%)<br><br>Signature: |

The parties have agreed to share the royalties as follows: Institute of Bioengineering and Nanotechnology – 70%, National University of Singapore – 20% and Singapore Institute of Manufacturing Technology – 10%.

**SECTION 5: ENDORSEMENT**

**Endorsed by:**

3/5/12

Prof. Jackie Y. Ying / Date:
Executive Director
Institute of Bioengineering and Nanotechnology

**Please attach any additional sections.**